SYNTHESIS AND CHARACTERIZATION OF NI(II), CU(II) AND ZN(II) COORDINATION POLYMERS AND THE APPLICATIONS IN ELECTROCHEMICAL STUDIES AND ADSORPTION OF DYES

BIBI SHERINO

FACULTY OF SCIENCE
UNIVERSITY OF MALAYA
KUALA LUMPUR

2018

SYNTHESIS AND CHARACTERIZATION OF Ni(II), Cu(II) and Zn(II) COORDINATION POLYMERS AND THE APPLICATIONS IN ELECTROCHEMICAL STUDIES AND ADSORPTION OF DYES

BIBI SHERINO

THESIS SUBMITTED IN FULFILMENT OF THE REQUIREMENTS FOR THE DEGREE OF DOCTOR OF PHILOSOPHY

DEPARTMENT OF CHEMISTRY
FACULTY OF SCIENCE
UNIVERSITY OF MALAYA
KUALA LUMPUR

2018

UNIVERSITY OF MALAYA

ORIGINAL LITERARY WORK DECLARATION

Name of Candidate: Bibi Sherino

Registration/Matric No: SHC 140045

Name of Degree: Doctor of Philosophy

Title of Project Paper/Research Report/Dissertation/Thesis (~~"t~~his Work"):

Synthesis and characterization of Ni(II), Cu(II) and Zn(II) coordination polymers and the applications in electrochemical studies and adsorption of dyes.

Field of Study:

I do solemnly and sincerely declare that:

(1) I am the sole author/writer of this Work;
(2) This Work is original;
(3) Any use of any work in which copyright exists was done by way of fair dealing and for permitted purposes and any excerpt or extract from, or reference to or reproduction of any copyright work has been disclosed expressly and sufficiently and the title of the Work and its authorship have been acknowledged in this Work;
(4) I do not have any actual knowledge nor do I ought reasonably to know that the making of this work constitutes an infringement of any copyright work;
(5) I hereby assign all and every rights in the copyright to this Work to the University of Malaya ("~~U~~UM"), who henceforth shall be owner of the copyright in this Work and that any reproduction or use in any form or by any means whatsoever is prohibited without the written consent of UM having been first had and obtained;
(6) I am fully aware that if in the course of making this Work I have infringed any copyright whether intentionally or otherwise, I may be subject to legal action or any other action as may be determined by UM.

Candidate's Signature Date:

Subscribed and solemnly declared before,

Witness's Signature Date:

Name:

Designation:

SYNTHESIS AND CHRACTERIZATION OF Ni(II), Cu(II) AND Zn(II) COORDINATION POLYMERS AND THE APPLICATIONS IN ELECTROCHEMICAL STUDIES AND ADSORPTION OF DYES

ABSTRACT

This work describes the synthesis and characterization of benzylimidazole and piperazine based coordination polymers with two different linkers (adipic acid (A) and terephthalic acid (T)) namely: TBim-Ni-CP (**a**), TBim-Cu-CP (**b**), TBim-Zn-CP (**c**), ABim-Ni-CP (**d**), ABim-Cu-CP (**e**), ABim-Zn-CP (**f**), TP-Ni-CP (**g**), TP-Cu-CP (**h**), TP-Zn-CP (**i**), AP-Ni-CP (**j**), AP-Cu-CP (**k**), AP-Zn-CP (**l**). The physical and chemical characterization of these coordination polymers have been studied by elemental analysis, Fourier transform infrared spectrometry, single crystal and powder X-ray diffraction, BET surface area analysis, thermogravimetric analysis and electrical impedance spectroscopy for conductivity analysis. The synthesized coordination polymers were used as a modifier for carbon paste electrode to study the electrochemical behaviour of ferricyanide. Electrochemical characterization revealed that the newly synthesized coordination polymers have excellent potential as electrode modifier for the redox reaction of ferricyanide. The redox reaction of ferricyanide was reversible and diffusion controlled and the calculated diffusion coefficient values were in the range of 1.89-5.96 $\times 10^{-5}$ cm^2 s^{-1}. BET and conductivity measurements showed that AP-Ni-CP has large pore size of 361.57 Å and high conductivity of 1.28×10^{-3} S/cm compared to other coordination polymers. Therefore, AP-Ni-CP was selected as electrochemical sensor to study the electrochemical detection of H_2O_2. Systematic optimization procedures were carried out for AP-Ni-CP/CPE by cyclic voltammetry and chrono-amperometry methods. Under optimized condition AP-Ni-CP/CPE response was linear for H_2O_2 in the concentration from 0.004 to 60 mM with the limit of

detection of 0.0009 mM. The effect of interfering species on the reduction peak current response show a minor change of signals (>5%). The modified electrode has good repeatability due to lifetime stability. AP-Ni-CP/CPE electrode was also applied in real samples (lens cleaner solution) for the detection of H_2O_2 with the recoveries of 94.7 to 107%. The application of the synthesized coordination polymers has been extended to adsorption study. Adsorption behaviour of the synthesized coordination polymers towards two oppositely charged dyes (Methylene Blue and Chicago Sky Blue) were explored through batch method by UV–vis spectrophotometer. Comparison study of adsorption of dyes show that coordination polymers were more selective toward anionic dyes Chicago Sky Blue (CSB) compared to cationic dye Methylene Blue (MB) due to the presence of cationic groups in coordination polymers. The % removal for CSB and MB are in the range of 65-95% and 4-48 % respectively. ABim-Zn-CP (**f**) was selected for the kinetic and isotherm study of CSB and MB due to it good % removal towards both dyes. Adsorption parameters, including adsorbent dosage, pH of solution, dye concentration, and time were optimized. ABim-Zn-CP has excellent percentage capacity of 144.26 mg/g and 174.64 mg/g for CSB and MB respectively. Kinetics studies indicated that the synthesized adsorbent ABim-Zn-CP **(f)** followed the pseudo-second order rate model with R^2 value 0.991 and 0.993 respectively, for CSB and MB. The Langmuir isotherm with high R^2 value as compared to Freundlich isotherm indicated that CSB and MB adsorption for the synthesized coordination polymer follows monolayer adsorption. The adsorbent also has excellent potential application in environmental water sample with recovery of 98% for mixture of both dyes.

Keywords: Coordination polymers; piperazine; benzylimidazole; H_2O_2; CSB.

SYNTHESIS AND CHRACTERIZATION OF Ni(II), Cu(II) AND Zn(II) COORDINATION POLYMERS AND THE APPLICATIONS IN ELECTROCHEMICAL STUDIES AND ADSORPTION OF DYES

ABSTRAK

Kerja ini menerangkan tentang sintesis dan pencirian polimer koordinatan berasaskan benzilimidazole dan piperazin dengan dua penghubung yang berbeza (asid adipik (A) dan asid terephtalik (T)) iaitu: TBim-Ni-CP (**a**), TBim-Cu-CP (**b**), TBim-Zn-CP (**c**), ABIM-Ni-CP (**d**), ABIM-Cu-CP (**e**), ABIM-Zn-CP (**f**), TP-Ni-CP (**g**), TP- Cu-CP (**h**), TP-Zn-CP (**i**), AP-Ni-CP (**j**), AP-Cu-CP (**k**), AP-Zn-CP (**l**). Pencirian fizikal dan kimia polimer koordinasi ini telah dikaji menggunakan, analisis elemen, pegubah Fourier inframerah, pembelauan hablur tunggal sinar X-ray, pembelauan serbuk sinar-X, analisis kawasan permukaan BET, analisis termogravimetri dan analisis kekonduksian EIS. Polimer koordinatan yang telah disintesis digunakan sebagai pengubahsuai pes karbon elektrod (CPE) untuk mengkaji tingkah laku elektrokimia ferrisianida. Keputusan pencirian elektrokimia mendedahkan bahawa polimer koordinatan yang baru disintesis mempunyai potensi yang sangat baik sebagai pengubahsuai elektrod untuk tindak balas redoks bagi ferrisianida. Tindak balas redoks ferrisianida adalah berbalik dan dikawal oleh pembauran dan nilai pekali resapan yang dikira adalah dalam julat $1.89\text{-}5.96\times10^{-5}$ cm^2 s^{-1}. BET dan ukuran kekonduksian ukuran polimer koordinasi menunjukkan bahawa AP-Ni-CP mempunyai saiz liang besar 361.57 Å dan kekonduksian lebih tinggi 1.28×10^{-3} S/cm berbanding polimer koordinasi lain. Oleh yang demikian, AP-Ni-CP telah dipilih sebagai penderia elektrokimia untuk mengkaji pengesanan elektrokimia bagi H_2O_2. Prosedur pengoptimunan yang sistematik telah dijalankan bagi AP-Ni-CP/CPE mengunakan kaedah kitaran voltammetri dan krono-amperometri. Di bawah keadaan yang dioptimumkan, sambutan AP-Ni-CP/CPE adalah linear untuk H_2O_2 dalam kepekatan dari 0.004 hingga 60 mM dengan had pengesanan

0.0009 mM. Kesan spesies pengganggu terhadap isyarat penurunan puncak arus menunjukkan perubahan isyarat yang kecil (> 5%). Elektrod yang terubahsuai mempunyaii kebolehulangan yang baik kerana kestabilan jangka hidup. AP-Ni-CP/CPE elektrod juga diaplikasikan dalam sampel sebenar (cecair pembersih kanta) untuk mengesan H_2O_2 dengan perolehan semula 94.77-107%. Penggunaan polimer koordinatan yang telah disintesis telah diperluaskan kepada kajian penjerapan. Sifat penjerapan polimer koordinasi yang disintesis terhadap dua pewarna yang bercas berlawanan (MB dan CSB) telah diteroka melalui kaedah kumpulan oleh UV-vis spektrofotometer. Kajian perbandingan penjerapan pewarna menunjukkan bahawa polimer koordinasi lebih selektif ke arah pewarna anionik CSB daripada pewarna kationik MB kerana kehadiran kumpulan kationik dalam polimer koordinasi. Peratus penyingkiran untuk CSB dan MB adalah masing-masing dalam lingkungan 65-95 % dan 4-48%. Tambahan pula, ABim-Zn-CP (f) telah dipilih untuk kajian kinetik dan isoterma daripada CSB dan MB kerana peratusan penyingkirannya yang baik ke atas kedua-dua pewarna. Parameter penjerapan, termasuk dos penjerap, pH larutan, kepekatan pewarna, dan masa, telah dioptimumkan. ABim-Zn-CP mempunyai peratusan kapasiti yang cemerlang iaitu 144.26 mg /g masing-masing dan 174.64 mg /g untuk CSB dan MB Kajian kinetik menunjukkan bahawa penjerap ABim-Zn-CP (f) yang sintesis mengikut model kadar tertib pseudo-kedua dengan nilai R^2 0.991 dan 0.993 masing-masing untuk CSB dan MB. Isoterma Langmuir dengan nilai R^2 lebih tinggi berbanding isoterma Freundlich menunjukkan bahawa CSB dan MB terjerap kepada polimer koordinatanang disintesis melalui monolapisan. Penjerap juga menunjukkan keupayaan aplikasi terhadap sampel air alam sekitar dengan perolehan semula 98% untuk campuran bagi kedua-dua pewarna.

Kata Kunci: polimer koordinatan; piperazin; benzilimidazole; H_2O_2; CSB.

ACKNOWLEDGEMENTS

All praises and graces to Almighty ALLAH who gave me knowledge, courage and strength to complete this work. All the respects for Prophet Muhammad (peace be upon him), who guided mankind to the path of rightness, who is the true source of wisdom, knowledge and whose love is the only way to reach ALLAH.

I express my sincere gratitude to my supervisor Associate Professor Dr. Sharifah Mohamad, Dr Siti Nadiah Abdul Halim and Dr. Ninie Suhana Abdul Manan for providing me full support, expert guidance, unlimited moral support, constant encouragement, intellectual help at many steps, sincerity and enlightening discussions throughout the course of the completion of my research work.

My special thanks to Dr. Afzal Kamboh for his kind help in adsorption study and to improve my writing skill and developing ideas in an academic way and to all my lab mats for their valuable support and sustaining friendly atmosphere in the laboratory.

I gratefully acknowledge University Malaya of Research Grant (RP011B-14SUS), IPPP grant (PG116-2014B) and Higher Education Commission of Pakistan under FDP for Financial support.

Finally, my deepest gratitude to my loving parents specially to my late mother (Rest in Peace) for their love, prayers and support throughout my life. Foremost, I wish to express my most heartfelt gratitude to my loving husband and children for their sacrifices, moral support, strength and motivation with positive energy throughout my research work. This is tribute to their affection, support and prayers which enable me to complete this task. Many thanks to my loving brother, sisters and my in-laws for their prayers and moral support. In the end, I also thank all my friends and well-wishers who remember me in their prayers.

TABLE OF CONTENTS

LIST OF FIGURES

LIST OF SCHEME

LIST OF TABLES

LIST OF SYMBOLS AND ABBREVIATIONS

Å	:	Angstrom
ABim-M-CP	:	Adipic acid benzylimidazol-metal-coordination polymer
AP-M-CP	:	Adipic acid piperazine-metal-coordination polymer
bdc	:	Benzenedicarboxylate
BDC-OH	:	2-hydroxybenzene1,4-dicarboxylic acid
BET	:	Brunauer–Emmett–Teller
bpy	:	Pyridine
CP	:	Coordination polymer
CPE	:	Carbon paste electrode
CS	:	Conventional Solvothermal
CSB	:	Chicago sky blue
CV		Cyclic voltammetry
DEF	:	N,N-diethylformamide
EC	:	Electrochemical
EIS	:	Electrochemical Impedance spectroscopic
et al	:	et alia
FESEM	:	Field Emission Scanning Electron Microscopy
FTIR	:	Fourier Transform Infrared
LOD	:	Limited of Detection
LOQ	:	Limit of Quantification
MBM	:	Molecular based Magnetism
MC	:	Mechanochemical
mL	:	Milliliter

mol	:	Mole
MW	:	Microwave
NMP	:	N-Methyl-2-pyrrolidone
NTE	:	Negative Thermal Expansion
PTE	:	Positive Thermal Expansion
PXRD	:	Powder X-ray diffraction
RSDs	:	Relative Standard Deviation
SC	:	Sonochemical
SCO	:	Spin crossover
SPE	:	Solid Phase Extraction
SXRD	:	Single Crystal X-ray diffraction
TBim-M-CP	:	Terephthalic acid benzylimidazole-metal-coordination polymer
TCNQ	:	Tetracyano-p-quinodimethane
TEA	:	Triethanolamine
TGA	:	Thermogravimetric Analysis
TMA	:	Trimesic acid
TNT	:	Trinitro toluene
UA	:	Uric acid
UV	:	Ultraviolet
υ	:	Scan rate
θ	:	Theta
λ	:	Limbda
^{o}C	:	Degree centigrade

LIST OF APPENDICES

CHAPTER 1: INTRODUCTION AND LITERATURE REVIEW

1.1 Background study

The word –coordination polymer" was firstly used by Shibata in 1916 to report the dimers and trimers of various cobalt(II) amine nitrate and the first review based on coordination polymer has been published in 1964 (Batten *et al*., 2012). In coordination chemistry, coordination polymers (CP) are defined as coordination complexes behaving as polymer units extending into polymeric chains through the coordination active sites (Biradha *et al*., 2009). Coordination polymers are composed of metal center, ligands and/or organic linkers, forming strong and stable complexes. The metal center coordinated to either same or more than one organic entity to make a polymeric array of coordination compounds into one-, two-, or three-dimensional frameworks (Figure 1.1) (Batten *et al*., 2012).

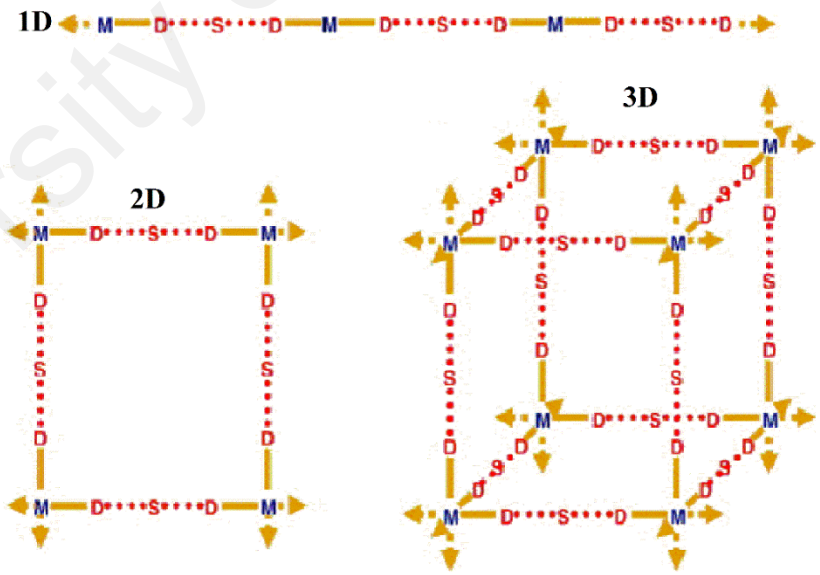

Figure 1.1: Coordination polymers into one-, two-, or three-dimensional frameworks. (S = spacer inside the ligand, D= donor groups of the ligand; M= metal ions) (Robin & Fromm, 2006)**.**

The study on the structure of porous coordination polymers has significantly increased since early 1990s and a large number of well-designed microporous

coordination polymers are reported in literature. The researches on coordination polymer were more motivated due to flexible framework based on variety of multifunctional organic bridging groups and metal center (Huang *et al*., 2012). The combination of the metal ion and the organic linker of a coordination polymer, size of the ligand, ability of interaction between metal ions and ligand are among the important element needed to construct different type of geometries of coordination polymer (Valente *et al*., 2010; Yaghi *et al*., 2003; Yaghi, 2000; Yaghi *et al*., 1997). There are various reports in the field of coordination polymers due to the following points.

(1) The coordination of metal ion in the network of supramolecular structure not only controls the position of metal ion but also give properties to the materials based on metal as well as binding ligands. In order to get stable coordination polymer which can be tuned, the types of metal centers and distances between them are very important for selection. (2) The selection of linkers and nodes suggested infinite opportunities for researchers to build new compounds with interesting structures and topologies. Furthermore, due to the computational resolution techniques and technological improvements in the field of X-ray measurements, the studies of crystals become much easier (Robin & Fromm, 2006). In coordination polymers the arrangement of constituents mostly present in solid state (in which the atoms or molecules occupying fixed positions with respect to one another and unable to move freely) (Janiak, 2003). The components are co-ordinated by coordination interactions and weaker forces such as van der Waals interactions, π–π stacking, hydrogen bonds in solution producing some small molecular units, and then, based on the same interaction self-assembly processes grow the coordination polymers (Figure. 1.2) (Kitagawa & Noro, 2004). Metal ions are usually called nodes whereas the ligands are the linkers. At the time of dissolution, the solid products are generally degrade

or insoluble. X-ray crystallographic methods are the only method to determine the structures of coordination polymers and characterizations in solution usually prove only the existence of oligomer fragments.

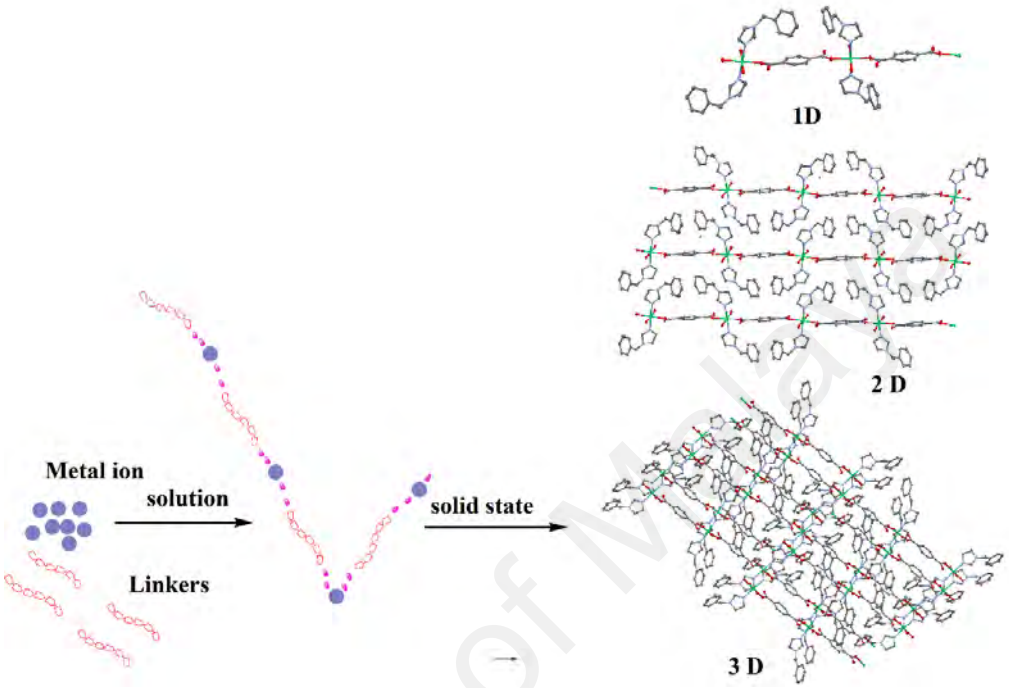

Figure 1.2: Formation of coordination polymers.

Coordination polymers are specific chemical species, their properties are different from the metal ions, ligands and linkers from which they are composed. For designing a target structure with distinct role and properties, first step is to understand the underlying geometric principles. The approach for such principle was determined by O'Keeffe and Yaghi by converting the crystal structures of coordination polymer into their underlying topological nets, which are basis for the design and description of other coordination polymer structures (Hu, 2011; Rosi *et al*., 2002). To achieve the desired structure from molecular building blocks there many synthetic approaches have been established. The structural chemistry has reached to a very mature level in a very short period of time. Coordination polymers (Figure 1.3) are now the new class that has been added in the conventional classification and occupied a significant position the area

materials (Kitagawa *et al*., 2004). However, the design of target complexes with the predicted structures and properties is still difficult and outstanding challenge due to many aspects, such as the nature of ligands used, metal ions, pH values, temperature, counter ions, the metal–ligand ratio and solvents (Ma *et al*., 2014; Cui *et al*., 2012; Hao *et al*., 2012; Effendy *et al*., 2004).

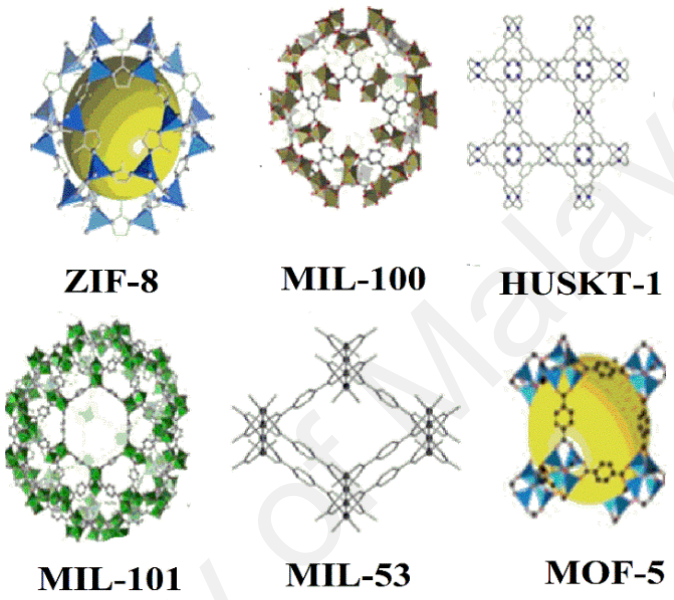

Figure 1.3: Types of porous coordination polymers (Lee *et al*., 2013**).**

1.2 Linkers and connectors

Linkers and connectors are the fundamental parts of coordination polymers. They are the starting substances which construct the basic framework of the coordination polymer. There are other secondary constituents, such as, counter ions, template molecules or nonbonding guests and ligands. The significant features of linkers and connectors are the coordination of their binding sites and coordination numbers (Kitagawa *et al*., 2004). The building of coordination polymers transition-metal ions is often used as connectors. Coordination numbers can vary from 2 to 7 giving numerous geometries depending on the central metal atom and its oxidation state such as linear, trigonal, tetrahedral, square-planar, square-pyramidal, trigonal-bipyramid, octahedral,

pentagonal-bipyramid, trigonal-prismatic, and the other distorted forms. By changing the reaction conditions such as ligands, counter ions and solvents, the metal ions with d^{10} configuration (Cu^{I} and Ag^{I} ion) giving rise different types of geometries with different coordination number (Khlobystov *et al*., 2001; Kitagawa & Munakata, 1993; Munakata, Wu, & Kuroda-Sowa, 1998). The polyhedral coordination geometry of the lanthanide ions and large coordination numbers from 7 to 10 are useful for the generation of novel and rare complex topologies. This reported coordination polymer $[Ni(C_{12}H_{30}N_6O_2)(1,4\text{-bdc})]\cdot 4\,H_2O$n ($C_{12}H_{30}N_6O_2$=macrocyclic ligand; bdc=benzenedicarboxylate) exhibit 1D chains, in which the bridging ligand 1,4-bdc occupied each axial site of the nickel–macrocyclic unit and 3D network forms by the hydrogen interaction between the chains (Choi & Suh, 1999).

Many organic linkers and ligands reported in literatures for the designing the coordination polymers. The linkers are the organic functional groups such as -COO, –NH_2, OH, –SH, –SO_3H, -PO_3H that are used to bind with metal ions in order to produce different geometries for various applications (Sel *et al*., 2015b). There are different linking sites which provided by linkers with coordinate binding directionality and strength. The composition, preparation, and application of coordination polymers based on flexible linker were reported by Kitagawa and coworker (Kitagawa, 2014). The simplest and smallest of all linkers are halides (F, Cl, Br, and I). In last two decades' carboxylates based linkers have been widely used to design different types of coordination frameworks in order to get high surface areas (600 to >5000 m^2/g) and uniform pore size distribution (Gagnon *et al.,* 2011*).* The most familiar and generally used organic linkers with carboxylic acid functional group are adipic acid, benzene 1,4-dicarboxylic (terephthalic) acid, benzene 1,3,5-tricarboxylic acid (TMA, trimesic acid), and benzene 1,2,4,5-tetracarboxylic acid (Figure 1.4). These are geometrically fixed organic linkers which are used to construct high topological frameworks and these

frameworks have good thermal and mechanical stability and having the ability to retain the porosity of compound after the removal of guest (solvent) molecule (Lin *et al*., 2014). Dicarboxylate are most common ligands used in coordination polymers and present in the form derivative with benzene or naphthalene (rigid ligand) or flexible species with alkyl chains between terminal carboxylate groups. The subclass of aliphatic carboxylates (malonate, succinate, glutarate and adipate) have a large conformational freedom property, which yield a wide variety of structural design and topologies to shows itself in a variety of connection modes (Baca *et al*., 2016; Batten *et al*., 2009). Terephthalic acid is a widely used ligand due to the rigidity of benzene ring. The attachment of carboxylic acid at para position facilitate polymer formation and discourages the formation of distinct complexes. Yaghi, O'Keeffe and co-workers have been widely study the synthesis of coordination polymers and to investigate the packing of infinite rod-shaped building blocks using large rigid dicarboxylate. Large number of terephthalate polymers have been synthesised for carbon dioxide uptake, the frameworks of those polymers are a-Po or distorted a-Po topology. For example a 3D polymer $[Gd_2(1,4\text{-bdc})_3(DEF)_2]$ H_2O (Poulsen *et al*., 2005) (DEF= N,N-diethylformamide) containing ligand terephthaic acid in which carboxylate chains are connected by the terephthalic acid linker (similar to those observed for monocarboxylate ligands) with the DEF ligands projecting into the 1D channels. A new Cu based microporous framework Cu(BDC-OH) (H_2O) 0.5DEF (where BDC-OH = 2-hydroxybenzene1,4-dicarboxylic acid) shows diamond pores in 3-D layers and almost square networks in 2-D microporous layers (Evans & Lin, 2002; Hoskins & Robson, 1990).

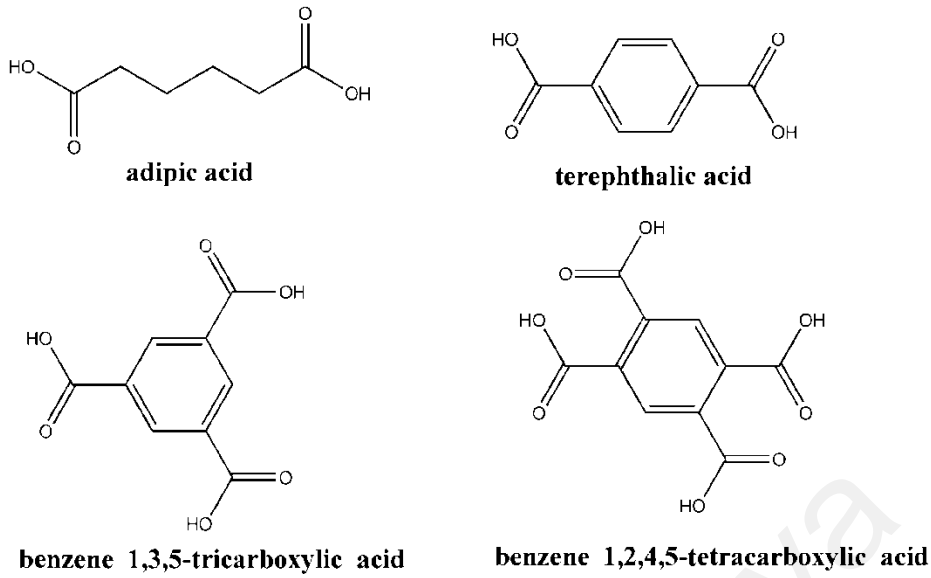

Figure 1.4: Structures of organic linkers with carboxylic acid functional group.

Coordination polymers contain ligands, which can be ions or neutral molecules, which have lone pairs that can be donated to the central metal atom. Benzylimidazole and piperazine are well-known N-donor ligands often used in coordination chemistry. Flexible N-donors ligands which have free conformation and rich structural information are more focused due to their flexibilities which allow them for greater structural diversity. Benzylimidazol ligands can rotate and bend when coordinating to metal centers due to the presence of $-(CH_2)_n-$ (n=1–6) spacers and consequently produce more strong and complex networks. The flexibility and steric hindrance of the N-donor organic ligands are very important in the formation of desired coordination polymers (Wang *et al*., 2013; Kan *et al*., 2012). Due to the remarkable flexible conformations and coordination ability of benzylimidazole derivatives, have been demonstrated to be good ligands in the composition of coordination polymers. Furthermore, this N-donor ligand able to act as hydrogen-bond donors and π–π stacking interactions due the presence of larger conjugated π system and imidazole ring to expand the supramolecular constructions (Li *et al*., 2015; Li *et al*., 2010a, 2010b). Zhang et al. (2017) reported a new coordination polymer (**NJU-Bai 19)** based on piperazine to enhance the CH_4

storage and demonstrated that the introduction of piperazine group in coordination polymer exhibits the following advantages compared with other aromatic ring functional groups: (1) it is cheaper and easier to introduce into coordination polymer (2) compared with other aromatic rings piperazine given more framework density and more balanced porosity to coordination polymer. N donor ligand are the good candidates to produce distinctive networks with advantageous applications. In addition, aromatic dicarboxylates have showed to be excellent co-ligands, due to their significant coordination ability and flexible coordination approaches (Li *et al*., 2015). Large number of porous materials has been prepared from mixture of N donor ligands and dicarboxylates linkers to build multidirectional configurations and topologies. Mixed-ligand assembly scheme including N-donor ligands and dicarboxylates has confirmed a productive approach for the building of distinctive frameworks (Krishnamurthy & Agarwal, 2014).

1.3 Synthetic techniques for coordination polymers

Coordination polymers have been synthesized by several methods. The most important methods are listed in Figure 1.5.

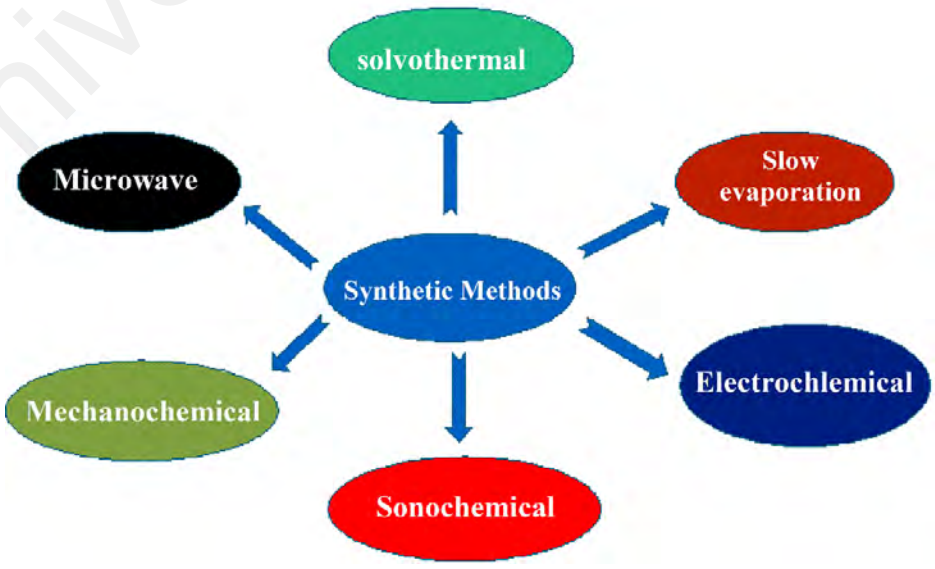

Figure 1.5: Types of synthetic methods.

The slow evaporation is the method in which no external energy is required to complete the reaction. It is also known as room temperature method in which the mixture is concentrated by slow evaporation of solvent at room temperature. The evaporation depends on the boiling point of the solvent, low boiling point solvent evaporate quickly whereas high boiling point solvent take long time to evaporate (Dey *et al*., 2014). Tranchemontagne and his co-workers reported the room temperature synthesis of MOF-74, MOF-5, MOF-177, MOF-199 and IRMOF-0 (Tranchemontagne *et al*., 2008). Slow evaporation is a method slow among all the methods. It takes several months for completion. Solvothermal/hydrothermal widely used method for the synthesis of coordination polymer. Gándara and his co-worker reported the solvothermal synthesis of MOF-519 MOF-520 at temperature of 150 °C in 4 days (Gándara *et al*., 2014). In solvothermal process the product yield increased with the increase of reaction time and the reaction time is from 24 hours to 96 hours. Crystal obtained by this method are suitable for single x-ray analysis but one drawback of solvothermal method is that the reaction condition is not suitable for those starting materials which are thermally sensitive (Krishnamurthy & Agarwal, 2014: Cravillon *et al*., 2009). Therefore, to produce good quality crystal for single X-ray and short synthesis time, other method were employed, i.e. sonochemical, microwave-assisted, ionothermal electrochemical, and mecanochemical methods (Martinez Joaristi *et al*., 2012; Klinowski *et al*., 2011; Klimakow *et al*., 2010; Li *et al.,* 2009; Parnham & Morris, 2007). Table 1.1 represents the synthesis conditions of different methods. Cr-MIL-100 was the first coordination polymer, which was prepared by microwave-assisted method in 4 h at 22 °C and has the same textural properties to that one, which was prepared by conventional method (4 days at 220 °C) (Jhung *et al*., 2007). Choi and his group reported the synthesis of MOFs-5 by the irradiation of microwave (Choi *et al*., 2008). This method has short synthesis time but the limitation of this method are related

to instrument and reaction condition because different instruments are not having same setting for temperature, reaction time and power of irradiation which effect the crystal structure (Lee *et al*., 2013). Sonochemical synthesis is the type of chemical reaction, which is concerned with the formation of acoustic cavitation (collapse and formation of bubbles) in solution. In this method the solution form of mixture is introduce into pyrex connected to a sonicator bar power output and sonicate the solution (Stock & Biswas, 2011; Gedanken, 2004; Suslick *et al*., 1986). Sonochemical is a fast and quick method and crystals formed by this method having small particles size as compared to the conventional solvothermal method. Recently, MOF-5, Mg-MOF-74, HKUST-1 and ZIF-8 have been prepared by sonochemical method (Azad *et al*., 2016; Cho *et al*., 2013; Yang *et al*., 2012; Son *et al*., 2008). Lee and his group demonstrated the production of IRMOF-3 membrane on an Al_2O_3 support disk by sonochemical and microwave assisted method, which was used for CO_2 adsorption. After comparison of the two different methods used for synthesizing of IRMOF-3 membrane they come to conclusions that sonochemical synthesis was superior to microwave method (Lee *et al*., 2015). Electrochemical method was first reported in 2005 for the synthesis of coordination polymers. In electrochemical method electric energy are used to complete the chemical reaction. The first coordination polymer which was prepared by electrochemical method was HKUST-1 in which copper metal used as electrode (anode and cathode) and H_3BTC used as organic linker dissolved in alcohol. The reaction time was 150 minutes and voltage was 12-19 V (Lee *et al*., 2013; Ulrich Mueller *et al*., 2009). The electrochemical process has following advantages; 1. Electrochemical synthesis is fast method 2. Complete utilization of organic linker with high faraday efficiency 3. Instead of metal salt metal electrode are used. 4. Synthesis occur under smooth condition as compared to microwave and solvothermal synthesis method (Martinez Joaristi *et al*., 2012).

Table 1.1: Synthesis conditions of different methods commonly used for preparation of coordination polymers.

Synthetic method	Source of energy	Time	Temperature	Solvent	References
Solvothermal	Thermal energy	48-96 hours	353-453 K	High boiling point organic solvent, DMF, DEF, methanol, ethanol, acetone, acetonitrile	(Banerjee *et al*., 2008)
Microwave-assisted	Microwave radiations	4 mints-4 hours	303-373 K	High boiling point organic solvent, DMF, DEF, methanol, ethanol, water	(Park, *et al*., 2009; Choi *et al*., 2008;)
Sonochemical	Ultrasonic radiation	30-180 mints	273-313 K	High boiling point organic solvent, DMF, DEF, methanol, ethanol, water, NMP+TEA	(Cho *et al*., 2013; Son, *et al*., 2008)
Electrochemical	Electrical energy	10-30 mints	273-303 K	High boiling point organic solvent, DMF, DEF, methanol, ethanol, water, TEA	(Martinez Joaristi *et al*., 2012)
Mechanochemical	Mechanical energy	30 mints 2 hours	298 K	Solvent free	(Martinez Joaristi *et al*., 2012)
Slow evaporation method	No external energy	7 days 7 month	298 K	High boiling point organic solvent, DMF, DEF, methanol, ethanol, acetone, acetonitrile	(Dey *et al*., 2014)

In mechanochemical method coordination polymers were synthesized without solvent or it is solvent free method. The first coordination polymer was synthesized by mechanochemical method by Pichon and his group (Pichon *et al*., 2006). The advantage mechanochemical method is that it is solvent free which is best to avoid the organic solvent as a medium. The reaction is completed in 10-60 minutes having short reaction time which gives a quantitive yield (Lee *et al*., 2013).

All the above methods have some drawbacks etc., instrument dependant, and low yield products, expansive and not suitable for industrial applications. Comparatively room temperature-method is more applicable in term of ease of synthesis, cheap, suitable for industrial application and an environment friendly but one drawback is of this method is time consuming method.

Comparison study (Table 1.2) indicated that these methods can be more improved by optimizing the reaction condition in order to get high quality, small and uniform single crystals in short synthesis time and high yield product.

Table 1.2: Comparison of synthetic methods for the preparation of coordination polymers.

Coordination polymers	Composition	CS Method	MW Method	SC Method	EC Method	MC Method	Ref.
MOF-5	$Zn(NO_3)_2 \cdot 4H_2O$ $+H_2BDC$ +DMF/ chlorobenzene	120 °C, 24 hr	800 W, 105 °C, 30 min	60 W, 30 min	300 W, 1 hr	30 Hz, 30 min-2 hr	(Lee *et al*., 2013; Banerjee *et al*., 2008; Son *et al*., 2008)
HKUST-1	$Cu(NO_3)_2 \cdot 3H_2$+ H_3BTC+H_2O /EtOH	180 °C, 12 hr	300 W, 140 °C, 1 hr	150 W, 1 hr	12-19 V, 1.3A, 150 min	25 Hz, 15 min	(Li *et al*., 2009; Seo *et al*., 2009; Pichon & James, 2008; Mueller *et al*., 2006; Chui *et al*., 1999)
ZIP-8	$Zn(NO_3)_2 \cdot 6H_2$+ HMeIm +DMF	85 °C, 72 hr	14 °C, 3 hr	300 W, 1 hr	Electrolyte [d]MTBS, 25 °C, 50 mA	5-60 min 30 Hz	(Cho *et al*., 2013; Lee *et al*., 2013; Martinez Joaristi *et al*., 2012; Park *et al*., 2009; Banerjee *et al*., 2008)
Cr-MIL-101	$Cr(NO_3)_3 \cdot 9H_2O$+ H_2BDC +H_2O	220 °C, 8 hr	60 W, 210 °C, 40 min	26.8 °C 30-180 min	29.85 °C 10-30 min	24.85 °C	(Lee *et al*., 2013; Jhung *et al*., 2007; Gerard Férey *et al*., 2005)

CS= Conventional Solvothermal, MW= Microwave, SC= Sonochemical, EC= Electrochemical, MC= Mechanochemical

1.4 Properties of coordination polymers

Coordination polymers have some unusual properties, such as luminescence, redox activity, conductivity and negative thermal expansion etc.

1.4.1 Luminescence

Luminescence is the emission of light due to the transition of electrons from an excited state to the ground state, caused by photoexcitation (Morsali & Hashemi, 2017; Feldmann *et al*., 2003). Luminescence can be divided into two types based on the nature of the excited state, i.e. fluorescence and phosphorescence. Fluorescence is a rapid process and the wavelength of emitted light increase compared to absorbed light while phosphorescence is slow process from a triplet excited state to a singlet ground state and this process is observed in the dark glow materials (Figure 1.6). Organic chromophoric ligands usually require for luminescent compounds, which absorb light and then transfer the excitation energy to the metal ion. The chromophoric ligands must have in excited state in order to sensitizing the metal ion emission. In this case the excitation of light is referred as a ligand-to-metal charge-transfer process (LMCT) while in reverse case called as metal-ligand charge-transfer (MLCT) (Dai *et al*., 2002).

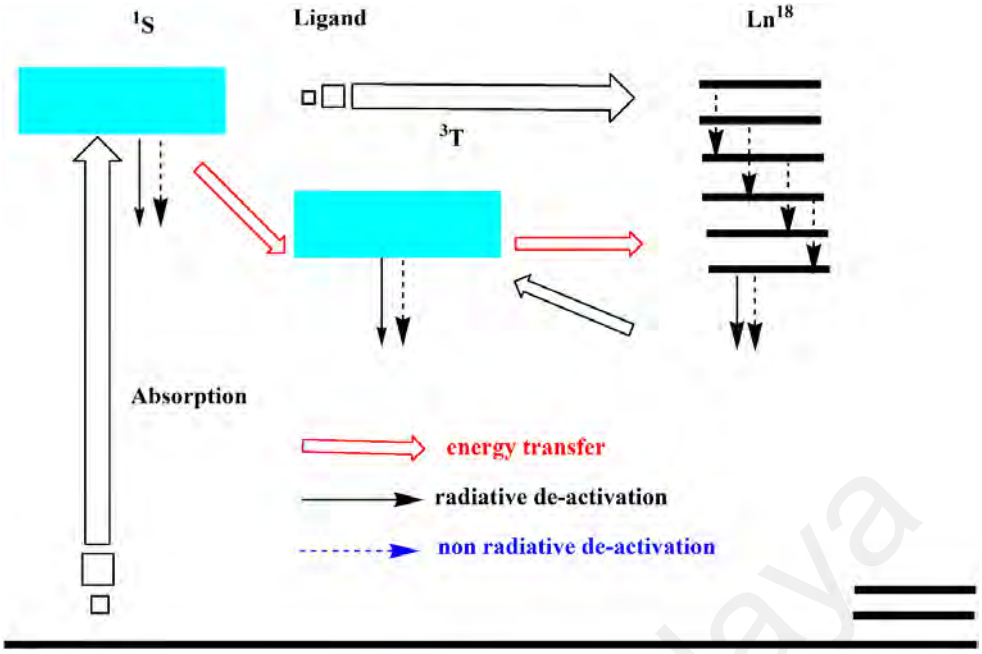

Figure 1.6: Luminescence occurs by either singlet–singlet decay (fluorescence) or triplet–singlet decay (phosphorescence).

Luminescence properties of coordination polymer are studied due to their higher thermal stability compare to organic ligand and have the capability to affect the emission wavelength of the organic material by metal coordination. Coordination polymers are the most flexible materials, which have the potential of emission properties with guest exchange. In some cases, it is suggested that the luminescence in coordination polymers is due to the ligand. For example, in the 2D coordination polymer of europium with carbamyldicyano-methanide (L_{34}) $[Eu(L_{34})_3(H_2O)_3].H_2O$, the fluorescence results are alike to that of the sodium salt, NaL_{34} where the emission arises from ligand (L_{34}) (Wang *et al*., 2011; Janiak, 2003). Carboxylate-based ligands are not the only bridging groups that can be used in luminescent materials but also more useful in bulk of other research areas. There are many examples of d-block coordination polymers with a range of different kinds of ligands reported. For example, bis(imidazolyl) ligands (Zhu *et al*., 2002), poly(pyridyl) ligands (Seward *et al*., 2004), Cu(I)–alkene polymer and bis(sulfonate) ligands (Fu *et al*., 2005), which have red

fluorescence due to MLCT process while $[Ag_4(Hbtc)_2]$ which are carboxylate-based Ag(I) polymers, exhibit intense blue emission (Ding *et al*., 2005).

1.4.2 Redox Activity

Redox activity of a compound is the ability to change in the oxidation states of atoms. The redox-active coordination polymers are interesting targets for us due to having significance role in catalysis or photophysical and electrical phenomena (Balzani *et al*., 1996). The coordination polymers are the solid-state materials so designing redox activity is challenging task because the change in the oxidation must be compensated by opposite change in the structure. The reported redox-active coordination polymer, $[Fe(III)(OH)_{0.8}F_{0.2}(O_2CC_6H_4CO_2)]$ is more attracted in Li based batteries applications due to reversible electrochemical consumption of lithium. In charging cycle the lithium is oxidised to Li(I) and the Fe(III) is reduced to Fe(II) and the reverse process occurs during discharge cycle (Férey *et al*., 2007).

A series of structures, i.e. Ni(II) complexes based on cyclam and bridged by polycarboxylate ligands have been reported by Suh et al. In these structures, Ni(II) is oxidized to Ni(III) and the absorption of these Ni complexes in the solution of $NaAuCl_4$ or $AgNO_3$ produce Ag and Au nanoparticles (Suh *et al*., 2006; Moon *et al*., 2005). The counter ions Cl^-, NO_3^- are absorbed into the structure and Ni(II) is oxidised to Ni(III). The molecule 7,7,8,8-tetracyano-p-quinodimethane (TCNQ) have been reported as one of the most important example of charge–transfer systems which is familiar as a good electron donor or acceptor, depending on its oxidation state (Pietraszkiewicz *et al*., 1998). In the structure of [Zn(TCNQ)(4,40-bipy)] $6H_2O$, the TCNQ is present as an aromatic species and dianion. In order to achieve good potential applications a number of other redox-active center can be intentionally imported into coordination polymers. Ferrocene moiety is one of the well-known redox species; ligands containing this

moiety have been incorporated into a number of nets, which have then been shown to be redox active. Ferrocenes have good redox activity as well as also show central role in the field of materials science, as nonlinear optical materials molecular magnets and components of catalysts (Horikoshi *et al*., 2002).

1.4.3 Conductivity

Electrical conductivity of coordination polymers is a measure of its ability to conduct electric current under certain conditions (as applied current, pressure, temperature). It is well known that the researchers of materials science were more attracted towards the electrical conductivity of coordination polymers. However, the researches on the conductivities of coordination polymers are still in early stage. In coordination polymers the conductivity is not the main focus of research such as in order to get good conductivity in extended metal-ligand structures short inorganic bridges are required to introduce in the structure (Givaja *et al*., 2012). The conductivity of metals are effected by temperature for example at room temperature the conductivity of metals are 104–105 S cm^{-1} and increases with decreasing of temperature. Stacked macrocyclic metal complexes of one dimensional coordination polymers have been studied for their conductivity and the conductivity significantly increases when doping with iodine (Janiak, 2003). The types of interaction of the d-orbitals of metal with the π orbitals of the bridging ligand affect the conductivity of these 1D coordination polymers. Conductivity is higher for those metals, which have better π-bonding (Os > Ru > Fe). The conductivity of coordination polymer $2\infty[Ni_2(L^{21})_4]$ (L^{21}= pyrimidine-2-thiolate) has 5.00×10^{-3} S cm^{-1} 28 °C due the μ_3-bridging ligand (pyrimidine-2-thiolate), which acts to bind the three nickel atoms by N and S atoms and decrease the conductivity with temperature, indicating a semiconductor nature .

In recent years, a new 2D Cu–S coordination polymer have been reported by Low and coworkers and which is formed by the self-assembly of Cu(I) ions with 4-hydroxythiophenol. Due to the ionic nature of the coordination network the electrical conductivity measured on pellets at room temperature of 120 S cm^{-1} (Low *et al*. 2010). Metallomacrocycles, are the types of low-dimensional compounds, which have been prepared in order to increase the electrical conductivity of coordination polymer by allowing the electron delocalization through π-π overlapping due to having a stacked co-planar arrangement with low interplanar distances. The ligand which are present in central metal–axises was considered to be a good pathway for conduction of electricity and in order to get this various types of bridging ligands were used between the metallomacrocycles to produce a linear coordination polymer (Givaja *et al*., 2012; Youngs *et al*., 1999).

1.4.4 Negative Thermal Expansion

The ability of a coordination polymer to shrink rather than expand with increase of temperature is called negative thermal expansion (NTE) (Barrera *et al*., 2005; Lightfoot *et al*., 2001). NTE of coordination polymers were more focused by researcher with the discovery of framework contraction of $Zn_4O(BDC)_3$ (BDC: 1,4-benzenedicarboxylate) (MOF-5 or IRMOF) with temperature which reported by Rowsell et al. In the same time Dubbeldam and coworkers reported three isoreticular coordination polymer (IRMOFs) including MOF-5 and suggested that NTE in the coordination polymers is due to the framework flexibility, thermal motion of linker and the coordination bonds of zinc atoms to oxygen of carboxylate (Dubbeldam *et al*., 2007; Rowsell, et al., 2005). In addition, it is revealed that the NTE more increases with increasing of linker size. Lock and his group members reported the elucidation of negative thermal expansion in MOF-5 and demonstrated that NTE in the framework

produced due to the vibrational motion of the aromatic ring and zinc carboxylate array (Lock *et al.*, 2010).

The reported structures such as $[Cu_2(CN)_3]$ $[Ag_4(CN)_5]$ and $[Cu_2(SCN)_3]$ contain two interpenetrating diamond nets in which cyanide is present as a bridge and NET is produce due to the thermal vibrations of bridge cyanide ligands around the metal–metal axis. The off-axis vibration increases when the temperature increases and the bridged metals are drawn closer (even though the individual ‗true' bonds increase in size). Shorter the ‗apparent' bond lengths, the cyanide atoms vibrate because of further away from the metal–metal axis (Figure 1.7) (Batten *et al*., 2009).

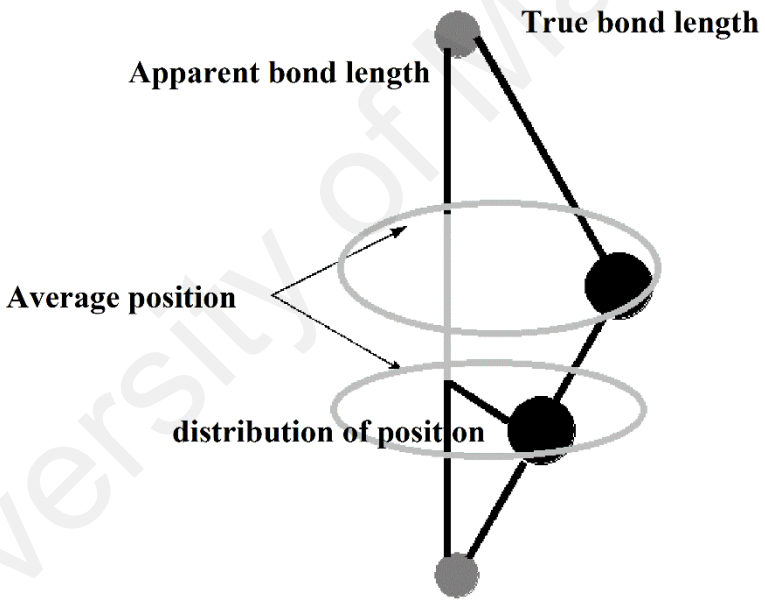

Figure 1.7: Transverse vibration of a two bridge atom, leading to NTE.

The guest species has been found to play an important role in thermal expansion properties, i.e. the compound $Er(III)[Co(III)(CN)_6].4H_2O$ shows negative thermal expansion (NTE) in the dehydrated form and positive thermal expansion (PTE) in the hydrated form. With the help of experimental evidence (reported in literatures large

NTE behaviour of carboxylate-based coordination polymer frameworks has been calculated (Wu *et al*., 2008).

1.4.5 Magnetism

One the most important property of coordination polymer is magnetism (Day & Underhill, 1999**).** It can be produced in coordination polymers by incorporating such groups which have magnetic moment for example open-shell organic ligands or paramagnetic metals or both (Kurmoo, 2009) . In magnetic material magnetic moment carrier not enough to explain magnetism, because magnetism is a phenomenon in which need some types of exchange among moment carriers. Thus, the distances of connection between moment carriers should be within the interacting range. In coordination polymers mostly magnetism can also be inserted in the form of guests while the structure remains non-magnetic. Up to now the first row transition metals (V, Cr, Mn, Fe, Co, Ni and Cu) (paramagnetic metal centres) are incorporating in the majority of coordination polymers network to make it magnetic. The allowance of variation of two important factors such as magnetic anisotropy and spin quantum number are present in that transition metal which exit in different oxidation state. Magnetic coordination polymers are well described within the classification of Molecular Magnets. There are two sub class of magnetic coordination polymers: 1. Those presenting long -range ordering 2. Those that show a spin crossover (SCO) properties. A class of magnetic materials which composed of molecular components such as molecules or molecular ions are called molecule-based magnets (MBMs). These magnetic materials opposed the metallic lattices or inorganic network solids, which are constructed from single atoms. Mostly, MBMs are formed by rare earth ions, transition metals, diamagnetic ligands, or free radicals (Batten *et al*., 2009).

The structure that allows for pairing of parallel spins, called ferromagnetism and pairing of antiparallel spins, termed ferrimagnetism. When antiparallel coupling of equal spins occurs, named antiferromagnetic, there is not observed the residual spin of the bulk material. Spin canting is an additional arrangement within these classes, which occurs when the local arrangement of spins differ in magnitude such that the moment is reduced but non-zero (Figure 1.8) (Batten *et al*., 2009; Janiak, 2003).

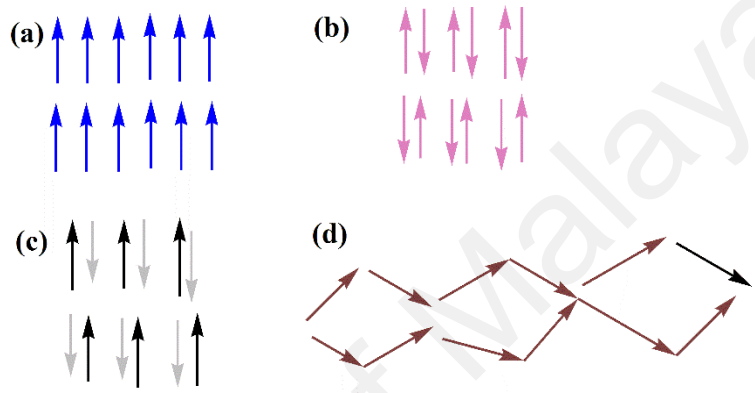

Figure 1.8: Drawing of the spin orientation in (a) a ferromagnet, (b) an antiferromagnet, (c) a ferrimagnet and (d) a spin-canted ferromagnetic.

1.5 Applications of coordination polymers

Recently much attention has been focused on the various design and synthesis of coordination polymer due to their possible applications in different fields such as in sensor technology, catalysis, gas storage (Rachuri *et al*., 2016; Sheng *et al*., 2016; Lee *et al*., 2009), separation, ion exchange, drug delivery (Figure 1.9) and in removal of dyes (Chen *et al*., 2016; Li *et al*., 2016; Wang *et al*., 2014; Wu *et al*., 2016). Robson and group reported a new coordination polymer in 1990, which has been used in an anion exchange application. Fujita et al. (1994) studied the catalytic properties of the 2D $[Cd(II)(4,4'\text{-bpy})_2]$ (bpy=bipyridine) coordination polymer.

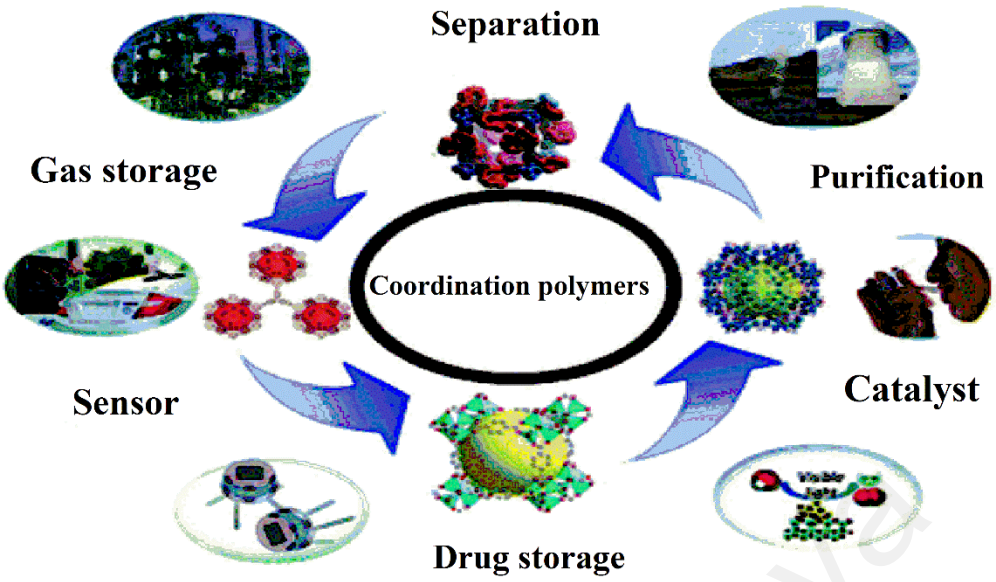

Figure 1.9: Applications of coordination polymers.

In many areas of chemistry, the host-guest behavior of coordination polymers was investigated by many researchers. The first host material (IRMOFs) was developed by Rosi and his co-worker for the application of energy storage (Rosi *et al*., 2003). High density hydrogen storage is one of the promising applications of coordination polymer due to its high volume. The advantage of coordination polymer has also been explored in heterogeneous catalysis like in zeolites. An amide group functionalized 3-D porous coordination polymer was reported by Hasegawa et al, which exhibited the ability to catalyzed Knoevenagel condensation (Hasegawa *et al*., 2007). Similarly, Sabo et al. have reported the coordination polymer (MOF-5), which could be use in catalysis of styrene within the cavities of MOF-5 that serve as palladium substrate (Sabo *et al*., 2007). Due to the biodegradability of coordination polymer, they can also use as a container material for drug delivery. Horcajada et al. have demonstrated MIL-53‘s ability for controlled release vehicle for ibuprofen (Hu, 2011; Horcajada *et al*., 2008).

1.5.1 Applications in electrochemical sensors

Coordination polymers have promising potential in electrochemistry and sensor technology. Zhang et al. (2014) have synthesized the first coordination polymer that has redox active sites which was used in lithium batteries as novel cathode active material. High porosity, adjustable chemical functionality and ordered structures make coordination polymers promising modifiers in electrochemical analysis and providing novel electrochemical sensors. Wang et al (2013) was developed an electrochemical sensor with $ZnO_4(BDC)_3$(MOF-5) for the detection of lead, which was modified to carbon paste electrode and suitable for the quantification of lead with the good reproducibility and high sensitivity and increase the scope of electrochemical sensor Ma and his co-workers demonstrated a redox-active Cu-based coordination polymers having good electrochemical ability towards electro-active probe ferricyanide ion $[Fe(CN)_6]^{3-}$ and as an excellent electrochemical sensor for nitrite ion. For the first time Ma et al. reported the ZIF material as a matrix to expand the electrochemical biosensors (Ma *et al*., 2013). Moreover, the electrochemical application of new stable coordination polymers is still one of the new challenges for researchers. Xu et al (2014) demonstrated the coordination polymer, NH_2-MIL125(Ti) modified carbon paste electrode as a photochemical sensor for the detection of Mn^{2+} under the irradiation of light they explored the photo oxidation character of NH_2-MIL125(Ti) for the sensing of Mn^{2+}. A novel carbon paste electrode (MIL-101($Cr_3X(H_2O)_2O(BDC)_3$; X = F, OH) with excellent electroanalytical performance can be used in the applications of electrochemical sensors. Li and his group reported the electrocatalytic oxidation of uric acid (UA) and dopamine (DA) by CV and electrochemical impedance spectroscopy (EIS) using modified electrode of MIL-CPE. In the absence of UA and DA there was no redox peaks in the CV of CPE and MIL-CPE. In phosphate buffered solution (PBS), MIL-101 (Cr) itself is totally inert in terms of direct electrochemistry. At the same time,

two well-defined redox peaks were detected on MIL-CPE in the presence of UA and DA. They concluded that electrocatalysis towards DA and UA is attributed to contact electrocatalysis from MIL-101 and they reported linear concentration ranges for UA and DA (Li *et al*., 2013). Coordination polymers are found to be promising candidate for sensing of volatile organic compounds due to following three properties (1) The tuning the intermolecular distance when Au(I) Pt(II), Ag(I), or those organic molecules which have π-π delocalized electrons are used (2) ligand-gas host guest interaction; (3) metal-gas interaction. The sensitivity of coordination polymers depends on the tuneable porosity, specific surface area and good thermal stability (Kumar *et al*., 2015). Coordination polymers also have important role in the detection of nitro explosives materials. Hu et al (2015) synthesized new Cd based coordination polymer and used as fluorescent sensor for the detection of explosives (TNT) material with good selectivity and reproducibility. Recently, the enzyme-free electrochemical sensors reports increase up to 343. The most widely used analytes for enzyme-free electrochemical sensors, are uric acid (UA), glucose and hydrogen peroxide (H_2O_2) due to their potential applications in various fields (Chen *et al*., 2014). Zhang et al. (2013) reported a new coordination polymer (Cu-MOF), which has good electrocatalytic activity toward H_2O_2 oxidation. H_2O_2 was oxidized to O_2 by Cu-MOF and a good linear relationship was obtained between the concentration of H_2O_2 and the anodic peak current (I_{pa}) in alkaline solution with a limit of detection of 0.068 μmol L^{-1}. The research on H_2O_2 detection is of practical importance for both industrial and academic purposes. Electrochemistry can offer rapid, simple, sensitive, and cost effective means as H_2O_2 is an electroactive molecule.

1.5.2 Applications in Adsorption of dyes

The adsorption of larger organic molecules (dyes) (Figure 1.10) by coordination polymers is another area where the pore dimensions, high porosities and large surface areas of coordination polymer provide distinctive opportunities as sorbents for environmental purification and remediation (Kitagawa *et al.,* 2004).

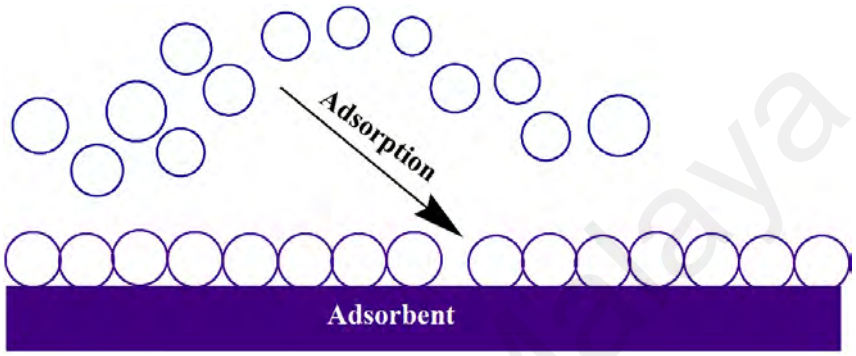

Figure 1.10: Adsorption of organic molecules by adsorbent.

Hague and co-workers demonstrated the results of the adsorption of cationic dye (MB) and an anionic dye (MO) by using coordination polymer MOF-235, $[Fe_3O(terephthalate)_3(DMF)_3][FeCl_4]$ and they observed that the adsorption capacities of the coordination polymers were higher than the commercially available activated carbon (Haque *et al*., 2011). Xu et al. (2015) reported the MSPE method for the removal of Congo red dye by using $Fe_3O_4@SiO_2$-Cu-BTC as adsorbents. The combination of coordination polymers with MSPE method will be an efficient way for water treatment and environmental protection. Various types of coordination polymer have been used for removal of different types of ionic dyes removed from polluted water reported in literature such as MCM-41, Cr-MIL-101, ED-MIL-101, MIL-53(Al) and MIL-53 (Fe) (Shakeel *et al*., 2016; Adeyemo *et al*., 2012). Leng et al. (2014) have been investigated the adsorption interaction of uranine dye with MIL-101. Hasan and co-worker reported the mechanisms of interactions for the selective adsorptions. The type of interactions for the adsorption mechanism are π–π stacking/interaction, electrostatic interaction,

hydrogen bonding, acid–base interaction and hydrophobic interaction (Hasan & Jhung, 2015). A novel anionic coordination polymer (**BUT-201**) were used to study the adsorption of cationic, anionic and neutral dyes by Sheng *et al*. and it was found that coordination polymer were more selective toward cationic dye with a smaller size, but show no adsorption towards cationic dyes with large size, anionic dyes, and neutral dyes, which indicated that adsorption not only effected by charge but also effected by the size of the dyes (Sheng *et al.*, 2016). Pore sizes of coordination polymers play a very important role in the adsorption of dyes. Porous properties of coordination polymers have attracted more attention not only in adsorption process but also in industrial applications, i.e. gas storage, separation and heterogeneous catalysis. In order to determine the porous properties of coordination polymers, the adsorption of guest molecules onto the solid surface plays an important role. The adsorption is not only influenced by interaction between the guest molecules and surfaces but also shape and pore size. Pores are classified according to their size (Table 1.3).

Table 1.3: Classification of pores.

Types of pore	**Pore size (Å)**
Ultramicropore	<5
Micropore	5-20
Mesopore	20-500
Macropore	>500

Variety of coordination designs with uniform pore structures own in porous coordination polymers. In inorganic zeolites and activated carbons (conventional porous materials) the pore shapes are often cylindrical like or slit respectively. Moreover, it is not necessary that coordination polymers possess only cylindrical like and slit pore

shapes, they also exhibit other shapes, such as triangles, squares and rectangles. In porous coordination polymers there are new adsorption profiles have been establish, which are characteristic of the uniform microporous nature such as, a square pore has four corner sites where a strong attractive potential is formed for guests (Kitagawa *et al*., 2004)

Haque et al. reported that the kinetic constant of adsorption increases with the increase of pore size, i.e. MIL-101 show high adsorption towards methyl orange then MIL153 due the large pore size of MIL-101 and this was observed in liquid phase as well as in gas phase. Coordination polymers with small pore size in microspore range limits the amount of dyes that can be adsorbed in the framework (Haque *et al*., 2010).

1.6 Objectives of research

Following are the objectives of this study:

i. To synthesize piperazine and benzylimidazole based coordination polymers with two different type of linkers (adipic acid, terephthalic acid) and three different metals, i.e. (Ni(II), Zn(II), Cu(II)).
ii. To characterize the synthesized coordination polymers by CHN, IR, SXRD, XRD, TGA, BET and EIS.
iii. To investigate electrochemical study of synthesized coordination polymers as electrode modifier.
iv. To apply the synthesized coordination polymers as electrochemical sensor for hydrogen peroxide detection.
v. To apply the synthesized coordination polymers as adsorbent for the removal of dyes.

1.7 Scope of study

Synthesis of new and more effective coordination polymers as a multifunctional material (as an electrode modifier in sensor technology and as an adsorbent for the removal of dyes) is the main objective of this study. In order to achieve this, we synthesized a series of coordination polymers (Scheme 1.1) with three different metals (Cu, Ni and Zn), two different linkers (adipic acid and terephthalic acid) and two different ligands (benzylimidazole and piperazine) for the purpose of analytical applications and characterized by various techniques CHN, IR, SXRD, XRD, TGA, BET and EIS.

The main consideration of these new materials are the presence of dicarboxylate linkers and N donor ligands, which are capable to improve the porosity of coordination polymer. Porosity play a very important role in dyes removal and sensor applications.

The synthesized coordination polymers were applied as modifier for carbon paste electrode to study the electrochemical behavior of ferricyanide and electrochemical detection of H_2O_2. In addition, the synthesized coordination polymers were also applied as an adsorbent to investigate the removal of two different dyes with two oppositely charged dyes such as Chicago sky blue (CSB) dye and methylene blue (MB) dye.

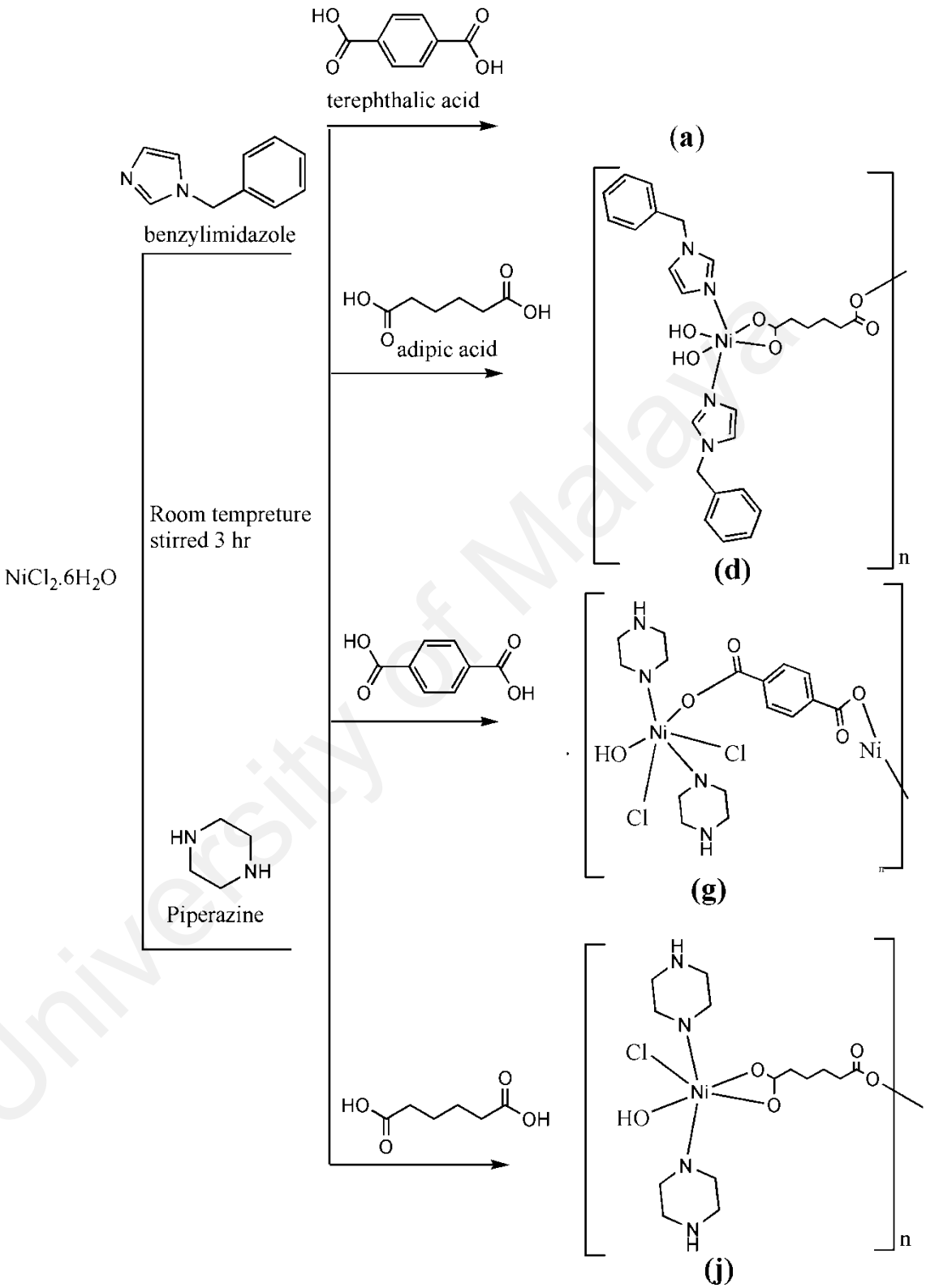

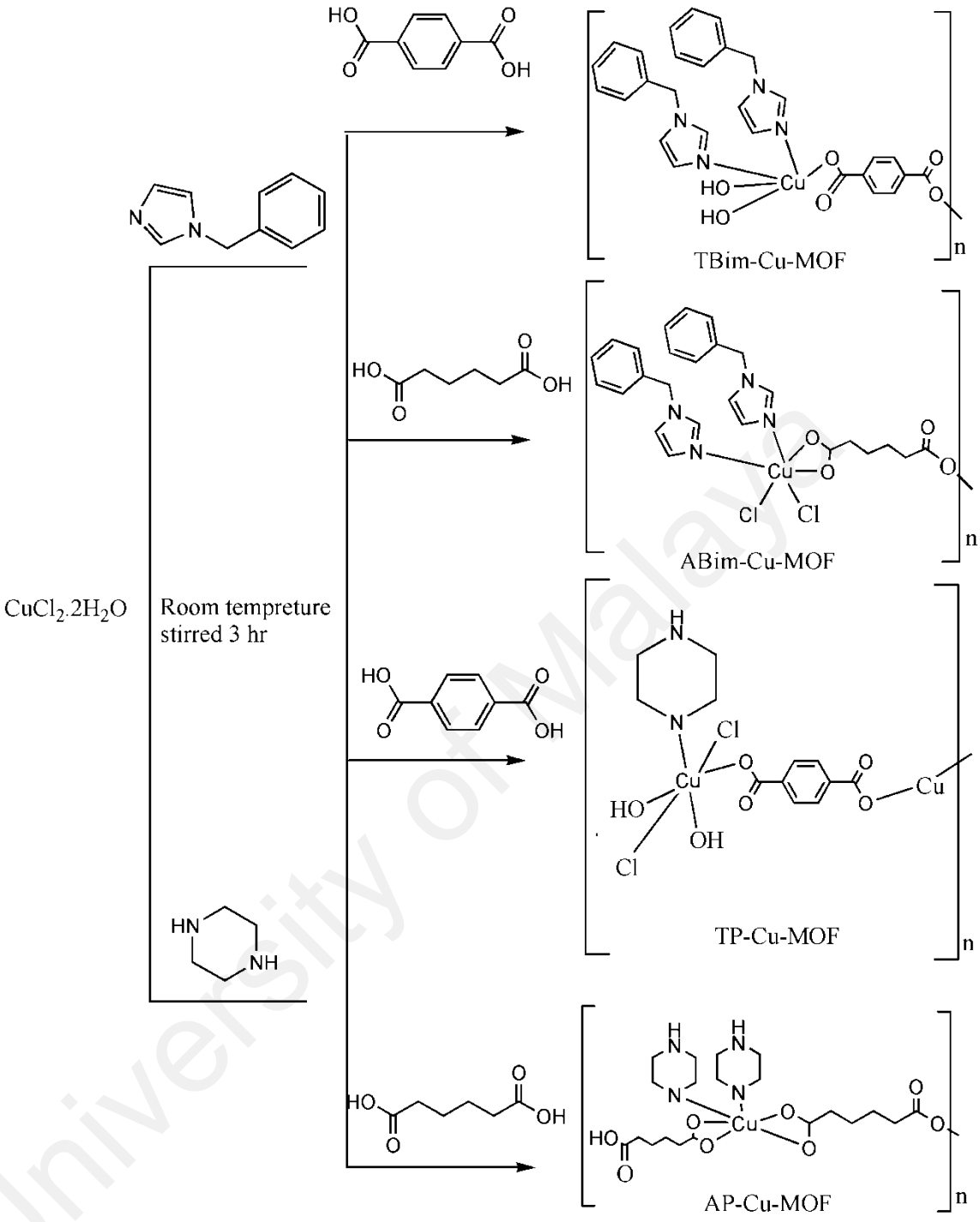

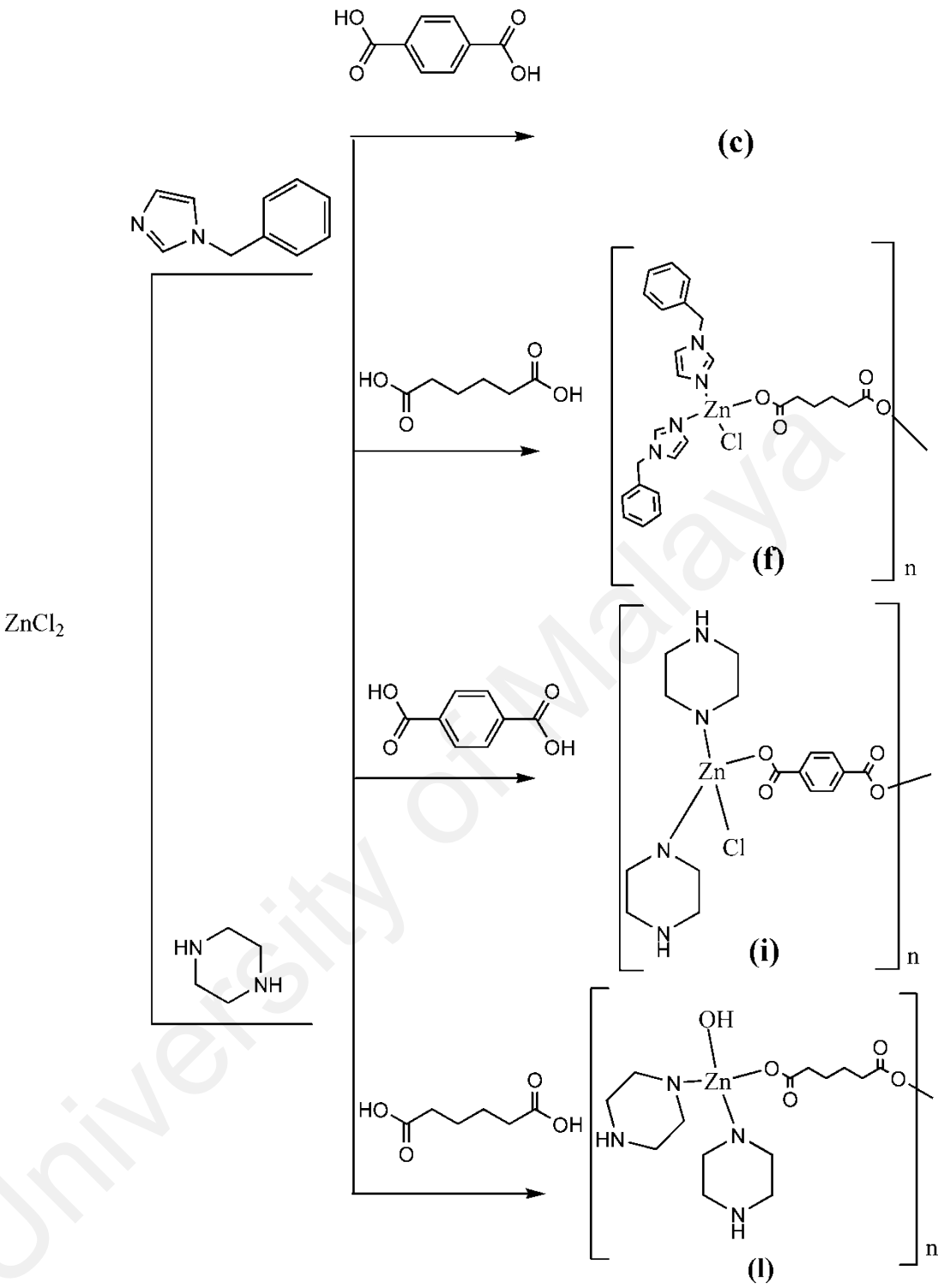

Scheme 1.1: Synthetic pathways.

CHAPTER 2: METHODOLOGY

2.1 Chemicals and reagents

Adipic acid, terephthalic acid, 1-benzylimidazole, chicago sky blue dye, methylene blue dye, sodium dihydrogen phosphate and sodium monohydrate phosphate were purchased from Sigma–Aldrich (Steinhem, Germany). Piperazine, $ZnCl_2$, $NiCl_2.6H_2O$, $CuCl_2.2H_2O$, KCl, potassium ferricyanide and hydrogen peroxide (30%) were obtained from R&M Chemicals (Essex, UK). Graphite was purchased from HmbG Chemicals (Hamburg, Germany). All the chemicals and solvent were analytical grade and used without further purification. All the working solutions were prepared in ultrapure water (UPW; Milli-Q water purification system, Millipore, Billerica, MA, USA).

2.2 Instrumentations and measurement parameters

Elemental analyses of coordination polymers were performed using CHN analyzer LECO model CHNS-932 and Perkin Elmer CHNS/O Analyzer series II 2400 (Waltham, MA, USA).

Fourier Transform Infrared Spectroscopy (FTIR) was used to collect the Infrared spectra by Perkin Elmer Spectrum 400 FTIR/FT-FIR spectrometer (Waltham, MA, USA). The ultraviolet-visible spectrometry (UV-vis) analyses were performed on UV-vis spectrophotometer UV-1650 (Shimadzu) (Kyoto, Japan) from 200 to 800 nm for the measurements of dyes.

X-ray single crystal data for coordination polymers were collected at 293(2) and 171(1) K on Oxford Supernova Dual Wavelength diffractometer (Oxford, England) ($\lambda_{Mo\ K\alpha}$ = 0.71073 Å). High quality crystals were chosen under a polarising microscope and mounted on a glass fibre. Data processing and absorption correction was performed by multi-scan method using CrysAlis PRO, with empirical absorption correction using spherical harmonics, implemented in SCALE3 ABSPACK scaling algorithm (Oxford Diffraction). The structures were solved by direct method using SHELXS solution

programme. All of the data were refined with full matrix least-squares refinement against $|F^2|$ using SHELXL refinement programm (Sheldrick, 2015) and the final refinement include atomic position for all the atoms, anisotropic thermal parameters for all the non-hydrogen atoms, and isotropic thermal parameters for all the hydrogen atoms. The programmes Olex2 (Dolomanov *et al*., 2009), PLATON (Spek, 2009) and Mercury (Macrae *et al.*, 2008) were used throughout the study. The crystallinity of coordination polymers were characterized by PANalytical, X'Pert HighScore diffractometer (Westborough, MA, US) with primary monochromatic high intensity Cu-K_α (λ=1.54184) radiation in the scanning range of 5° to 40°.

Thermogravimetric analysis (TGA) was conducted under nitrogen atmosphere in the range of 50 ˚C to 900 ˚C at a heating rate of 10 ˚C/min by using TGA7, Perkin Elmer (Waltham, MA, USA). The surface area, pore size and pore volume of coordination polymers were measured using Brunauer–Emmett–Teller (BET) by nitrogen adsorption-desorption isotherms at 77.35 K in Micromeritics ASAP2020 (Norcross, GA 30093 USA). Surface morphology were determined by field emission scanning electron microscope (FESEM, FEI, Quanta 400, Carl-Zeiss, Germany).

For conductivity measurement, the synthesized coordination polymers were first dried in a vacuum oven at 60 ºC for 24 h, then compressed to form disks by applying about 10 tons. The prepared disks have area of about 1.326 m^2 and thickness of about 11.15-26.16 mm. The sample disks were sandwiched between two stainless steel holder which act as electrode. The conductivity of synthesized coordination polymers was determined by Cole-Cole impedance plot of imaginary impedance against real impedance using HIOKI3532-50LCRHiTESTER (Cranbury, NJ 08512, USA) from room temperature to 373 K. The frequency range is from 50Hz to 5MHz. Impedance spectroscopy is the main analysis carried out to calculate and study the conductivity of prepared coordination polymers.

All electrochemical experiments (CV and chronoamapherometry) were performed on a computer-controlled Auto lab potentiostat using PGSTAT 101 (Utrecht, Netherlands).

2.3 Synthesis method

2.3.1 Synthesis of benzyl imidazole based coordination polymers

2.3.1.1 Synthesis of TBim-Ni-CP (a)

a has been prepared according to the reported method (Groeneman *et al*., 1999). An aqueous solution (20 mL) of $NiCl_2.6H_2O$ (0.0025 M, 0.594 g) was slowly added to a methanol solution (10 mL) of 1-benzylimidazole (0.01 M, 1.582 g) resulting an aqueous light green solution. The mixture was left stirred for about an hour. The DMF solution of terephthalic acid (0.0025 M, 0.415 g) was then added into the green solution and was left for continuous stirring for about 3 hours. No precipitate was obtained and the light green solution was left for slow evaporation. Light green crystals suitable for single crystal X-ray data collection were obtained after a week.

2.3.1.2 Synthesis of TBim-Cu-CP (b)

The synthetic method as in 2.2.1.1 was repeated by changing the metal salt to $CuCl_2.6H_2O$ (0.0025 M, 0.426 g) resulting light blue precipitate. No crystals were obtained for this compound.

2.3.1.3 Synthesis of TBim-Zn-CP (c)

The synthetic method as in 2.2.1.1 was applied by replacing $NiCl_2.6H_2O$ with $ZnCl_2$ (0.0025 M, 0.341 g) resulting colorless precipitate. No crystals were obtained for this compound.

2.3.1.4 Synthesis of ABim-Ni-CP (d)

The synthetic method as in 2.2.1.1 was employed by changing the organic linker terephthalic acid to adipic acid (0.365 g, 0.0025 M) and the solvent from DMF to methanol. Compound **d** precipitated out as light green powder.

2.3.1.5 Synthesis of ABim-Cu-CP (e)

The synthetic method as in 2.2.1.1 was repeated by changing the organic linker and metal salt to adipic acid (0.365 g, 0.0025 M) and $CuCl_2.6H_2O$ (0.0025 M, 0.426 g) respectively. Blue powder was obtained for compound **e**.

2.3.1.6 Synthesis of ABim-Zn-CP (f)

The synthetic method as in 2.2.1.1 was performed by changing the organic linker and metal salt to adipic acid (0.365 g, 0.0025 M) and $ZnCl_2$ (0.0025 M, 0.341 g) respectively. Colorless precipitate was obtained for this compound.

2.3.2 Synthesis of piperazine based coordination polymers

2.3.2.1 Synthesis of TP-Ni-CP (g)

g has been prepared according to the 2.2.1.1 method. An aqueous solution (20 mL) of $NiCl_2.6H_2O$ (0.0025 M, 0.594 g) was slowly added to an aqueous solution (10 mL) of piperazine (0.215 g, 0.0025 M) resulting an aqueous light blue solution. The mixture was left stirred for about an hour. The DMF solution of terephthalic acid (0.0025 M, 0.415 g) was then added into the blue solution and was left for continuous stirring for about 3 hours. The resultant sky blue precipitate of **g** was filtered off and washed thoroughly with DI water, and then dried in oven at 100 °C for 24 hr.

2.3.2.2 Synthesis of TP-Cu-CP (h)

A similar procedure as in 2.2.2.1. was carried out by changing the metal salt to $CuCl_2.6H_2O$ (0.0025 M, 0.426 g) resulting dark green color precipitate.

2.3.2.3 Synthesis of TP-Zn-CP (i)

A similar procedure as in 2.2.2.1 was applied by changing the metal salt to $ZnCl_2$ (0.0025 M, 0.341 g) resulting colorless precipitate.

2.3.2.4 Synthesis of AP-Ni-CP (j)

The synthetic method as in 2.2.2.1 was repeated by changing the organic linker to adipic acid (0.365 g, 0.0025 M). Turquoise powder were obtained for this compound.

2.3.2.5 Synthesis of AP-Cu-CP (k)

The synthetic method as in 2.2.2.1 was performed by replacing the metal salt to $CuCl_2.6H_2O$ (0.0025 M, 0.426 g) and organic linker to adipic acid (0.365g, 0.0025M). Green powder was obtained for this compound.

2.3.2.6 Synthesis of AP-Zn-CP (l)

The synthetic method as in 2.2.2.1 was employed by changing the metal salt to $ZnCl_2$ (0.0025 M, 0.341 g) and organic linker to adipic acid (0.365 g, 0.0025 M). Colourless precipitate was obtained for this compound.

2.4 Electrochemical study

2.4.1 Fabrication of working electrode

The CPs/CPE were prepared by mixing 0.3 g of graphite powder with 0.015 g of coordination polymers. 0.1 mL paraffin oil was added to the mixture as binder. The mixture was firmly packed into a syringe with tip internal diameter of 3.0 mm and copper wire was used as the electrical contact. The modified electrode was dried at 60 °C for 1 hour, before use.

2.4.2 Study of electrochemical behavior of ferricyanide at modified carbon paste electrode

A 15 mL solution of 10 mM $[Fe(CN)_6]^{-3}$ and 0.1 M KCl (electrolyte) was analyzed by cyclic voltamogramm at CPs/CPE. For the electrochemical study the coordination polymer modified carbon paste electrodes (CPs/CPE) were used as the working electrode, platinum wire as the auxiliary electrode and Ag/AgCl (saturated KCl) as the reference electrode.

2.4.3 Electrochemical detection of H_2O_2

In chronoamperometic method, a 10 mL solution containing various concentration of H_2O_2 ranged from 0.004 to 60 mM and 0.1 M of phosphate buffer solution (pH 7.0) was transferred into an electrochemical cell. A conventional three electrode system was used consisting of AP-Ni-CP/CPE as the working electrode, platinum wire as the auxiliary electrode and Ag/AgCl (saturated KCl) as the reference electrode. The electrode surface was mechanically renewed by smoothing 2-3 mm AP-Ni-CP/CPE paste off, and then polishing for the next measurement. The potential of H_2O_2 was at −0.25 V vs Ag/AgCl (saturated KCl).

2.4.3.1 Interference study

For the purpose of good selectivity of the proposed electrochemical sensor, the effect of interfering species (glucose, urea, ascorbic acid, ethanol, $FeCl_2$ and $CuCl_2$) were studied. The amperometric current response were recorded by the successive addition of 0.5 mM H_2O_2 followed by glucose, urea, ascorbic acid, ethanol, $FeCl_2$ and $CuCl_2$ (0.5 mM) containing 0.1 M PBS (pH 7) and change in the current signal were calculated by using the following equation.

$$\%\, signal = \frac{Am(i) - Am(int)}{Am(i)} \times 100 \qquad \text{Eq. 2.1}$$

Where *Am (i)* is the initial current change of H_2O_2, *Am* (*int)* is the current change of interfering species.

2.4.3.2 Reproducibility

The reproducibility of AP-Ni-CP/CPE electrode was determined by seven modified electrodes which were prepared under optimum condition and used continuously 10 days. The relative standard deviation (RSD%) of amperometric response of these seven electrodes were calculated by the following equation:

$$\% RSD = \frac{SD}{\bar{x}} \times 100 \qquad \text{Eq. 2.2}$$

Where SD is calculating from the following equation.

$$SD = \frac{\sqrt{\Sigma(x - \bar{x})^2}}{n-1} \qquad \text{Eq. 2.3}$$

Where $\bar{x}$ is representing mean value, x is the result of every run, and n is the number of measurements

In order to check the stability of AP-Ni-CP/CPE electrode, it was stored in refrigerator at 4°C and the amperometric current were monitored consecutively for 10 days. The change in the current response were calculated by the following equation.

$$\% \, Change \; in \; current \; response = \frac{Am(f)}{Am(i)} \times 100 \qquad \text{Eq. 2.4}$$

Where *Am(f)* is the current response of final day, and *Am (i)* is the current response of initial day.

2.4.3.3 Limit of detection (LOD) and Limit of quantification (LOQ)

The limit of detection (LOD) and the limit of quantification (LOQ) are two important factors that determined the lowest concentration of an analyte that can be reliably detected by an analytical procedure. The limit of detection and quantification were determined from the standard deviation of the blank (S_B) and slope of calibration curve (b) (Konieczka & Namiesnik, 2016) by using following equations:

$$LOD = \frac{S_B}{b} \qquad \text{Eq. 2.5}$$

$$LOQ = \frac{\boldsymbol{S_B}}{b} \qquad \text{Eq. 2.6}$$

2.4.3.4 Real sample analysis

The real samples (lens cleaning solutions were purchased from a shopping mall were filtered and adjusted to pH 7 using phosphate buffer solution (pH 7). Later 0.1, 0.5, 1, 5, 50 mM of H_2O_2 were spiked into real sample solutions and transferred to voltammetric cell for detection of H_2O_2. by AP-Ni-CP/CPE sensor. The percent recovery (% R) was determined by using equation 2.7.

$$\% R = \frac{Cf}{Ci} \times 100 \qquad \text{Eq. 2.7}$$

Where *Cf* is the final concentration of H_2O_2 and *Ci* is the initial concentration of H_2O_2.

2.4.3.5 Standard addition method

The determination of H_2O_2 in real sample were carried out by using standard addition method. Standard addition method is a type of quantitative method often used in analytical chemistry whereby the standard is added to an unknown which already contains some analyte. This method is used in situations where the intensity of the signal of the analyte is affected by the composition of the matrix, by the temperature or by other factors.

2.5 Adsorption procedure (batch method)

Sorption experiments were determined by the following batch method: in each experiment 10 mg/5 mg of adsorbent (coordination polymers) was mixed with 10 mL of an aqueous solution of CSB or MB at a known concentration in a tightly sealed vial. The solution was shaken for 30 min on a shaker (180 rpm) at room temperature. After the adsorption process, the adsorbent was separated by filtration and the residual concentration was determined using Ultraviolet-Visible spectroscopy (UV–Vis) equipped with 1 cm quartz cells at 280 nm. The percentage of adsorbate adsorbed on the

coordination polymer (removal efficiency, R (%)) was calculated by the following equation:

$$\% \text{ Removal} = (\frac{C_i - C_e}{C_i}) \times 100 \qquad \text{Eq. 2.8}$$

where C_i (mol L^{-1}) is the initial concentration of solution before the adsorption and C_e (mol L^{-1} is the final concentration after the adsorption of CSB and MB.

The amount of dyes (CSB/MB) adsorbed per unit mass of adsorbent (qe) was calculated by following equation.

$$q_e = \frac{V}{m}(C_i - C_e) \qquad \text{Eq. 2.9}$$

where C_i and C_e are the initial and equilibrium concentrations of CSB and MB (mgL^{-1}), respectively, ***m*** is the mass of adsorbent (g), and ***V*** is volume of the solution.

2.5.1 Optimization factors effecting adsorption process

(i) Effect of adsorbent dosage

The effect of dosage was studied in the range of 5-30 mg. The dyes initial concentration was fixed at 10 mg L^{-1} in 10 mL of an aqueous solution of CSB or MB dyes. The percentage of removal was determined by Eq. 2.8.

(ii) Effect of pH

The effect of pH was studied in the range of pH (4.5–10.5) at room temperature. The desired pH was adjusted with 0.01 M HCL and 0.01 M NaOH using pH meter (Model Ella Instrument). The initial concentration of dyes was fixed at 10 mg L^{-1} in 10 mL. The percentage of removal was determined by Eq. 2.8.

(iii) Effect of contact time

The effect of contact time was studied at different time intervals (5-60 min) at room temperature. The initial concentration of dyes was fixed at 10 mg L^{-1} in 10 mL of pH 7.5.

(vi) Equilibrium studies

The equilibrium studies were done at different dye initial concentrations (10–500 mg L^{-1}) at pH 7.5.

2.5.2 Real Sample analysis

Real sample (lake water) was collected from a lake located in University of Malaya, Kuala Lumpur. The collected lake water sample were filtered off by filter paper. Later 10 ppm solution of mixture of both dyes were spiked into the lake water and added 10 mg of adsorbent and were analysed by UV-Vis spectrophotometer. The percent recovery (% R) was determined by using equation 2.7.

CHAPTER 3: RESULTS AND DISCUSSION

3.1 Characterization of synthesized coordination polymers

Twelve coordination polymers (**a, b, c, d, e, f, g, h, i, j, k, l**) based on two different ligands (benzylimidazole and piperazine), two different linkers (adipic acid and terephthalic acid) and three different metals (Ni, Cu and Zn) were synthesized. Chemical and physical characterization of these compounds were carried out via CHN analysis, infrared spectroscopy, single crystal X-ray diffraction, powder X-ray diffraction, BET analysis, thermal gravimetric analysis, electrical impedance spectroscopy (for conductivity measurement) and electrochemical characterization.

3.1.1 Physical characterization

Results tabulated in Table 3.1 summarised the molecular formula, IUPAC names, molecular weight, % yield, and elemental analyses for the synthesized coordination polymers. The molecular weight of coordination polymers was calculated from the proposed structures of the compounds (Scheme 1.1). The yields of most of the compounds are considered as moderate, but compounds synthesized are the expected compounds as confirmed by elemental (CHN) analysis, which are well matched the calculated CHN results of proposed structures.

Table 3.1: Physical data (molecular weight, yield, CHN analysis) for piperazine and benzylimdazole based coordination polymer.

S.No	Coordination polymers	Molecular formula	IUPAC Name	M.W	Yield (%)	Found (Calculated)		
						C	H	N
1.	**a**	$C_{30}H_{28}N_2NiO_6$	poly[[diaquadibenzylimdazolenickle(II)]di-μ-terephtalato κ^2 O,O′]	575.3	87.0	58.71 (58.46)	4.80 (4.90)	8.7 (9.74)
2.	**b**	$C_{29}H_{30}CuN_4O_7$	poly[[dibenzylimdazoledihydoxocopper (II)]di-μ-terephtalato κ^2 O,O′]	594.1	75.7	59.45 (59.09)	4.53 (4.96)	10.67 (10.18)
3.	**c**	$C_{14.5}H_{12}ClN_2O_2Zn$	poly[[benzylimidazole](chlorozinc(II))d i-μ-terephtalato κ^2 O,O′]	341.1	63.6	48.19 (49.29)	4.33 (3.54)	8.50 (8.21)
4.	**d**	$C_{27}H_{34}N_4NiO_6$	poly[[di-μ-adipato κ^2 O,O′] dibenzylimdazoledihyroxonickle(II)]	568.2	79.3	56.48 (56.79)	6.07 (6.02)	10.06 (9.84)
5.	**e**	$C_{28}H_{37}CuN_4O_6$	poly[[di-μ-adipato κ^2 O,O′]dibenzylimdazoledichlorocopper(II)]	589.2	52.5	58.22 (57.08)	5.94 (6.33)	10.56 (9.51)
6.	**f**	$C_{27}H_{31}ClN_4O_4Zn$	poly[[di-μ-adipato κ^2 O,O′] dibenzylimdazolechlorozinc(II)]	576.4	84.0	55.97 (56.26)	6.51 (5.42)	10.96 (9.72)
7.	**g**	$C_{21}H_{39}Cl_2N_4Ni_2O_5$	poly[[chlorohyroxodipiperazinenickle(II)] di-μ-terephtalato κ^2 O,O′]	617.1	50.3	41.9 (41.7)	5.81 (5.38)	9.56 (9.10)
8.	**h**	$C_{15}H_{24}Cl_2Cu_2N_2O_6$	poly[[dichlorodihydroxopiperazinecopper (II)]di-μ-terephtalato κ^2 O,O′]	526.4	71.1	32.93 (34.23)	3.23 (4.60)	4.75 (5.32)
9.	**i**	$C_{18}H_{27}ClN_4O_4Zn$	poly[[chlorodipiperazinezinc(II)]di-μ-terephtalato κ^2 O,O′]	464.3	58.5	45.66 (46.57)	5.84 (5.86)	11.44 (12.07)
10.	**j**	$C_{15}H_{31}ClN_4NiO_5$	poly[[di-μ-adipato κ^2 O,O′] chlorohyroxodipiperazinenickle(II)]	444.1	56.4	42.01 (43.29)	7.39 (7.91)	12.60 (11.88)
11.	**k**	$C_{22}H_{44}CuN_4O_8$	poly[[di-μ-adipato κ^2 O,O′] dipiperazinecopper(II)]	556.2	79.5	46.34 (47.51)	7.11 (7.97)	10.04 (10.07)
12.	**l**	$C_{16}H_{33}N_4O_5Zn$	poly[[di-μ-adipato κ^2 O,O′] hydroxodipiperazinezinc(II)]]	426.8	54.4	44.10 (45.02)	7.51 (7.79)	12.96 (13.13)

3.1.2 IR Spectroscopic characterization

The IR spectral data for free linkers (terephthalic acid and adipic acid) and the synthesized coordination polymers are represented in Table 3.2. It was observed that the IR spectra of linkers and coordination polymers (Appendix A, B) depicts peaks in nearly similar region. However, some significant variations have been illustrated in the spectra of the coordination polymers and their free linkers. The IR peaks for terephthalic acid at 3060, 1670 are attributed to C–H (aromatic) and C=O stretching, respectively. By comparing the infrared spectra of free terephthalic acid with its coordination polymers, the coordination mode and sites of the ligand and linker to the metal ion were explored. The IR stretching vibrations of TBim -M-CP **s**how**s** some additional bands at 3100-3152 cm^{-1} (N-H), 1513-1577 cm^{-1} (COO^- asymmetric), 1318-1355 cm^{-1} (COO^- symmetric), 670-708 cm^{-1} (M-O) and 464-511 cm^{-1} (M-N), respectively. A broad band (OH^-) in the range of 3426-3430 cm^{-1} were only seen in **a**, **b**. It has been observed that the stretching frequency of COO^- at 1670 cm^{-1} in terephthalic acid has been shifted to the higher wave length (lower wave number) 1513-1577 cm^{-1} (ν_{as}) and 1318-1355 cm^{-1} (ν_s) in TBim-M-CP due to the interaction with metal ion (Liu *et al*., 2015; Demirci *et al*., 2015b; Refat *et al*., 2008). The IR stretching frequency for adipic acid at 2959 cm^{-1} and 1682 cm^{-1} are attributed to C–H and C=O stretching respectively. Similarly, like TBim-M-CP, ABim-M-CP also show some additional bands in the range of 3109-3164 cm^{-1}, 1519-1565 cm^{-1}, 1361-1390 cm^{-1}, 594-702 cm^{-1} and 456-517 cm^{-1} for OH^- broad band, N-H, COO^- asymmetric, COO^- symmetric, M-O and M-N respectively. The stretching vibrations for the $\upsilon(COO^-)$ bond experienced a significant shift from 1682 to 1519-1565 cm^{-1} (ν_{as}) and 1361-1390 cm^{-1} (ν_s) in ABim-M-CP.

Piperazine based coordination polymers also show particular peaks almost in the same range like benzylimizole based coordination polymers. New characteristic peaks, which were absent in the spectrum of linkers were observed in piperazine based coordination polymers in the range of 3355-3599 cm^{-1} (OH^-), 3135-3300 cm^{-1} (N-H), 1507-1594cm^{-1} (COO^- asymmetric), 1308-1396 cm^{-1} (COO^- symmetric), 588-640 cm^{-1} (M-O) and 446-488 cm^{-1} (M-N), respectively.

Yang and co-workers reported that if $\Delta(\nu_{as}-\nu_s) > 200cm^{-1}$, carboxyl is monodetate while if $\Delta(\nu_{as}-\nu_s) < 200\ cm^{-1}$, carboxyl is bidentate (Yang *et al*., 2005). The calculated results of **a**, **b**, **c**, **d**, **e**, **f**, **g**, **i**, **j**, **k** and **l** are 136, 236, 195, 162, 131, 204, 205, 228, 245, 199, 204 and 192, respectively, which indicated the coordination of metal with linker. According to the calculated values, the linkers in **a**, **c, f**, **g**, **h, i, l** are monodentate whereas in the remaining compounds the linker is bidentate.

Table 3.2: Selected IR absorption bands of linkers (terephthalic acid and adipic acid) and coordination polymers.

IR spectral data of 1- benzylimidazole based coordination polymers									
	Wave number υ(cm^{-1})								
Coordination polymers	**ν(O-H**	**ν(N-H)**	**ν(C-H)**	**ν(COOH)**	**ν(COO^- asymmetric)**	**ν(COO^- symmetric)**	**ν(M-O)**	**ν(M-N)**	**Δ($ν_{as}$-$ν_s$)**
Linker terephthalic acid	-	-	3060	1670	-	-	-	-	-
a	3426	3100	2953	-	1577	1355	670	464	222
b	3430	3152	-	-	1573	1337	690	511	236
c	-	3117	-	-	1520	1310	708	482	210
Linker adipic acid	-	-	2959	1682	-	-	-	-	-
d	3423	3109	2942	-	1552	1390	684	517	162
e	-	3134	2948	-	1519	1388	702	456	131
f	-	3164	2930	-	1565	1361	594	505	204
IR spectral data of piperazine based coordination polymers									
Linker terephthalic acid	-	-	3060	1670	-	-	-	-	-
g	3355	3170	2959	-	1530	1325	588	485	205
h	3400	3146	2948	-	1589	1361	594	488	228
i	-	3135	2954	-	1594	1349	640	482	245
Linker adipic acid	-	-	2959	1682	-	-	-	-	-
j	3599	3300	2958	-	1507	1308	616	464	199
k	-	3171	2960	-	1582	1390	592	471	192
l	3384	3174	2927	-	1580	1376	594	446	204

3.1.3 Single crystal X-ray diffraction

Out of twelve coordination polymers we able to get crystal structure for two compounds (TBim-Ni-CP (**a**), TBim-Zn-CP (**c**)) and the rest of the compounds we obtained in precipitate form without any crystal structure due to solubility problem

3.1.3.1 Crystal structure of $[Ni(bim)_2(L1)(H_2O)_2]_n$ (a)

X-Ray single-crystal diffraction analysis revealed that **a** crystallized in the triclinic system with space group $P\bar{1}$, whilst **c** crystallized in the monoclinic system with space group $P2_1/n$. Crystallographic data and structural refinement details for both crystals are listed in Table 3.3.

The asymmetric unit of **a** consists of two [aqua(benzylmidazole)Ni(II)] fragments linked by a terephthalate bridge through coordination between the carboxylato oxygen atoms to the central nickel atoms (Figure. 3.1). The crystal structure of **a** consists of a one-dimensional network symmetrically generated, with the center of inversion at the terephthalate ring (Figure. 3.2). The nickel atom is coordinated to two benzylmidazole ligands through their nitrogen atoms, two water ligands, and carboxylato oxygen atoms of the bridging terephthalate ligands in an almost perfect octahedral environment. The Ni-O1W bond length of 2.1077(12) Å is slightly longer than the Ni-N1, Ni-O2 and Ni-O4 distances, of 2.0961(14), 2.0586(10) and 2.0778(11) Å respectively. Therefore, the two water ligands occupy the axial positions and N1, O2, N1A and O2A occupy the equatorial positions. The O2-Ni-N1, O2A-Ni-N1, O2-Ni-O1W and O2-Ni1-N1A cis-angles are all between 87 and 91°. Other bond lengths and angles are in the normal ranges (Table. 3.4) and in agreement with other previously reported nickel complexes (Mukhopadhyay *et al*., 2003).

The crystal structure is stabilized by both intra and intermolecular O-H…O, C-H…O and C-H…N hydrogen bonds (Table. 3.5).

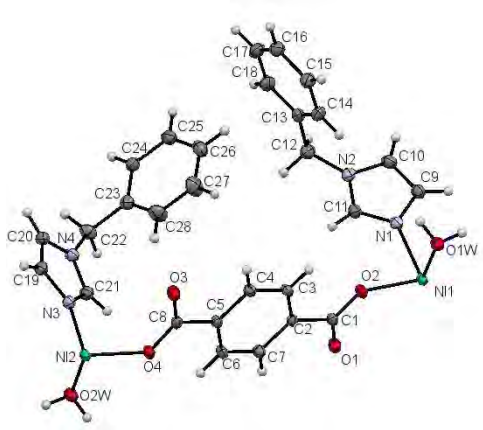

Figure 3.1: Asymmetric unit of **a** drawn with 50% probability ellipsoids.

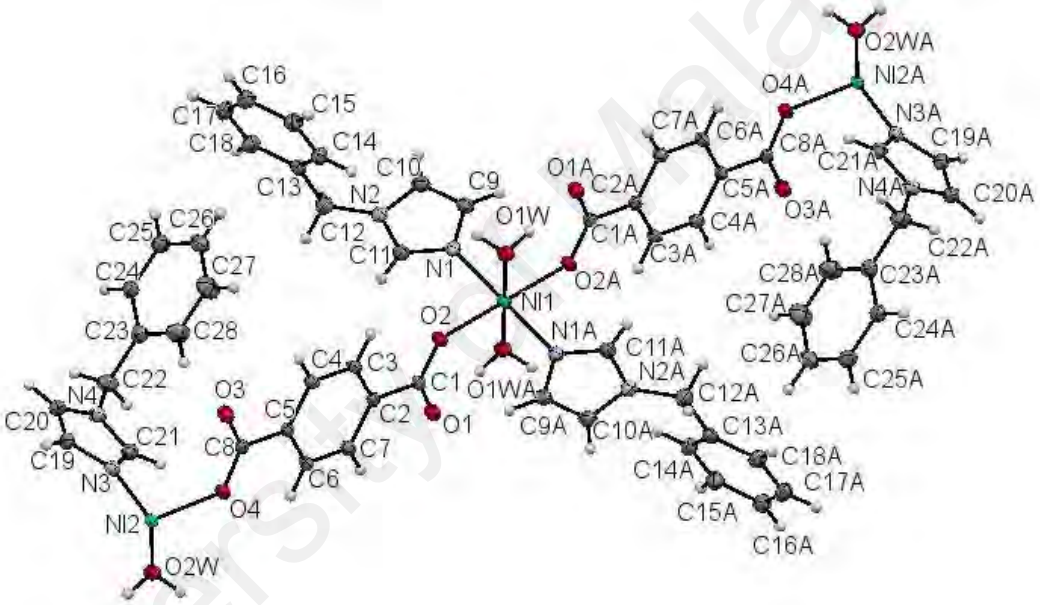

Figure 3.2: One-dimensional structure of **a** catenation complex drawn at 50% probability ellipsoids.

3.1.3.2 Crystal structure of $[Zn(bim)(L1)(Cl)]_n$ (c)

Unlike **a**, the asymmetric unit of **c** consists of a Zn complex with half of a terephthalate ligand, one chloride, and one benzylimidazole ligand (Figure. 3.3). A one-dimensional polymeric chain is also produced by symmetry. The two zinc atoms are linked by two pairs of carboxylate oxygen atoms to give a dinuclear zinc complex (Figure. 3.4). The central zinc has a distorted tetrahedral geometry with bond angles about the Zn atom between 107 and 112°. Each zinc atom is attached to one

benzylimidazole ligand through a nitrogen atom, plus one chlorine and two oxygens from the monodentate cabroxylates of two terephthalate ligands, forming a heterocyclic eight membered ring incorporating two Zn atoms. The Zn1/O2/C11/O1/Zn1A/O2A/C11A/O1 cyclooctyl ring adopts a chair conformation, with the chlorine ligands on the two zinc atoms oriented in opposite directions. The dinuclear zinc complexes are linked through the two phthalate ligands, giving a one-dimensional framework. The Zn1-N1, Zn1-O1, Zn1-Cl1, and Zn1-O2 bond lengths of 1.993(3), 1.962(2), 2.2240(9), and 1.954(2) Å, respectively are all slightly shorter than the previously reported bond lengths (2.001, 2.0746, 2.2511(6), and 2.093 Å, respectively) for similar zinc coordination polymers (Bibi *et al*., 2017; Krishnamurthy & Agarwal, 2014) Other bond lengths and angles are in normal ranges (Table 3.4) and comparable to those found in **a**.

There is only one intermolecular hydrogen bond, C14-H14…O2 (symmetry code: x, 1+y, z) with D-H= 0.93, H...A= 2.56, D…A= 3.268(4) Å and D-H-A= 134° in the solid structure, compared to the multiple hydrogen bonds observed in **a**. It is clear that the coordination geometry and metals play an important role in the formation of multi-dimensional metallic polymers or metal-organic frameworks, although the reaction conditions for **a** and **c** were the same.

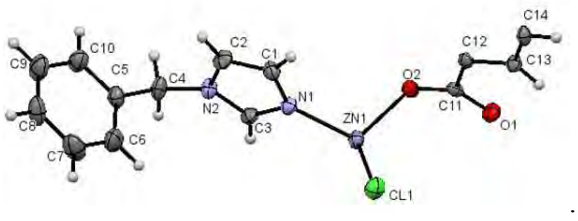

Figure 3.3: Asymmetric unit of **c** drawn with 50% probability ellipsoids.

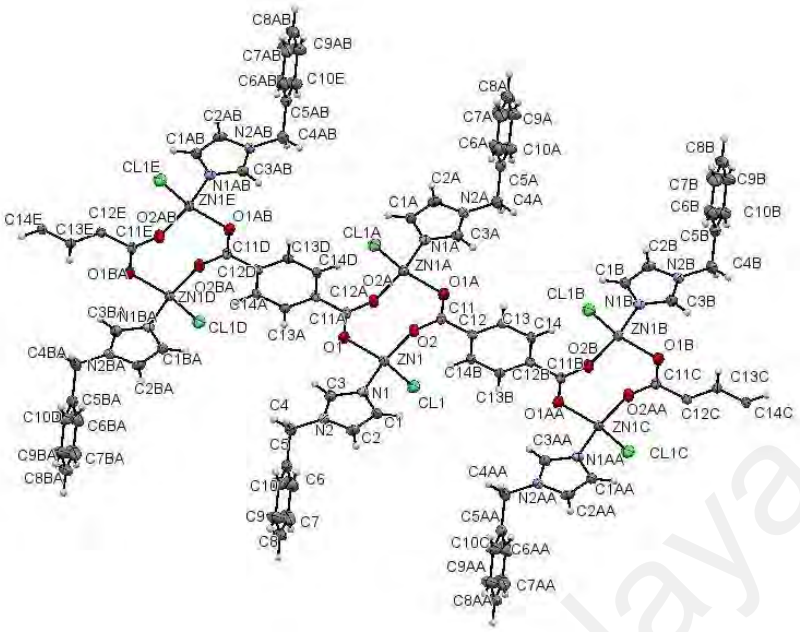

Figure 3.4: One-dimensional linear polymeric chain structure of **c** along the a-axis, drawn at 50% probability ellipsoids.

Table 3.3: Crystal data and structure parameters for crystal $[Ni(bim)_2(L1)(H_2O)_2]_n$ (**a**) and $[Zn(bim)(L1)(Cl)]_n$ (**c**).

	$[Ni(bim)_2(L1)(H_2O)_2]_n$ (a)	**$[Zn(bim)(L1)(Cl)]_n$ (c)**
CCDC No	1513753	1545205
Empirical formula	$C_{28}H_{28}N_4NiO_6$	$C_{14}H_{12}ClN_2O_2Zn$
Formula weight	575.25	341.08
Temperature/K	293(2)	171(1)
Wavelength	CuKα (λ = 1.54184)	MoKα (λ = 0.71073)
Crystal system	triclinic	monoclinic
Space group	$P\bar{1}$	$P2_1/n$
a/Å	6.5366(4)	6.5058(6)
b/Å	9.2294(5)	7.4002(5)
c/Å	21.7393(6)	28.996(3)
α /°	91.686(3)	90
β/°	90.884(4)	95.690(9)
γ/°	93.765(5)	90
Volume/ $Å^3$	1307.90(11)	1389.1(2)
Z	2	4
$\rho_{calc}g/cm^3$	1.461	1.631
μ/mm^{-1}	1.500	1.961
F(000)	600	692
2Θ range range for data collection/°	4.8 to 74.5	3.5 to 29.6
Reflections collected	8802	11272
Independent reflections	5122	3410
Data/restraints/parameters	5122/0/357	3410/0/181
Goodness-of-fit on F^2	1.091	1.051
Final R indices [I>2sigma(I)]	R1 = 0.0345, wR2 =0.0967	R1 = 0.0480, wR2 = 0.0844
Final R indices (all data)	R1= 0.0373, wR2=0.0996	R1 = 0.0818, wR2 = 0.1010
Largest diff. peak/hole/ $e.Å^{-3}$	0.338/-0.453	0.543/-0.495

Table 3.4: Selected bond lengths (Å) and bond angles (˚) for **a** and **c**.

$[NiC_{28}H_{28}N_4O_6]_n$ (a)					
Atom	**Length/Å**	**Atom**	**Angles/ ˚**	**Atom**	**Angles/ ˚**
Ni1-O1W	2.1077(12)	O2-Ni1-N1	91.53(5)	N1-Ni1-O1W	90.98(5)
Ni1-O2	2.0586(10)	O2-Ni1-N1	88.47(5)	N3-Ni2-O4	89.46(5)
Ni1-N1	2.0961(14)	O1W-Ni1-O1W	180.0	N3-Ni2-O4	90.54(5)
Ni2-O2W	2.1152(12)	N1-Ni1-N1	180.0	N3-Ni2-O2W	93.05(5)
Ni2-O4	2.0778(11)	O2-Ni1-O1W	87.99(5)	N3-Ni2-O2W	86.95(5)
Ni2-N3	2.0487(14)	O2-Ni1-O1W	92.01(5)	O4-Ni2-O2W	93.36(5)
O2-Ni1-O2	180.0	N1-Ni1-O1W	89.02(5)	O4-Ni2-O2W	86.64(5)
$[ZnC_{14}H_{12}ClN_2O_2]_n$ (c)					
Zn1-O2	1.954(2)	O2-Zn1-Cl1	107.65(7)	N1-Zn1 Cl1	112.70(8)
Zn1-Cl1	2.2240(9)	O2-Zn1-N1	110.77(10)	O1-Zn1 Cl1	118.37(7)
Zn1-N1	1.993(3)	O2-Zn1-O1	109.93(10)	O1-Zn1 N1	97.10(10)
Zn1-O1	1.962(2)	N1-Zn1-Cl1	112.70(8)	C11-O2-Zn1	129.4(2)
O2-C11	1.267(4)	O1-Zn1-N1	97.10(10)	C11-O1-Zn1	118.7(2)

[1]1-X, -Y,1-Z; [2]2-X, -Y, -Z

Table 3.5: Hydrogen Bond (Å) for $[Ni(bim)_2(L1)(H_2O)_2]_n$.

$[NiC_{28}H_{28}N_4O_6]_n$				
D-H……A	**d(D-H)**	**d(H…..A)**	**d(D…A)**	**d(D-H…..A)**
intermolecular hydrogen				
O1W-H1WB….O1^{i}	0.82(2)	2.05(2)	2.8331(17)	160(2)
O1W-H1WA….O1^{ii}	0.820(18)	1.914(17)	2.7166(16)	166(2)
O2W-H2WB….O3^{iii}	0.82(3)	2.06(3)	2.8574(17)	164(2)
C14-H14….O1^{iv}	0.93	2.52	3.350(2)	149
C24-H24….O3^{v}	0.93	2.58	3.480(2)	162
Intramolecular hydrogen bonds				
O2W-H2WA….O3^{vi}	0.824(18)	1.890(16)	2.6930(16)	165(3)

Symmetry codes *(i) 1+x, y, z, (ii) 1-x, -y, 1-z, (iii) 1+x, y, z, (iv) 1+x, y,z, (v) x, 1+y, z, (vi) 2-x, -y,-z.*

3.1.4 Powder X-ray diffraction

3.1.4.1 Powder X-ray diffraction patterns of coordination polymers

XRD spectra were obtained to elucidate the crystal structure of benzylimidazole and piperazine based coordination polymers. The XRD signals of the prepared coordination polymers **a, b, c, d**, **e** and **f** are given in Figure.3.5. Comparison of peaks of metal-linker (adipic acid, terephthalic acid) and metal-ligand (benzylimidazole) with the peaks of coordination polymers (**b, d, e, f**) indicated the successful synthesis of coordination polymers due to the presence of new peaks which confirmed the insertion of linker in the metal complex to form a polymeric structure. The sharp and strong diffraction peaks in the range of 14-28° of 2θ for **b, d, e** and **f** indicated high crystallinity and confirmed the purity of coordination polymers, which can also justified by the CHN and IR results. However, the powder X-ray diffraction patterns of coordination polymer **a** and **c** compared with simulated patterns, which are well in position and shows that the single X-ray is the representative of bulk material.

Similarly, comparison of peaks of metal piperazine and metal linker with coordination polymers **g**, **h**, **i**, **j**, **k**, **l** (Figure 3.6) shows many new diffraction peaks in the range of 14° to 25° of 2θ. The diffraction peaks in the range of 14° to 28° of 2θ usually observed for inorganic porous materials (Chandra *et al*., 2008; Szostak, 1989). Furthermore, the diffraction patterns of coordination polymers could not match with other coordination polymers known in literatures, indicating that the synthesized coordination polymers have new phases.

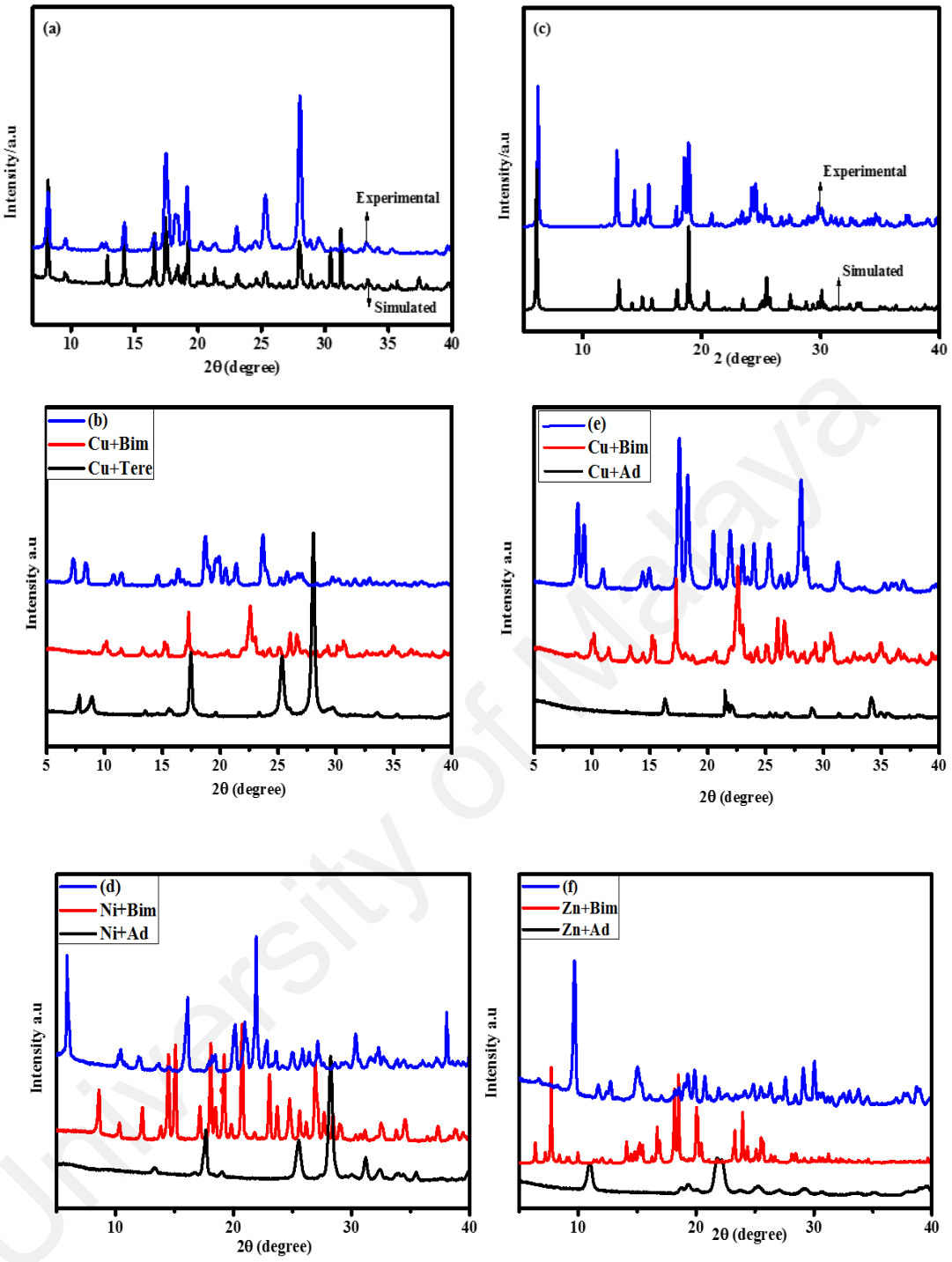

Figure 3.5: X-ray diffraction patterns of benzylimdazole based coordination polymers.

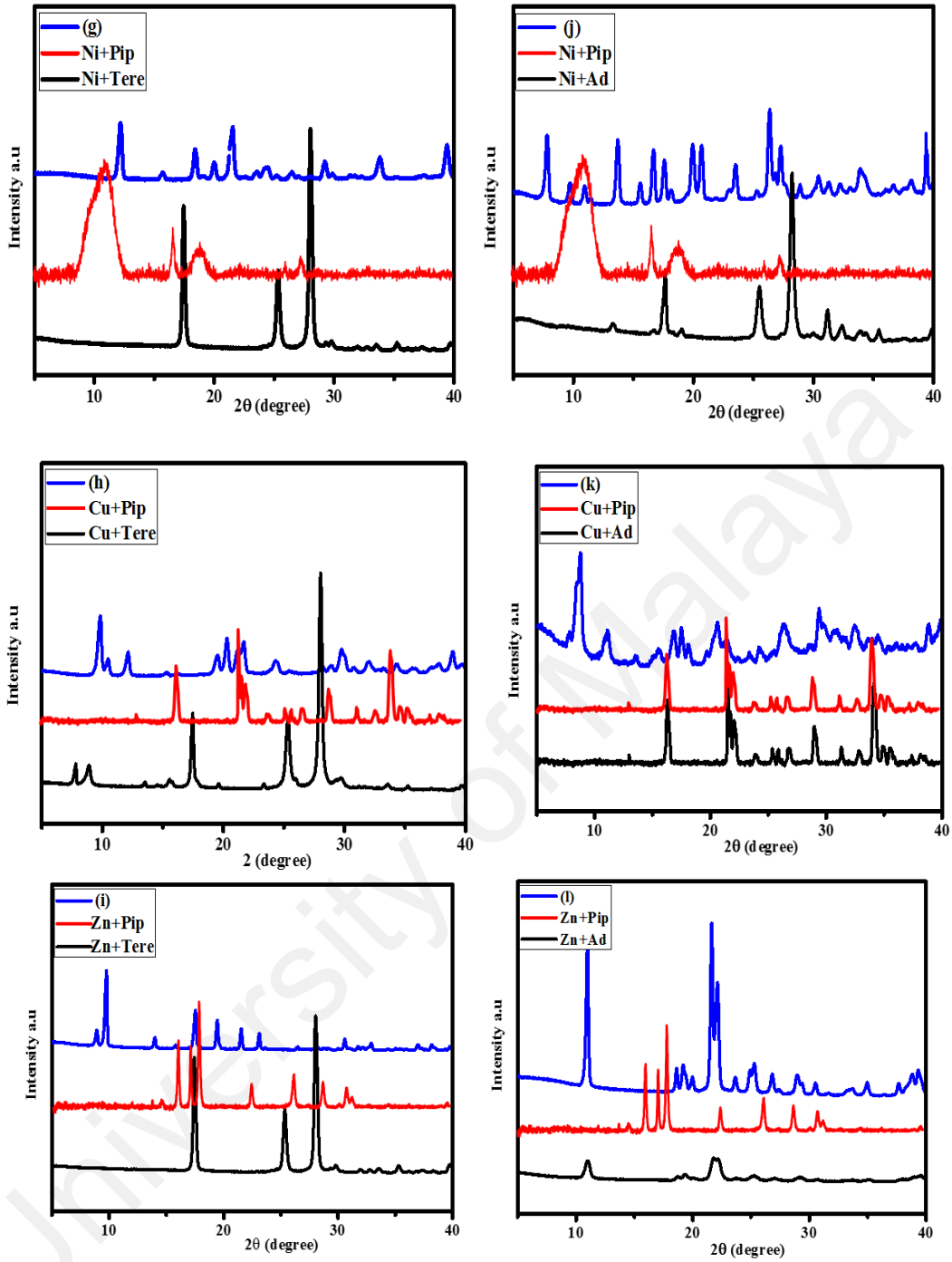

Figure 3.6: X-ray diffraction patterns of piperazine based coordination polymers.

3.1.5 Thermal gravimetric analysis

Figure 3.7 and 3.8 display the thermograms of prepared benzylimidazole and piperazine based coordination polymers to evaluate their thermal behaviour and thermal stability. In benzyl imidazole series the TG profile of complex **d** exhibits four steps, **a**, **b**, **c**, **e** three steps and **f** shows two steps pyrolysis. The initial weight loss (6-19 %) at temperature range of 71-271 °C from **a** to **d** is attributed to loss of solvated/ coordinated

water/solvents whereas in **e** and **f** the initial temperatures range of 106-473°C show the weight loss from 43 to 72.2 %, which were correspond to the loss of organic linkers. The second curve from **a**-**f** shows weight loss in the range of 15.5-54 % at temperature range of 236-664 °C, third and fourth curve from compound **a**-**e** and **d** show weight loss in the range of 3.1-50.3 % and 13 %, which are attributed to decomposition of all the ligands and leaving 12.3-33.9 % as their final residues, which are well matched with the calculated residues (NiO, CuO, ZnO, 2NiO, Cu_3N and metallic zinc). The degradation temperatures ranges and weight loss of coordination polymers are given in Table 3.6. In this series the coordination polymers **e** (large amount of residue left) and **d** (due to high degradation temperature of 477-664 °C) are the most stable compounds.

On the other hand, the TG curve for piperazine series; **i**, **k** show two steps, **h**, **l** three steps and **g**, **j** show four steps degradation profile, respectively. As obvious from Table.3.6 the initial weight loss (3.5-16 %) of complexes **g**, **h**, **j**, and **l** was attributed to removal of water molecules at temperatures range of 90-293 °C while in **i** and **k** the initial temperatures range of 181-410 °C show the weight loss from 32 to 37 % which were corresponds to the loss of organic linkers. In piperazine series, compound **k** is more stable than the other compounds due to high thermal degradation temperature (640 °C). Moreover, in piperazine series the decomposition starts at temperature range of 167-640 °C was due to loss of all organic contents and ligands that give abrupt weight reduction of 63-89 % and leaving behind 11.95- 37 % as their final residues, which were correspond to NiO, 2Cu(II), ZnO, 2 Ni(II), Cu_3N and 2 Zn(II).

From the results it was found that the thermal stability of coordination polymers was affected by the ligands, linkers, and central metal atom. As obvious from the Table 3.6 that the compounds containing piperazine (ligand), comparatively more stable than benzylimiazole based compounds because piperazine is more thermally stable (degradation temperature 106 °C) then benzylimdazole (degradation temperature 71

°C). On the other hand, in case of linker, the coordination polymers containing adipic acid are thermally more stable than those containing terephthalic acid because in most of the synthesized compounds adipic acid is present in bidentate (two site attached with metal ion) form, while terephthalic acid is present in monodentate (one site attached with metal ion) form, which are also justified by IR results. Thus, adipic acid is more strongly attached to metal ion and requires more energy for degradation. Furthermore, metal ion also effects the thermal stability of synthesized coordination polymers. As we observed that copper containing compounds with bidentate adipic acid have high thermal stability then Ni and Zn containing compounds because Cu has d^9 system which make strong bond with bidentate linker while Ni and Zn has d^8 and d^{10} system which make comparatively weak bond with bidentate adipic acid.

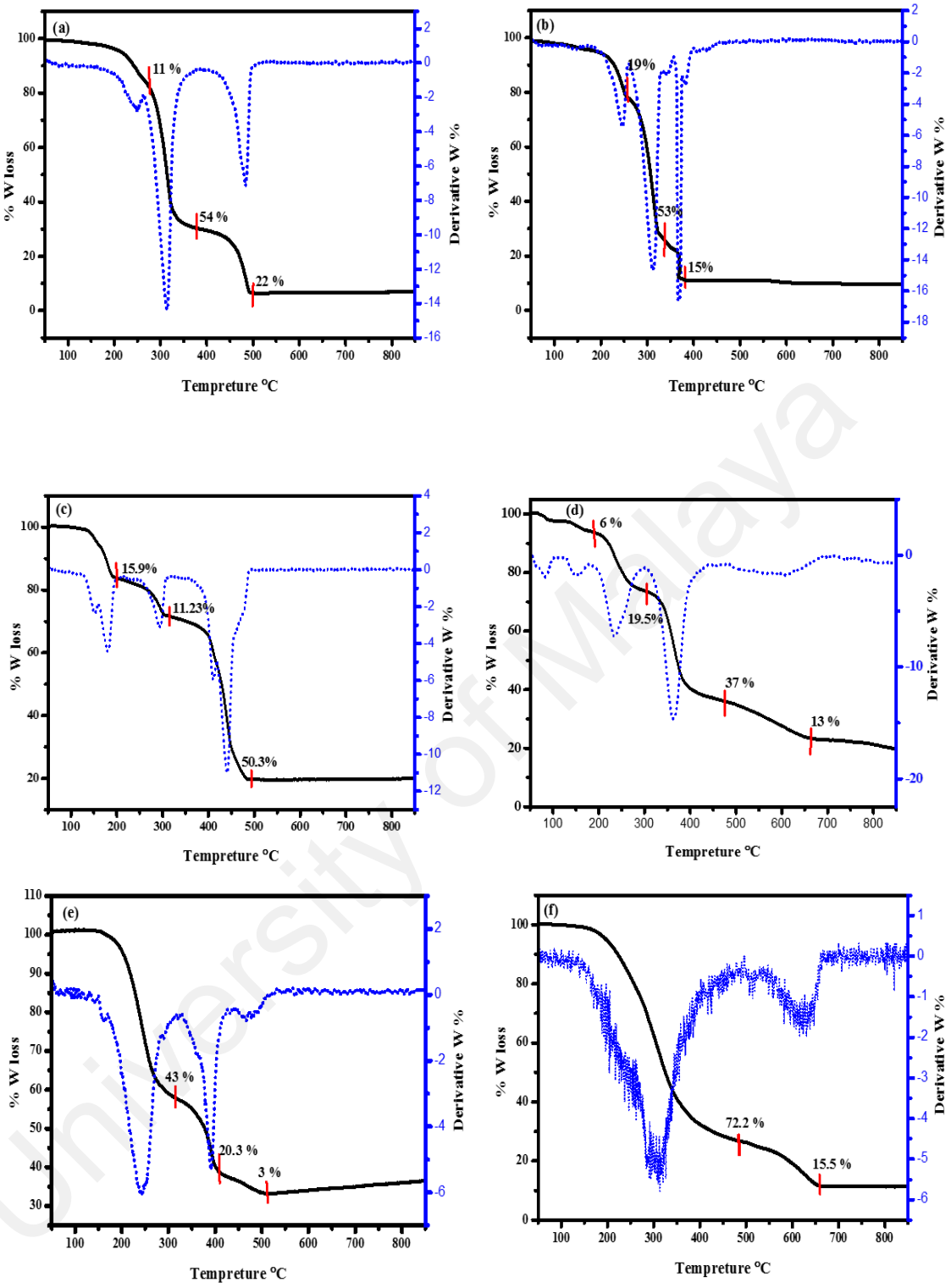

Figure 3.7: TGA thermograms for benzylimidazole series (a), (b), (c), (d), (e), (f).

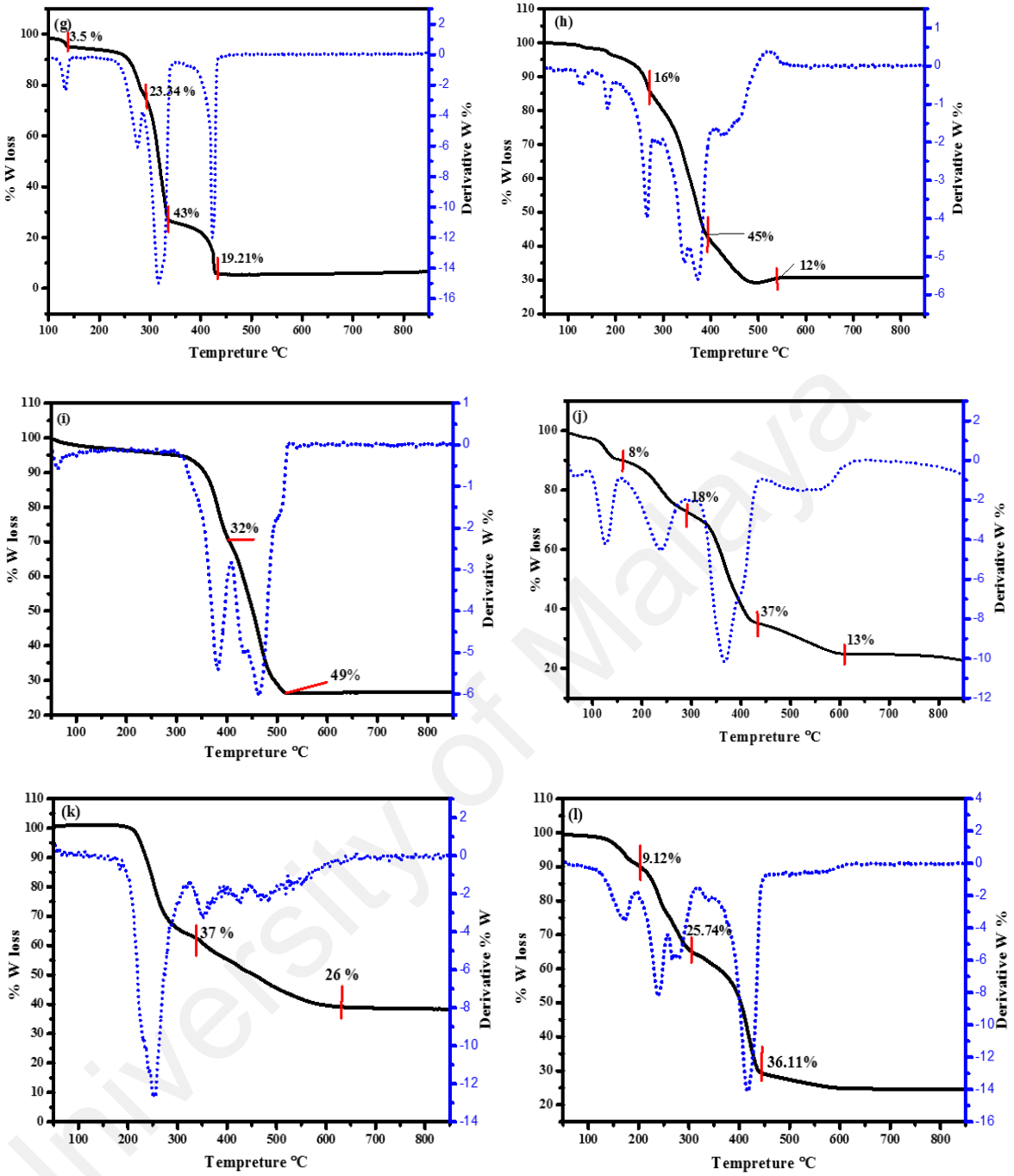

Figure 3.8: TGA thermograms for piperazine series (g), (h), (i), (j), (k), (l).

Table 3.6: TGA temperature range and decomposition steps for benzylimidazole and piperazine based coordination polymers.

Coordination polymers	Decomposition Range		Weight of remaining residue Exp, (Calc) (%)	Expected residues
	Temperature range (°C)	Weight loss (%)		
(**a**)	197-271 272-388 411-530	11 54 22	13 (12.8)	NiO
(**b**)	190-262 263-335 356-408	19 53 15	13 (13.3)	CuO
(**c**)	103-218. 240-327 368-509	15.9 10.23 50.3	23.57 (23.87)	ZnO
(**d**)	71-190 191-306 307-476 477-664	6 19.5 37 13	25.5 (26)	2 NiO
(**e**)	131-318 330-415 448-505	43 20.8 3.1	33.9 (34.7)	Cu_3N
(**f**)	106-473 528-655	72.2 15.5	12.3 (11.2)	metallic zinc
(**g**)	116-151 236-286 287-346 347–433	3.5 23.34 42 19.21	11.95 (12.6)	NiO
(**h**)	100-293 295-415 418-558	16 45 12	25 (24)	2 Cu(II)
(**i**)	274-410 411-500	32 49	19 (17.4)	ZnO
(**j**)	90-160 167-298 301-450 450-621	8 18 37 12	24 (24.5)	2 Ni(II)
(**k**)	181-336 337-640	37 26	37 (37)	Cu_3N
(**l**)	150-200 201-263 264-440	9.12 25.74 36.11	29.03 (30.6)	2 Zn(II)

3.1.6 BET analysis and morphology of coordination polymers

Figure 3.9 and 3.10 display the nitrogen adsorption desorption isotherms of synthesized benzylimidazole and piperazine based coordination polymers to investigate their pore size, surface area and pore volume**.** Table 3.7 represents the BET results for both series. It is found from the Table 3.7 that piperazine based coordination polymers have pore size in the range of 116.26-361.57 Å with BET surface area in the range of 0.62-9.50 m^2/g, while benzylimidazole based coordination polymers have pore size of 20.70-193.14 Å with BET surface area of 0.90-5.37 m^2/g. It can be seen from the results that the coordination polymer AP-Ni-CP (**j**) has highest pore size among both series and the SEM images of AP-Ni-CP are display in Figure 3.11 (a- d) which showed that AP-Ni-CP (**j**) has irregular plate like shape and has distinctive pores in the structure.

From the BET results of both series we observe that there is a big change in the pore size of coordination polymers and it was found that the pore size was also effected by ligand, linker and metal ion of coordination polymers. The tabulated results shows that piperazine based coordination polymers have high pore size compared to benzylimidazole based coordination polymers because the insertion of piperazine in the coordination compounds brings more balanced porosity compared to other aromatic ring ligands (Zhang *et al*., 2017; Sachdev *et al.,* 2016; Mowat *et al*., 2009) and in the structure of piperazine suppose two sites are available for attachment, one with metal ion and second to continue the polymeric chain while in case of benzyimidazole only one site (N atom) is available, which attached with metal ion and there is no further site available to continue the polymer chain. Thus, piperazine makes more porous structure then benzylimidazole. Moreover, in case of linker, adipic acid containing compounds have comparatively high pore size then terephthalic acid because adipic acid is non rigid aliphatic dicarboxylate and terephthalic acid is rigid aromatic dicarboxyltes (Kaskel, 2002). So adipic acid brings more porosity in the compounds due to the flexible and

bending nature of its structure while terephathlic acid has fixed and non-bending structure, which decrease the porosity of compounds.

In addition, the metal ion (Ni(II), Cu(II), Zn(II)) also play an important role in the pore size of coordination polymers. The result shows that the pore size of Ni (II) and Cu (II) compounds are higher than Zn (II) compounds in the series of coordination polymers having same linker and ligand and this is due the geometry of compound which arise from metal ion such as in case of Ni and Cu the geometry is octahedral while in zinc compounds mostly the geometry is tetrahedral, which effect the porosity of compound (Schoedel & Yaghi, 2016).

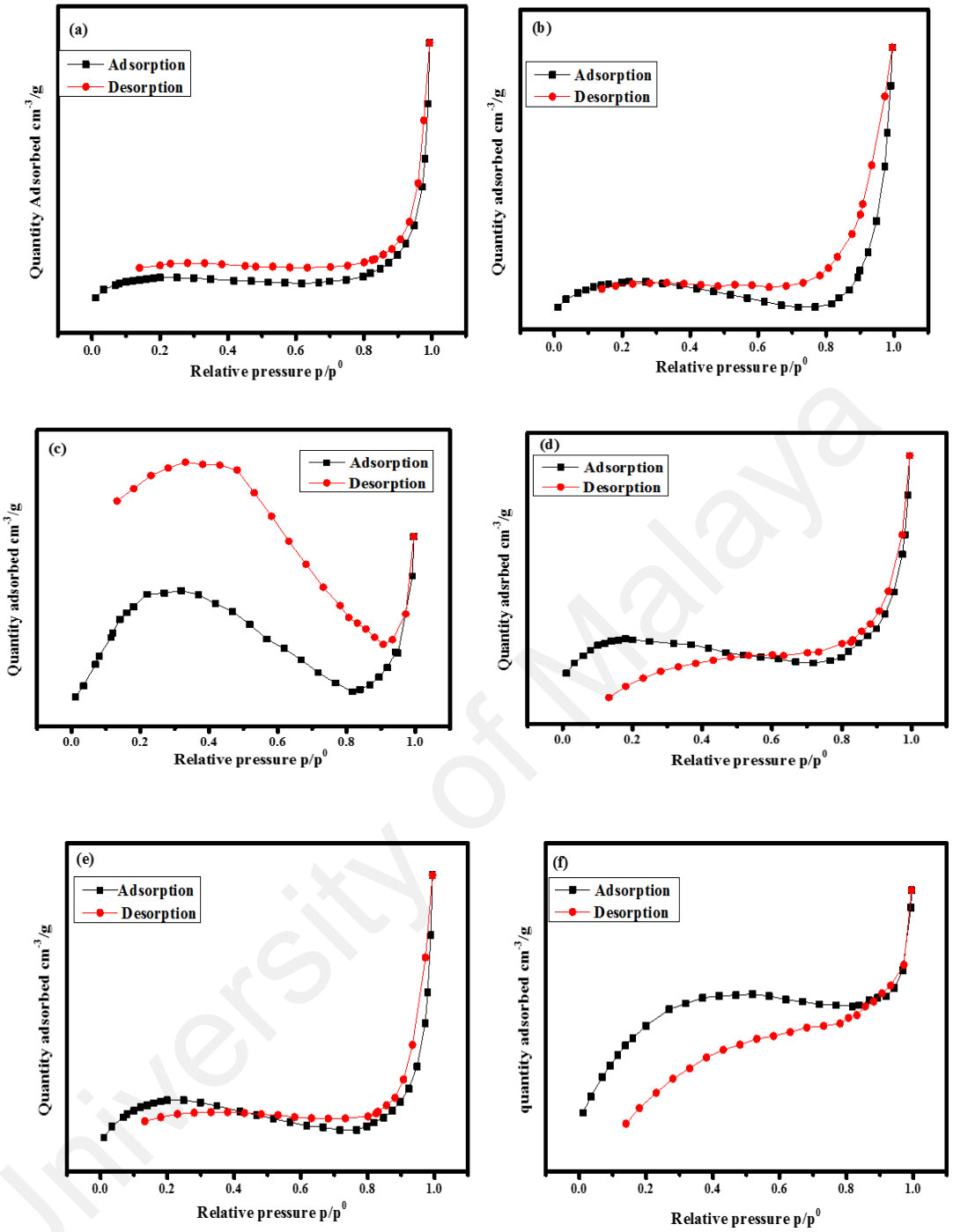

Figure 3.9: Nitrogen adsorption –desorption isotherm for benylimidazole series coordination polymers.

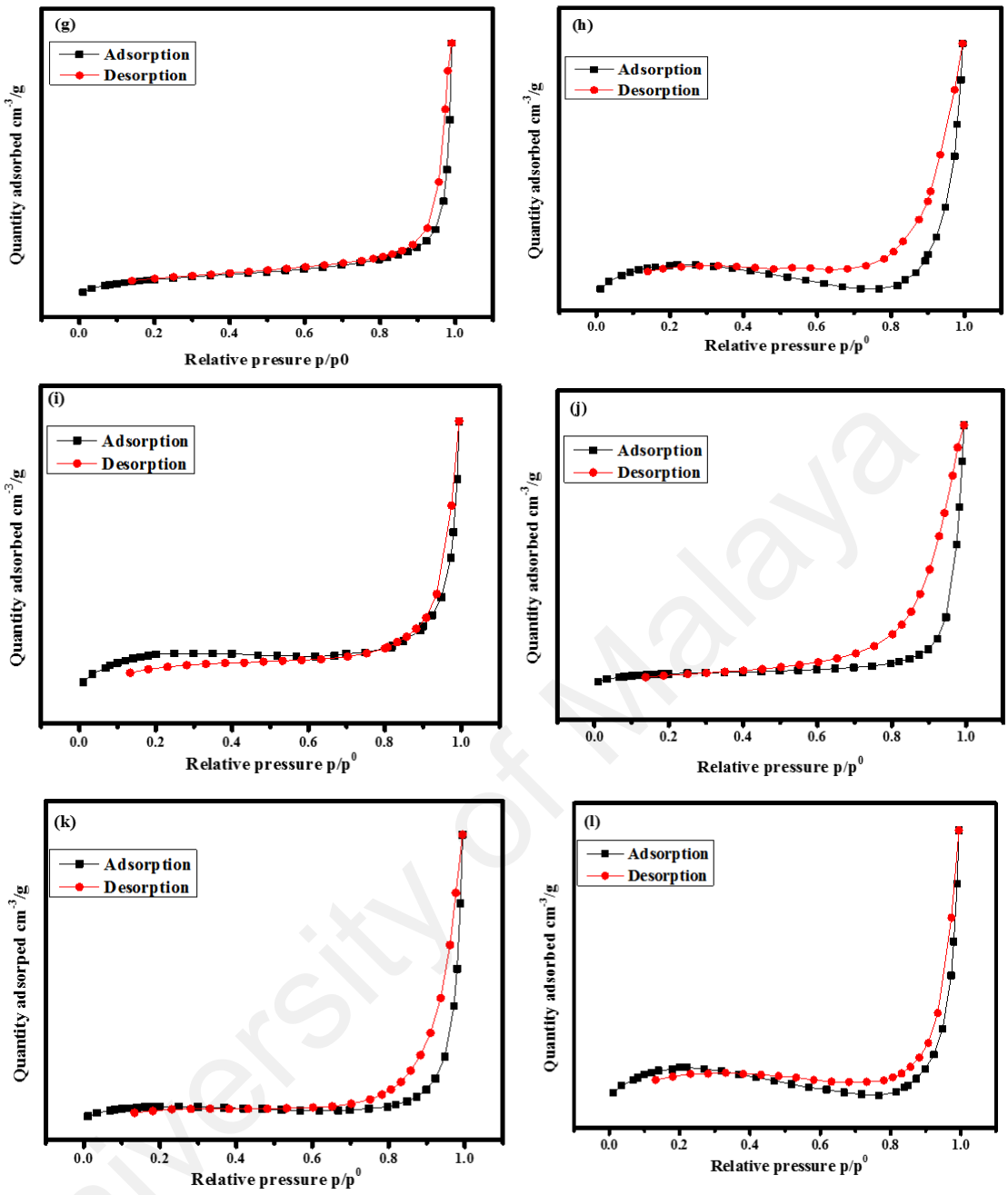

Figure 3.10: Nitrogen adsorption –desorption isotherm for piperazine series coordination polymers.

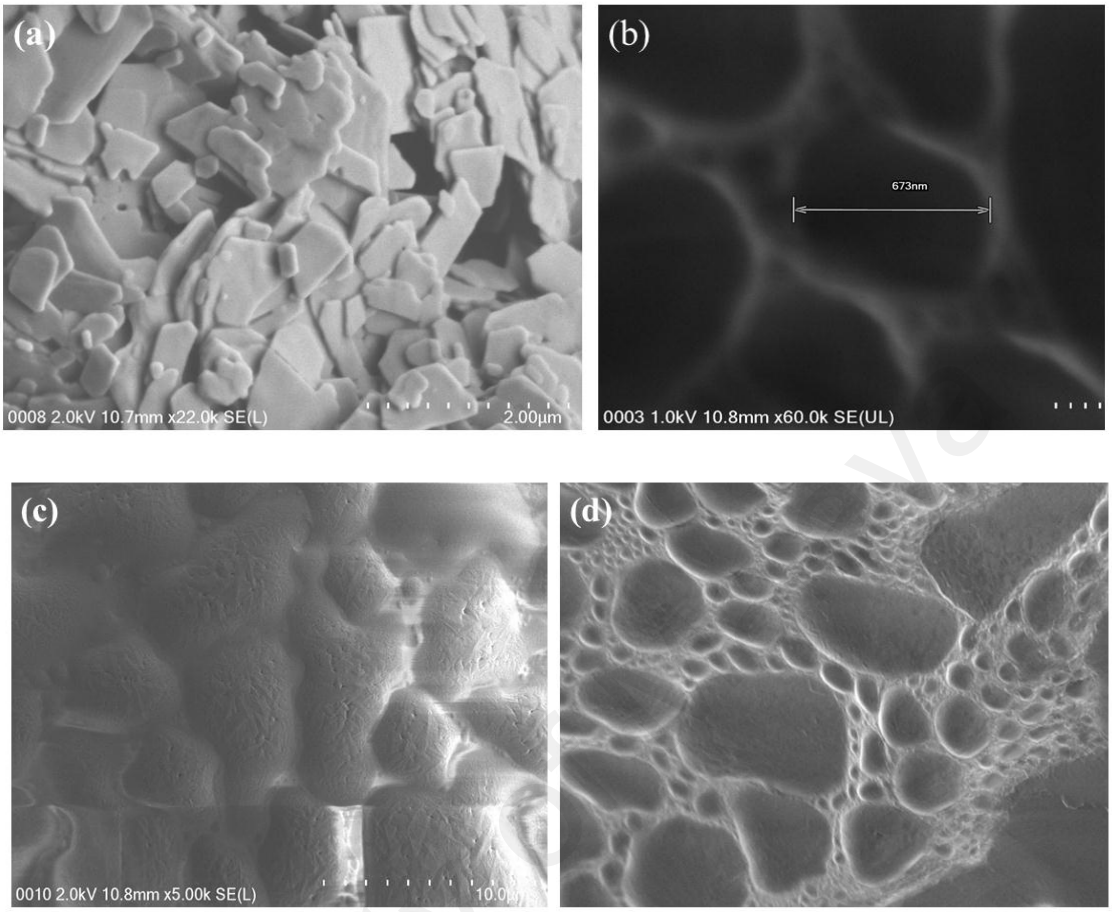

Figure 3.11: SEM images of AP-Ni-CP (a) solid structure morphology (b, c, d) different morphology of porous structure.

Table 3.7: BET surface area analysis of coordination polymers.

Types of coordination polymers.	BET surface area (m^2/g)	BET pore size (Å)	BET Volume (cm^3/g)
AP-Ni-CP	2.56	361.57	0.02
AP-Cu-CP	1.55	303.25	0.01
TP-Ni-CP	9.50	250.14	0.05
TBim-Ni-CP	5.37	193.14	0.02
TP-Cu-CP	1.40	135.92	0.004
AP-Zn-CP	1.40	134.32	0.68
TP-Zn-CP	0.62	116.26	0.001
ABim-Ni-CP	0.62	109.52	0.006
ABim-Cu-CP	2.49	87.53	0.002
TBim-Cu-CP	1.31	80.51	0.002
ABim-Zn-CP	1.31	25.78	0.001
TBim-Zn-CP	0.90	20.70	0.004

3.2 Electrochemical studies

This electrochemical part is further divided into three sub parts. First part introduces the electrochemical characterization of coordination polymers, second part discussed the conductivity of the synthesized compounds and the third part gives a brief discussion of electrochemical detection of hydrogen peroxide by AP-Ni-CP/CPE.

3.2.1 Electrochemical characterization of coordination polymers

Ferricyanide is one of the widely used redox active specie to increase the solutions redox potential in physiological experiments (Jiao *et al*., 2016). It also has an important role as an electrode transfer mediator and as a potential standard. It can be used to determine electrode areas and to detect the problems related with new electrochemical cell design. Ferricyande, as a redox couple, has good electrochemical reversibility and known to be good behaved both electrochemically and chemically. Moreover, it is also used as a model system in electrochemical experiments (Niranjana

et al., 2009) and also internal potential standard in many electrochemical reaction (Behadon *et al.,* 2013).

Carbon paste electrodes (CPEs) are being prepared from a non-conductive binder and graphite powder with specific mixing ratio (Kachoosangi *et al*., 2007). The CPEs are favoured due to low background, current, wide potential window and low costs. Different types of materials can be mixed easily with CPEs and their modified forms have been widely applied in electrochemical processes (Rubianes & Rivas, 2003). Nowadays various studies focused on chemically modified electrodes due to their significant advantages (Nezamzadeh-Ejhieh & Hashemi, 2012). Applications and properties of CPEs modified with zeolites and coordination polymers have attracted much attention due to its easy fabrication and good stability (Nezamzadeh-Ejhieh & Esmaeilian, 2012).

In this study, we applied piperazine and benzylimidazole based coordination polymers modified carbon paste electrode to study the electrochemical behaviour of $Fe(CN)_6^{4-}/Fe(CN)_6^{3-}$. The piperazine and benzylimdazole based coordination polymers are new type of materials, which have π bonds in the structure, potentially allowing for fast electron transfer, electrolyte diffusion, and excellent electrolyte penetrability during the electrochemical reaction process, and therefore showing high electrochemical performance towards ferricyanide.

Table 3.8 summaries the results of electrochemical study of benzylimidazole and piperazine based CPs/CPE. The electrochemical of electrode-electrolyte interface were studied by CV in 0.1 M KCl solution at various scan rate (0.01-0.5 mV) using benzylimidazole based CPs/CPE (Figure. 3.12 (A**)** a-f) and piperazine based CPs/CPE (Figure. 3.13 (A**)** g-l) for 10 mM $[Fe(CN)_6]^{3-}$ containing 0.1 M KCl solution at various scan rate (υ) (0.01-0.5 mV). It was observed that bare CPE electrode (Figure 3.12 B (a-

f**)** & 3.13 B (g-l)) showed no electrochemical response while in the presence of CPs/CPE show typical redox peaks for ferricyanide. The plots of anodic peak current (i_{pa}) and cathodic peak current (i_{pc}) as a function of square root of scan rate are presented in Figure. 3.12 C (a-f) & 3.13 C (g-l). There are two redox couples (**1**, **2**) appeared in the CV of ferricyanide, at nickel based CPs/CPE (Figure 3.12 A (a), A (d) and Figure 3.13 A (g), A (j)) where peak **1** represents the electrochemical event of $[Fe(CN)_6]^{3-/4-}$ in the range of 0.2-0.8 (Yuan *et al*., 2015) and the peak **2,** which appear in the range of -0.2 to 0.4 V represents the redox reaction of Ni(II) and Ni(0) (Gale *et al*., 1979). Furthermore, the CV of ferricyanide at copper and zinc containing CPs/CPE (Figure 3.12 A (b), A (c), A (e), A (f) and Figure 3.13 A (h), A (i), A (k), A (l)) shows only one redox couple peak appear, which corresponds to ferricyanide (in the range of 0-0.4 V). The Cu and Zn has a d^9, d^{10} system which make it difficult to undergo redox reaction. The peak current ratio of the anodic and cathodic scan of ferricyanide at CPs/CPE was close to unity (i_{pa}/i_{pc}=1) and peak potential separation (E_{pc}-E_{pa}) were in the range of 570-300 mV. The results show that $[Fe(CN)_6]^{3-}$ undergoes a linear diffusion controlled process at CP/CPE. It means that this redox active specie showed diffusional behaviour at CP/CPE and the reversibility of carbon paste electrode for ferricyanide was strengthened due the presence of coordination polymers (Li *et al*., 2013). The redox couple of $[Fe(CN)_6]^{3-/4-}$ are represented as below:

$$[Fe(CN)_6]^{3-} + e^- \rightleftharpoons [Fe(CN)_6]^{4-} \qquad \text{Eq. (3.1)}$$

Where e^- is the exchanged electron.

The peak current for a reversible process obeys Randles Sevick equation (Eq. 3.2), which is used for determination of diffusion coefficient (D) (Comminges *et al*., 2006; Zuman, 1970). Randles Sevick equation state that mass transfer occurs only by a diffusion process in which i_{pa} and i_{pc} are proportional to $\upsilon^{1/2}$. Diffusion coefficient can

be define as the mass of the substance diffuses through a unit surface in a unit time at a concentration gradient of unity.

$$i_p = (2.69*10^5)\, n^{3/2} A C D^{1/2} \upsilon^{1/2} \qquad \text{Eq. (3.2)}$$

Where i_p is the peak current (A), n is the number of electrons transfer during redox process, A is the electrode area (cm^2), D is the diffusion coefficient of electroactive species ($cm^2\ s^{-2}$), υ is the scan rate (Vs^{-1}), C is the bulk concentration of electroactive species (mol cm^{-3}). The calculated diffusion coefficient (D) values (1.89×10^{-5}-5.96×10^{-5} $cm^2\ s^{-1}$) from the above equation for ferricyanide suggesting that the electrochemical process between $[Fe(CN)_6]^{3-}$and $[Fe(CN)_6]^{4-}$ were reversible and diffusion controlled.

Table 3.7: Electrochemical study of coordination polymers.

Types of coordination polymers	**i_{pa}/i_{pc}**	**E=Ec-Ea**	**Diffusion coefficient (D) ($\times10^{-5}$) $cm^2\ s^{-1}$**
AP-Ni-CP (**j**)	1.07	0.57	5.96
TP-Cu-CP (**h**)	1.36	0.51	4.86
AP-Zn-CP (**l**)	1.12	0.32	3.44
AP-Cu-CP (**k**)	1.08	0.24	3.44
TP-Ni-CP (**g**)	1.08	0.78	2.66
TP-Zn-CP (**i**)	1.18	0.27	1.89
TBim-Cu-CP (**b**)	1.21	0.39	4.87
ABim-Ni-CP (**d**)	1.08	0.44	3.44
ABim-Zn-CP (**f**)	1.03	0.21	3.44
TBim-Zn-CP (**c**)	1.03	0.41	3.44
ABim-Cu-CP (**e**)	1.29	0.41	2.88
TBim-Ni-CP (**a**)	0.91	0.30	1.89

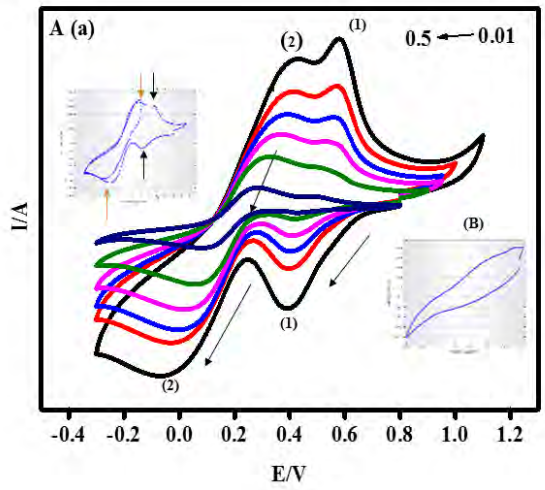

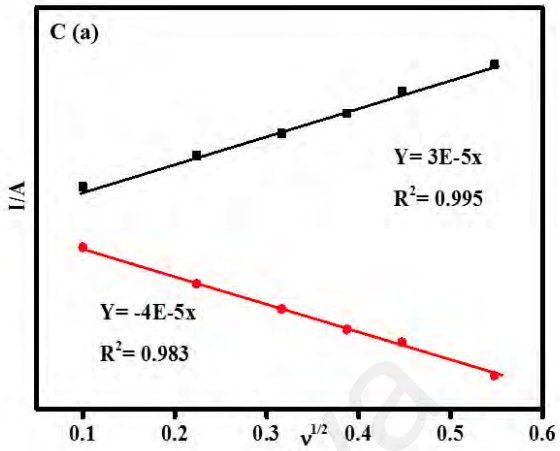

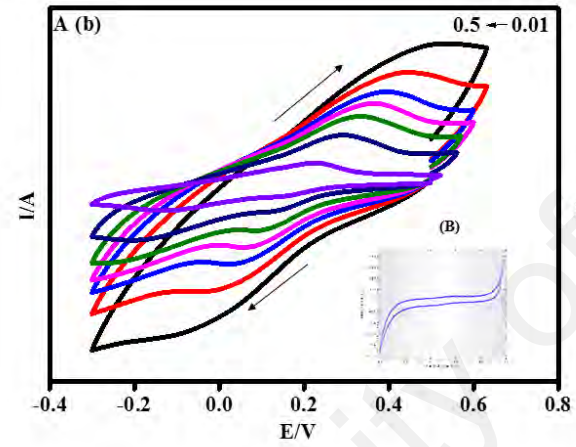

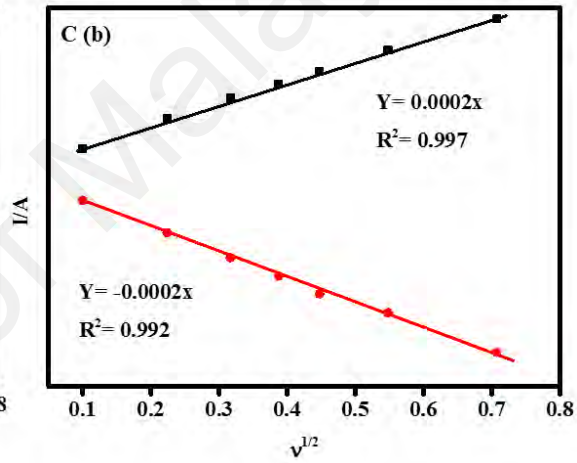

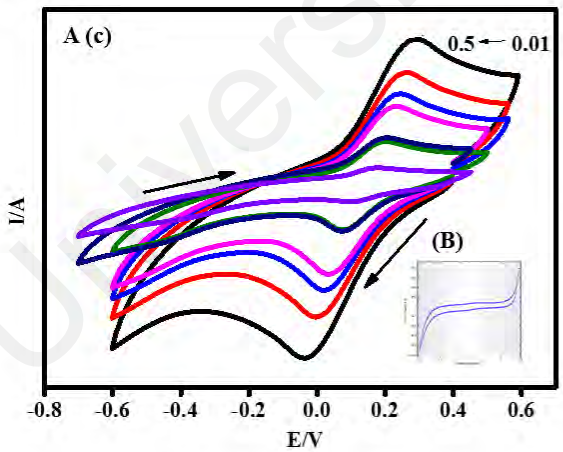

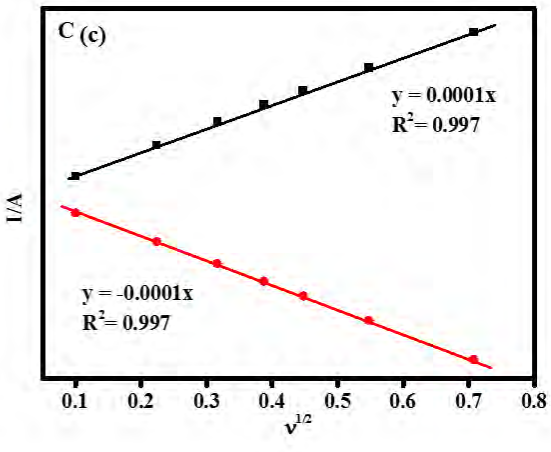

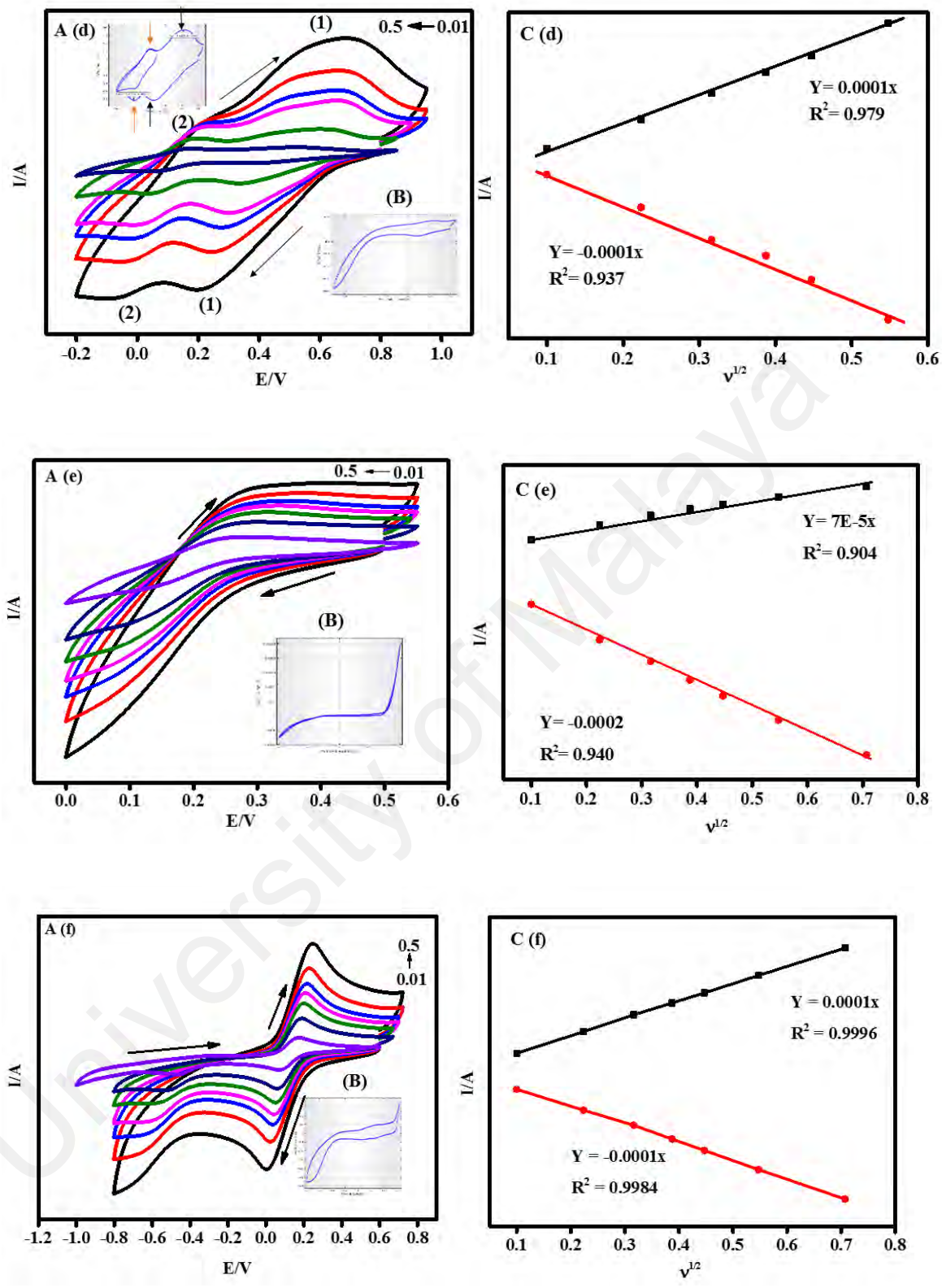

Figure 3.12: (A) (a-f) CV for $[Fe(C)_6]^{3-}$ at benzylimdazole based CPs/CPE in 0.1M KCl at different scan rate (0.01 to 0.5 mV) (B) CV for $[Fe(C)_6]^{-3}$ at CPE without CPs (C (a-f)) Plot of I_p verses $\upsilon^{1/2}$.

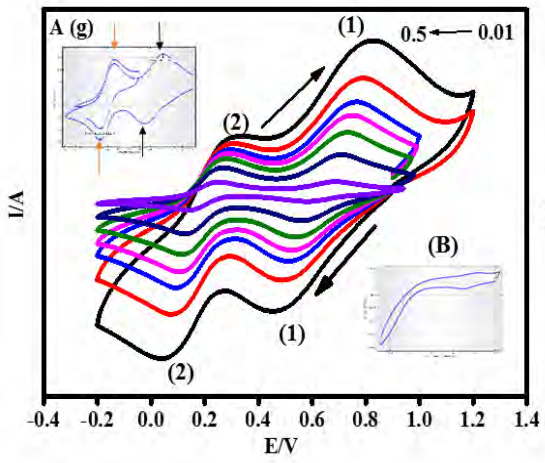

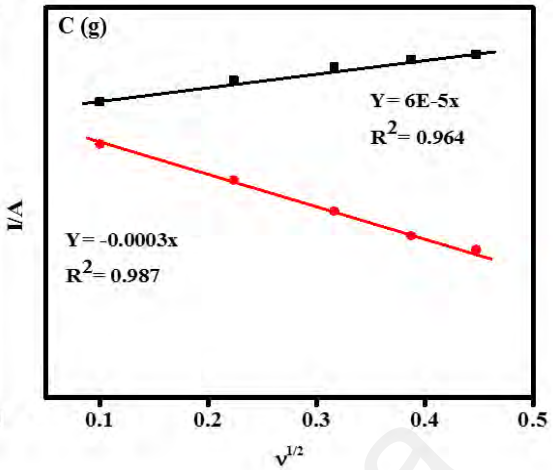

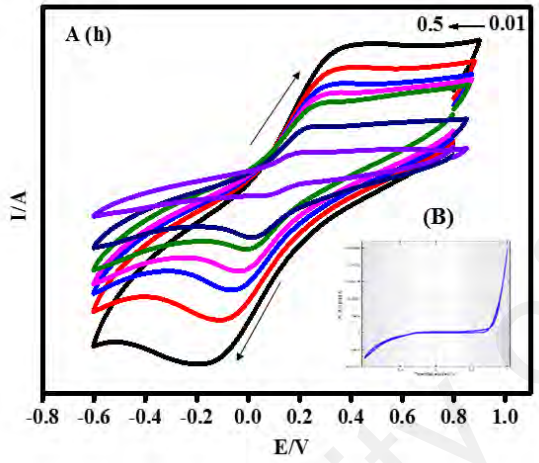

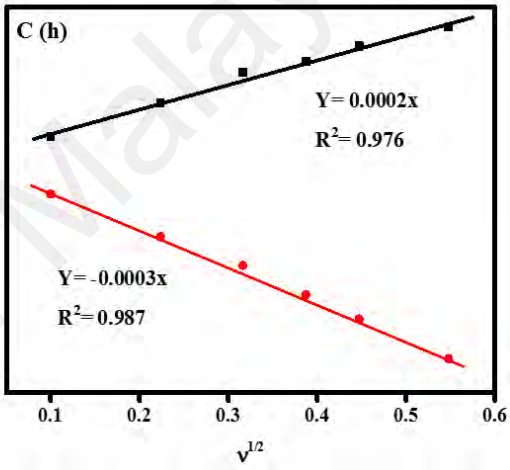

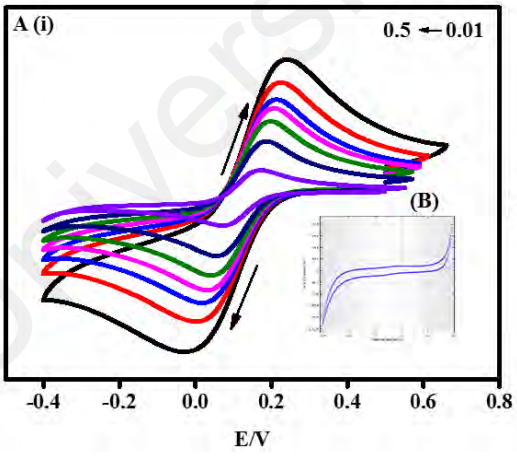

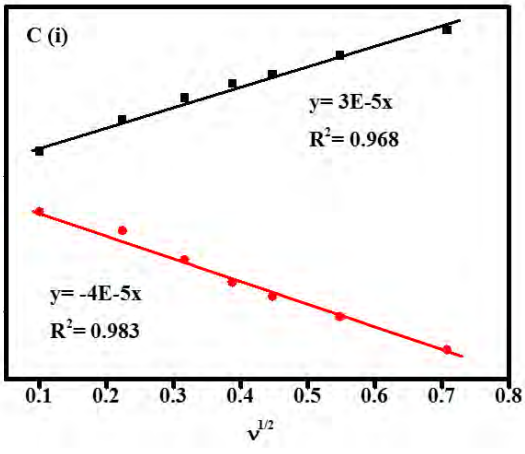

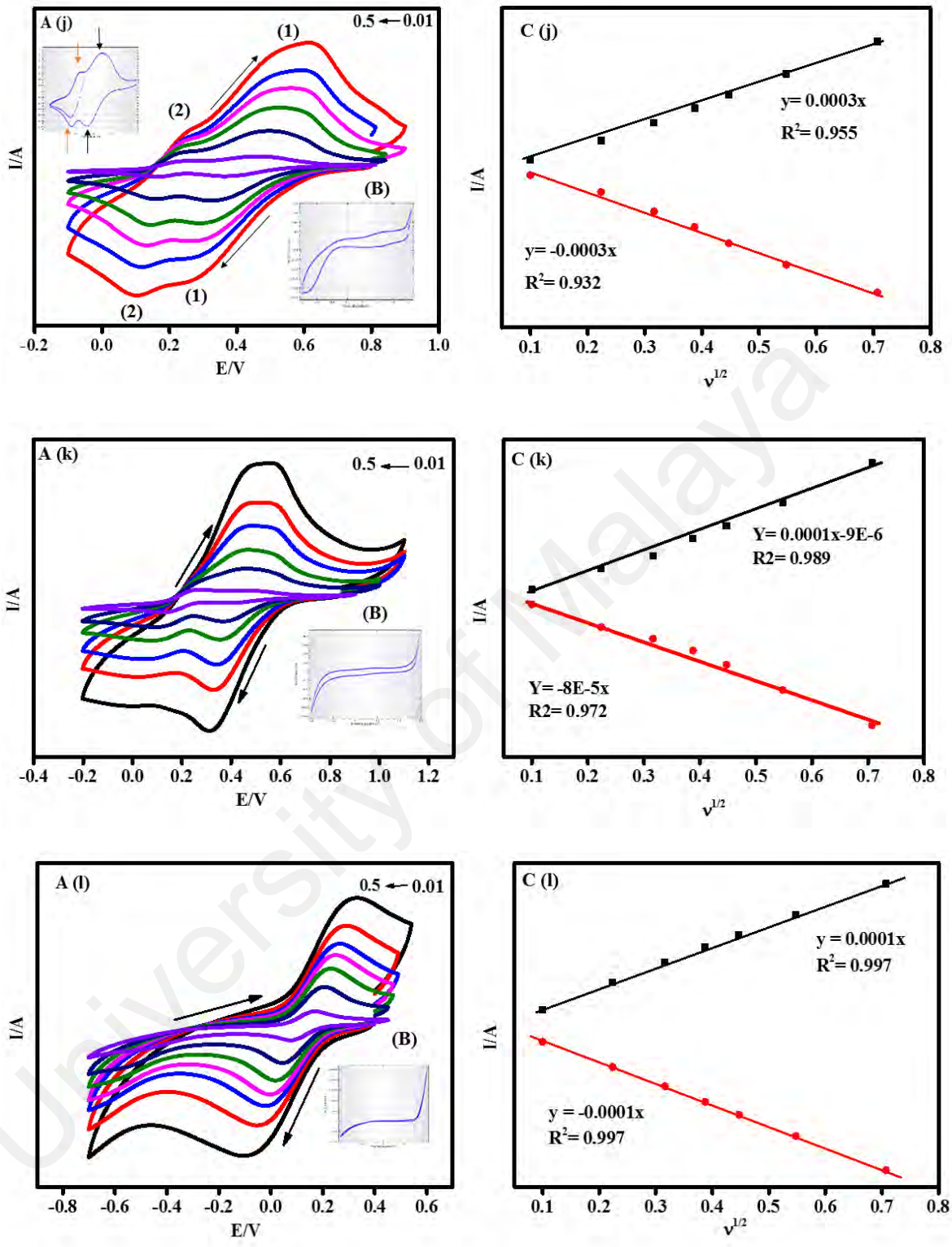

Figure 3.13: (A) (g-l) CV for $[Fe(C)_6]^{3-}$ at piperazine based CPs/CPE in 0.1M KCl at different scan rate (B) CV for $[Fe(C)_6]^{3-}$ at CPE without CPs (C (a-f)) Plot of I_p verses $\upsilon^{1/2}$.

3.2.2 Electrical Impedance spectroscopy/conductivity analysis

The conductivity of synthesized coordination polymers was studied in order to investigate their electrical properties. The conductivity (σ) of the coordination polymers were determined from the ohmic region of Cole-Cole impedance plot (Appendix C & D.) and calculated by using Eq.3.3.

$$\sigma = l/(R.A) \qquad \text{Eq. (3.3)}$$

where l is the thickness, R is the resistance of the disks, and A is the cross-sectional area of the electrodes. The calculated conductivity of synthesized coordination polymers are given in Table 3.9. The tabulated results show that the conductivity of the coordination polymers are in the range of 9.07×10^{-8}-1.28×10^{-3} S/cm. As obvious from the results that conductivity of AP-Ni-CP (1.28×10^{-3} S/cm) (Figure. 3.14) is very high among all the synthesized coordination polymers as well as with respect to the other reported coordination polymers (Table 3.10). The high conductivity of AP-Ni-CP make it as a good conducting material and having potential use in sensor applications.

It can be seen that the conductivity increases in the same range as increase in the pore size of coordination polymers, for example those compounds having high pore size, their conductivity is very high. It indicates that in more porous structure, more space is available for the conduction of electrons, so we can conclude that conductivity value is proportional to the pore size of coordination polymers.

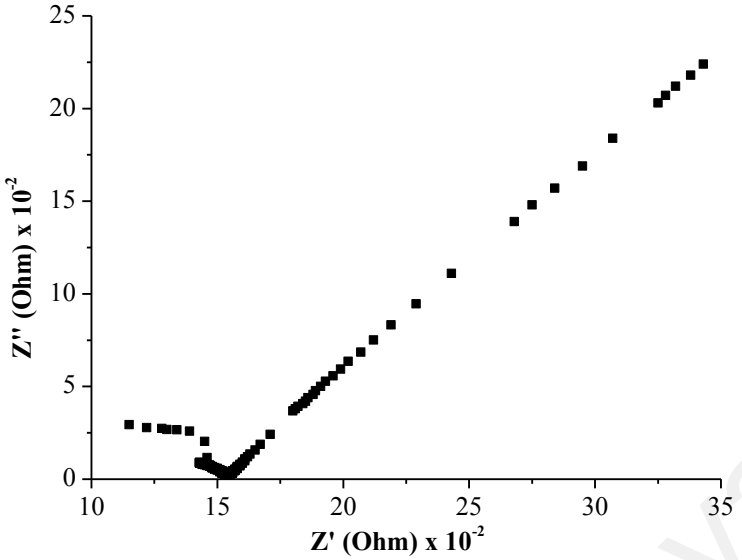

Figure 3.14 : Cole-Cole plot of AP-Ni-CP.

Table 3.8: The calculated conductivity values of coordination polymers.

S.No	Coordination polymers	Conductivity S/cm
1.	AP-Ni-CP (**j**)	1.28×10^{-03}
2.	AP-Cu-CP (**k**)	3.75×10^{-7}
3.	TP-Ni-CP (**g**)	3.02×10^{-07}
4.	TBim-Ni-CP (**a**)	2.97×10^{-07}
5.	AP-Zn-CP (**l**)	2.80×10^{-07}
6.	TP-Cu-CP (**h**)	2.28×10^{-07}
7.	TP-Zn-CP (**i**)	1.71×10^{-07}
8.	ABim-Ni-CP (**d**)	1.32×10^{-07}
9.	ABim-Cu-CP (**e**)	9.07×10^{-08}
10.	TBim-Cu-CP (**b**)	2.15×10^{-08}
11.	ABim-Zn-CP (**f**)	7.74×10^{-09}
12.	TBim-Zn-CP (**c**)	6.84×10^{-09}

Table 3.9: Comparison study of conductivity values of AP-Ni-CP with previously reported coordination polymers.

Coordination polymers	Conductivity (S/cm)	References
TMA–Ni	2.65×10^{-08}	(Sel *et al*., 2015a)
TMA-Cd	7.6×10^{-11}	(Sel *et al*., 2015)
TMA-Cu($CH_3COOH)_2$ (DIW)	4.16×10^{-10}	(Sahiner *et al*., 2014)
Cu[Cu($pdt)_2$]	6×10^{-4}	(Takaishi *et al.*, 2008)
Cu[Ni($pdt)_2$]	1×10^{-08}	(Kobayashi *et al*., 2010)
Fe_2(DSBDC)	3.9×10^{-6}	(Sun *et al*., 2015)
Mn_2(DOBDC)	2.5×10^{-12}	(Sun *et al*., 2015; Sun *et al*., 2013)
AP-Ni-MOF_	1.28×10^{-3}	This work

3.2.3 Electrochemical detection of H_2O_2

The increasing demand of hydrogen peroxide (H_2O_2) sensor were more focused in recent years due to the significance role of hydrogen peroxide in various field such as food industry, fuel cell, chemical synthesis, biotechnology, environmental, clinical and pharmaceutical application (Yang *et al*., 2015; Zhang *et al*., 2015; Hosseini *et al*., 2014). In the past decade's electrochemical biosensor based on enzymes have been greatly studied due to their high performance (Wang *et al*., 2010; Ding *et al.,* 2007). However, the enzyme based electrochemical biosensors are expensive, complicated and effected by temperature and pH due to activity of enzyme. Alternatively, non-enzymatic electrochemical sensors are attracted more attention for the determination of H_2O_2 due to long term stability, high sensitivity, pH free, quick response time and low cost (Shang & Dong, 2009; Zhao *et al*., 2009; Cai *et al*., 1995). Transition metal oxide, nobel metals, alloy and nano particles are employed as non-enzyme electrochemical sensor but their application were limited due to poor operating stability and low electronic conductivity (Heli & Pishahang, 2014; Wang *et al.,* 2014; Gu & Hasebe, 2006). In order to overcome this problems, the development of new highly sensitive, selective, fast, low cost non enzyme electrode material with the high performance for H_2O_2 detection is still needed.

Design and synthesis of different types of coordination polymers for electroanalysis application have become an interesting field of research. Literature survey clarified that coordination polymers showed attractive electrocatalytic activity towards oxidation of L-cysteine (Hosseini *et al*., 2013), methanol (Lu *et al*., 2012), hydrazine (Hosseini *et al*., 2013), oxygen reduction reaction NADH (Zhang *et al*., 2013) and H_2O_2 (Yang *et al*., 2015; Zhang *et al*., 2013).

The application of CPs as electrochemical sensor is still very rare and one of the main reason could be due to the fact that most CPs are nonconducting materials (Fateeva *et al*., 2010; De Combarieu *et al*., 2009). As a result, it is a tough challenge to fabricate a high performance sensor for H_2O_2 detection based on CPs. In order to address the above issue, we have designed a new type of nickel-based CPs (AP-Ni-CP) which have very high conductivity compared to previously reported coordination polymers (Sel *et al*., 2015; Sun *et al*., 2015; Takaishi *et al*., 2008) potentially allowing for fast electron transfer and thus showing high electrochemical performance.

Herein, we select AP-Ni-CP (**j**) as non-enzyme electrochemical sensor for the detection of H_2O_2 due to its high conductivity and diffusion coefficient value. For sensing study, AP-Ni-CP was modified with carbon paste (CP) due to its easy fabrication, renewability, good reproducibility and good stability.

3.2.3.1 The morphology and surface characteristics of AP-Ni-CP, CPE and AP-Ni-CP/CPE

The FESEM images of AP-Ni-CP, CPE and AP-Ni-CP/CPE were given in Figure 3.15 respectively. Figure 3.15a shows that AP-Ni-CP exhibited rod like structure with average length of 732 nm and 495 nm. The image of the surface of CPE was seen in Figure 3.15b, which is consist of unrecognized and isolated flake graphite with clearly distinguished layers. Moreover, the surface of AP-Ni-CP material as seen in Figure

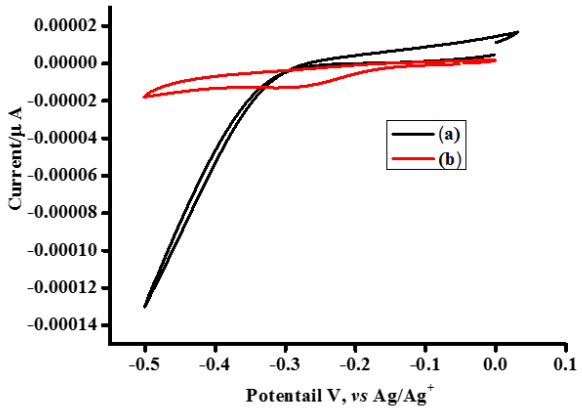

Figure 3.16: CV of 1mM H_2O_2 in the presence of 0.1M PBS at pH 7 at scan rate of 100 mVs^{-1} (a) CPE (b) AP-Ni-CP/CPE.

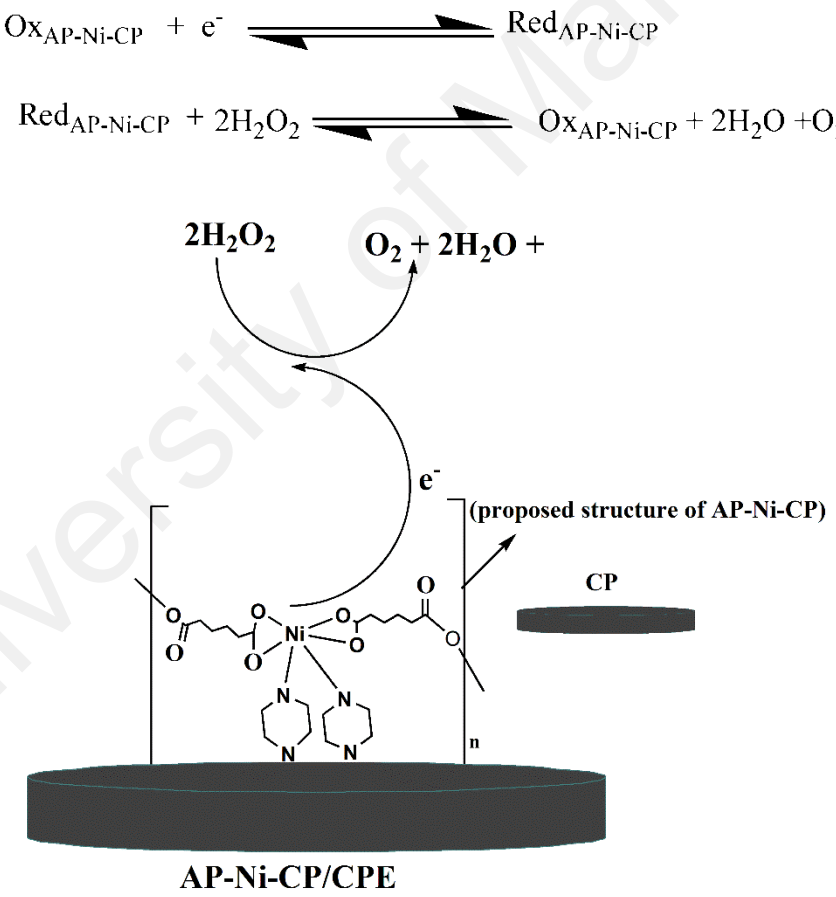

Scheme 3.1. Electroactive mechanism of AP-Ni-CP/CPE for H_2O_2.

3.2.3.3 Sensor optimization

To obtain a high performance of sensor, the effect of the amount of AP-Ni-MOF on the reduction peak current of H_2O_2 were investigated with different weight percentages of AP-Ni-CP/graphite/mineral oil based on previously reported literatures (Li *et al*., 2013; Wang *et al*., 2013). The ratio of weight percentages are (a) 2:68:30 (b) 5:65:30 (c) 17:53:30 and (d) 27:43:30. From the results, it was found that 2:68:30 showed the best signal of current toward H_2O_2 and was selected for further experiment.

Figure 3.17a displays the voltammograms of different pH ranged from 5 to 8.5 of the phosphate buffer solution (0.1 M). The reduction peak current increases steadily from pH 5 to 7. However, the effect of the pH of 0.1M phosphate buffer solution (PBS) (pH range from 5 to 8) on the reduction peak current of H_2O_2 on AP-Ni-CP/CPE electrode was studied using CV (Figure 3.17a). From pH 5 to 7 the reduction peak current increases and after pH 7 the current decreased slowly (Figure 3.17b). It is obvious from the results that pH 7 was the optimized condition for electrochemical reduction of H_2O_2. The decrease of current in alkaline solution might be related to self-degradation of H_2O_2 (Špalek *et al*., 1982). Therefore pH 7 phosphate buffer solution was used for further experiment.

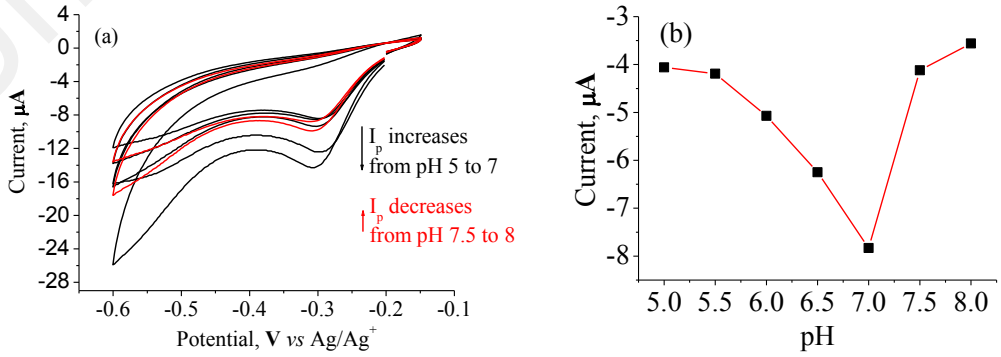

Figure 3.17: (a) CV of 1 mM H_2O_2 in 0.1 M PBS at scan rate of 0.1 Vs^{-1} on AP-Ni-CP/CPE electrode at 5 to 8 pH solutions (b) pH verses peak current.

The kinetic process at AP-Ni-CP/CPE electrode was studied by CV. The scan rate verses the electrochemical response of 1 mM H_2O_2 in 0.1 M PBS (pH 7) were recorded (Figure.3.18a). It is obvious from Figure 3.18b that there is a linear relationship between cathodic peak current intensity and square root of scan rate, indicating that reduction process of H_2O_2 at AP-Ni-CP/CPE electrode is a typical diffusion controlled reaction (Yang *et al*., 2015).

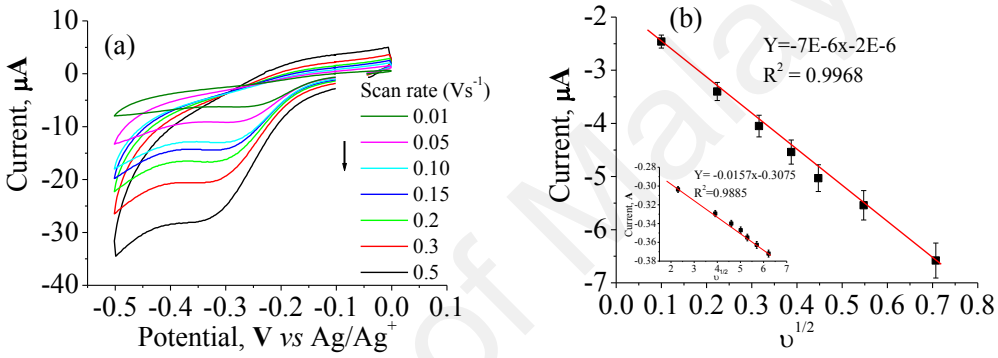

Figure 3.18: **(a)** CV of 1 mM H_2O_2 in 0.1 M PBS (pH 7) on AP-Ni-CP/CPE electrode at various scan rates (from 0.01 to 0.50 Vs^{-1}). (b) Plot of I vs $\upsilon^{1/2}$. Inset plot of E_{pc} vs ln υ. The error bar length accounts for the relative standard deviations for 3 measurements.

The sensing performance of an electrochemical sensor is usually effected by the applied potential and therefore, in this work, the applied potential was studied and optimized. The hydrodynamic voltammogramms of H_2O_2 was optimized by amperometric method as shown in Figure 3.19a. The increase of applied potential were increase the reduction peak current of H_2O_2 (line 1) and background current (line 2). Due to that reason, the alternative of current signal (hydrodynamic of signal to background ratio) was studied as shown in Figure 3.19b. The signal to background ratio measured at -0.25 V exhibited highest sensitivity for detection of H_2O_2, thus -0.25 V was selected for further experiments as an amperometric detection applied potential.

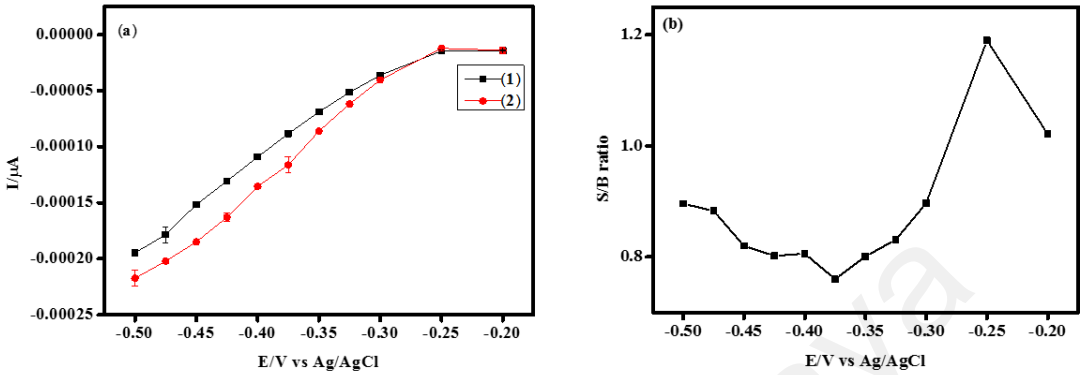

Figure 3.19: **(a)** Hydrodynamic voltammogram of 1 mM H_2O_2 (line 1), and background (line 2) in 0.1 M PBS pH 7 at 15 s sampling time measured on AP-Ni-CP/CPE and (b) hydrodynamic voltammogram of the signal-to-background ratios extracted from the data in (a).

3.2.3.4 Analytical performance of AP-Ni-CP/CPE sensor

The amperometric method were used to assess the electrocatalytic activities of AP-Ni-CP/CPE sensor due to its wide applicability and high sensitivity. The amperometric response of AP-Ni-CP/CPE to various concentration of H_2O_2 was carried out under optimum conditions. The concentration of H_2O_2 and reduction current responses were used to derive the calibration curve (Figure 3.20). The calibration curve shows a linear relationship between the reduction peak current and concentration of H_2O_2 in the wide range of 0.004-60 mM and after 60 mM saturation were started. The limit of detection was estimated to be 0.0009 mM and the limit of quantification is 0.003 mM.

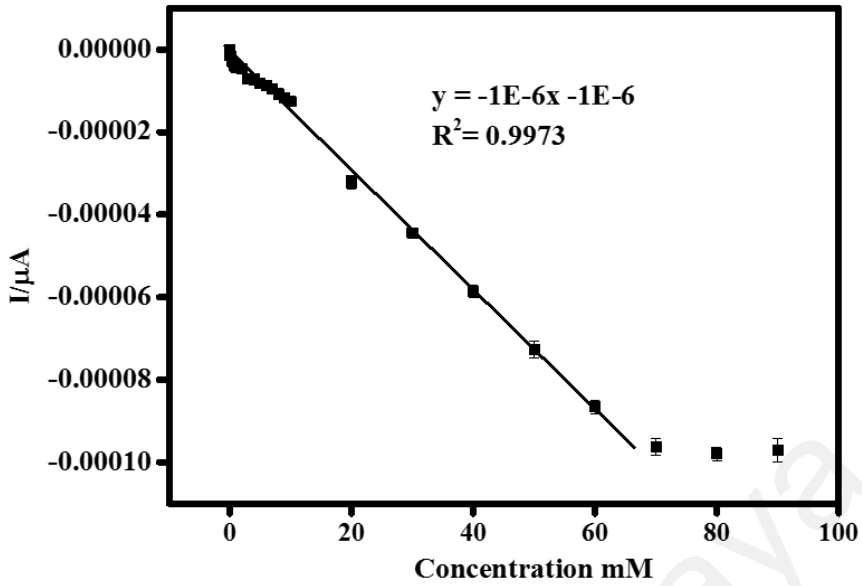

Figure 3.20: The calibration curve of amperometric response of H_2O_2 with the concentration of 0.004-60 mM. The error bar length accounts for the relative standard deviations for 3 measurements.

3.2.3.5 Interference study

In order to examine the selectivity of AP-Ni-CP/CPE towards H_2O_2, the effect of various species including glucose, urea, ascorbic acid, ethanol, Fe^{2+}, Cu^{2+}, Co^{2+}, Na^{+}, K^{+}, Ca^{2+}, Ba^{2+} and Mg^{2+} were studied on AP-Ni-CP/CPE in 0.1 M PBS (pH 7) containing 0.5 mM H_2O_2. It is obvious from the results of Table 3.10 that the change in signals of H_2O_2 has quiet negligible by all interfering species and signal changes of below 5%. Thus, AP-Ni-CP/CPE has good selectivity toward H_2O_2.

Table 3.10: The effect of some interfering species (0.5 mM) on the determination of 0.5 mM H_2O_2.

Interfering species	% Signal
Glucose	1.59
Urea	3.73
Ascorbic acid	3.19
Ethanol	0.19
Fe^{2+}	4.65
Cu^{2+}	0.07
Co^{2+}	0.22
Na^{+}	1.08
K^{+}	1.74
Ca^{2+}	1.30
Ba^{2+}	2.83
Mg^{2+}	3.26

3.2.3.6 Reversibility, Reproducibility and lifetime stability

Reversibility, reproducibility and stability of sensor are important factors in practical applications (Gupta *et al*., 2015; Jain e*t al*., 2010). The reversibility of AP-Ni-CP/CPE electrode was investigated by cyclic voltammetry. The cyclic voltamogramm of 1 mM H_2O_2 in the presence of 0.1M PBS (pH 7) at scan rate of 100 mVs^{-1} exhibit well defined reduction peak in the range of -0.3 to -0.35 V (Figure 3.21) and this peak is still retaining after reverse scans (30 cycle at the same scan rate), suggesting the reversible nature of electrode process.

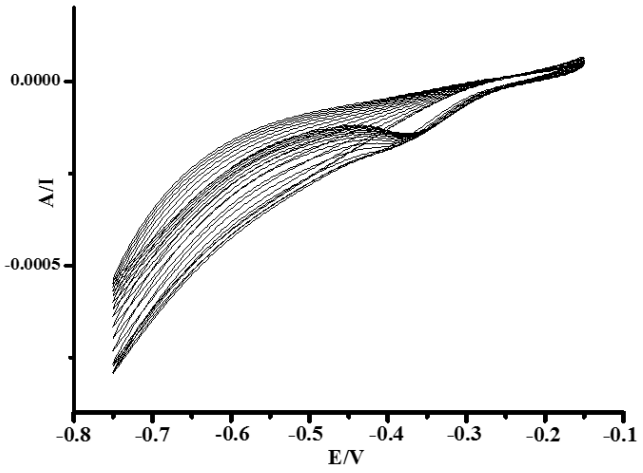

Figure 3.21. Cyclic voltamogramm (30 cycle) of 1 mM H_2O_2 in the presence of 0.1M PBS (pH 7) at scan rate of 100 mVs^{-1}.

The reproducibility and stability of the prepared AP-Ni-CP/CPE electrode were studied by amperometric response towards H_2O_2. Seven modified electrodes were prepared under optimum condition and relative standard deviation (RSD%) of the amperometric response of modified electrode toward 1 mM H_2O_2 was found to be 1.47 % after 10 consecutive days, indicating that the results can be reproducible. In addition to study the stability of AP-Ni-CP/CPE sensor, the AP-Ni-CP/CPE electrode was store in refrigerator at 4°C and the current were continuously monitored for 10 days, the sensor retained 86-97% of its initial current response after 10 days. The suggested results indicated that AP-Ni-CP have good reproducibility and stability.

3.2.3.7 Real sample analysis

In order to check the reliability of the AP-Ni-CP/CPE sensor for the detection of H_2O_2, the lens cleaning solution was used. The phosphate buffer solution (pH 7) was used to dilute the samples before measuring the current response. H_2O_2 solutions were then added to the cell by using standard addition method. The data collection was repeated four times for each sample. The average recoveries of all samples are listed in Table 3.11 The calculated relative standard deviation (RSD) values and recoveries from

Table 3.11, indicated that the as synthesized sensor has promising use in the determination of certain concentration range of H_2O_2.

Table 3.11: Determination of H_2O_2 in Real samples.

Samples	Add (mM)	Found (mM)	[n] RSD%	% Recovery
1.	0.1	0.11	1.31	107
2.	0.5	0.49	0.46	97.7
3.	1	0.96	0.35	96.1
4.	5	4.78	0.55	95.6
5.	50	47.3	4.53	94.7

[n] RSD% calculated from four measurements

3.2.3.8 Comparison of AP-Ni-CP/CPE sensor with other published H_2O_2 sensors

Comparison of the limit of detection and the linear range of synthesized AP-Ni-CP/CPE electrode with the published coordination polymers and other compounds which are used for the detection of H_2O_2 are given in Table 3.12. On the basis of this comparative study, it is found that the AP-Ni-CP/CPE electrode is able to get favourable LOD and linear range for the detection of H_2O_2.

Table 3.12: Comparative study of as prepared sensor with published sensors.

Modified electrodes	Linear range ($mmolL^{-1}$)	LOD ($\mu molL^{-1}$)	References
Cu-bipy BTC/MWCNTs/GCE	0.003-0.07	0.46	(He *et al*., 2011)
[Co(pbda)(4,4-bpy)(2H2O)]n/GCE	0.05-9	3.76	(Yang *et al*., 2015)
Cu-MOF/MPC/GCE	0.01-11.6	3.2	(Zhang *et al*., 2013)
[Cu(adp)(BIB)(H_2O)]n/GC	0.0001-0.00275	0.068	(Zhang *et al*., 2013)
$Ni(OH)_2$/ERGO.MWNT/GC	0.01-9.05	4	(Gu *et al.,* 2010)
Co_3O_4/MWCNTs/CPE	0.02-0.43	2.46	(Heli & Pishahang, 2014)
AP-Ni-CP/CPE	0.004-60	0.9	This work

3.3 Adsorption of dye studies

3.3.1 Introduction

Recently, annual utilization of more than 10000 different types of textile dyes has exceeded 7×10^5 tons (Al-Degs *et al.,* 2006; Crini, 2006). Dyes are widely used for coloring in several industries, such as pulp mill electroplating printing, paper, cosmetic, medicine, and textile, wherein huge amounts of colored wastewater is produced (Gao *et al*., 2016; Yu *et al*., 2015; Li *et al*., 2014; Kamboh *et al*., 2013; Mittal *et al*., 2007). Dyes not only influence water quality but also impact human health, including mutagenic, carcinogenic, teratogenic, and other inflammatory effects (Polak *et al*., 2016; Yap & Neuhaus, 2016; Chen *et al*., 2010). The toxicity and bio-resistivity of dyes have been comprehensively reviewed (Bedekar *et al*., 2015; Sponza, 2006; Golka *et al*., 2004). Dye are difficult to degrade because of their stability towards light and oxidation (Chen *et al*., 2011). Hence, removal of dyes from wastewater is very essential for safer environment, various methods have been reported in literature for the removal of dyestuffs (Lig *et al*., 2016; Shahabuddin *et al.*, 2016; Coasne *et al*., 2009; El-Gohary & Tawfik, 2009; El-Naas *et al*., 2009; Unuabonah *et al*., 2008). Adsorption technique is one of the competitive technologies used for dye removal and purification of colored contaminated water (Zare *et al*., 2017).

Design and synthesis of different types of CPs for the removal of dyes have become an interesting research (Hasan & Jhung, 2015). Literature survey clarified that CPs are considered attractive and optimistic adsorbents for the detoxification of dye effluents owing to their unique features, such as high surface area, high adsorption capacity, microporosity, and potentially strong interactions with dye molecules (Kligler *et al*., 2016; Lin & Lee, 2016; Liu *et al*., 2016; Jhung *et al*., 2012). Various type of CPs, such as Cr-MIL-101, PED-MIL-101, MIL-53 (Fe), MCM-41, MIL-100(Fe), MIL-

53(Al), and MOF-235, have been reported for the removal of different types of textile dyes from contaminated water (Adeyemo *et al*., 2016). Recently research attention has focused on design of new innovative and highly efficient CPs to treat dye-contaminated effluents.

The structures of adsorbents and dyes play an important role for the removal of dyes. Most of the dyes have a conjugated system, thus the coordination polymers could stabilize the dyes through π–π interactions or stacking with dyes (Hasan & Jhung, 2015). Herein, we select two oppositely charged dyes, methylene blue (cationic dye) and Chicago sky blue (anionic dye) as a main dye contaminant to evaluate the adsorption property of the synthesized coordination polymers. The effect of structure of coordination polymers on the removal of methylene blue and Chicago sky blue dye (Figure 3.22) was also investigated. The extraction behavior was explored through solid-phase adsorption (batch method) using UV–vis spectrophotometry.

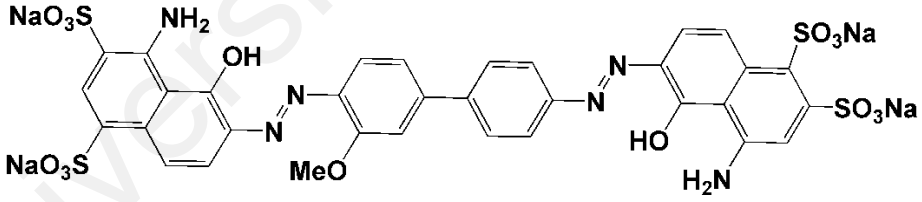

Chicago sky blue dye

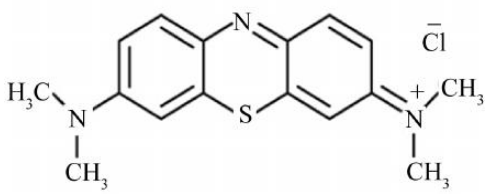

Methylene blue

Figure 3.22: Chemical structures of selected dyes used in the study.

3.3.2 Adsorption of methylene blue and Chicago sky blue by coordination polymers

The adsorption of the dyes were studied because of porous nature of coordination polymers. To assess the adsorption property of benzylimidazole and piperazine based coordination polymers, two dyes were selected, which possess different charges, cationic dye (methylene blue (MB)) and anionic dye (Chicago Sky Blue (CSB)). Figure. 3.23 depicts the screening results for the % removal of dyes by coordination polymers. It was observed that percentage removal of methylene blue is less than 50% while the percentage removal for Chicago sky blue is in the range of 65 to 95 % which is quite high compare to methylene blue. The result indicated that adsorption not only depend on the pore size of coordination polymers but also effected by the types of interactions between dye and coordination polymers. A comparative study shows that coordination polymers were more selective toward the adsorption of anionic dyes than cationic dyes because of the different types of interactions between the coordination polymer and anionic dyes (Figure. 3.24).

(a) ***Electrostatic interactions:*** Following the dissociation process in aqueous media, the Na^+ and SO_3^{-2} groups of the dyes become positively and negatively charged, respectively. In this situation, the lone-pair electron of the nitrogen atom in the piperzine/imidazole ring in coordination polymers forms an attractive interaction with the positive Na^+ ion.

(b) ***Metal ion interactions:*** The metal ions of coordination polymers can bind the lone pair of electrons of oxygen of the CSB molecules, and thus the dye can be extracted via metal–dye coordination.

(c) ***π–π interactions:*** CSB is a benzidine-based dye with a rich aromatic core (π–π arrangement), and the synthesized coordination polymers adsorbents also have aromatic cores (terephthalic acid units). Thus, due to the formation of π–π electron interactions, the dye is extracted.

(d) ***Hydrogen bonding:*** Hydrogen atoms of the dye molecules form hydrogen bonds with oxygen atoms of the linker present in coordination polymers, thereby extracting the dye.

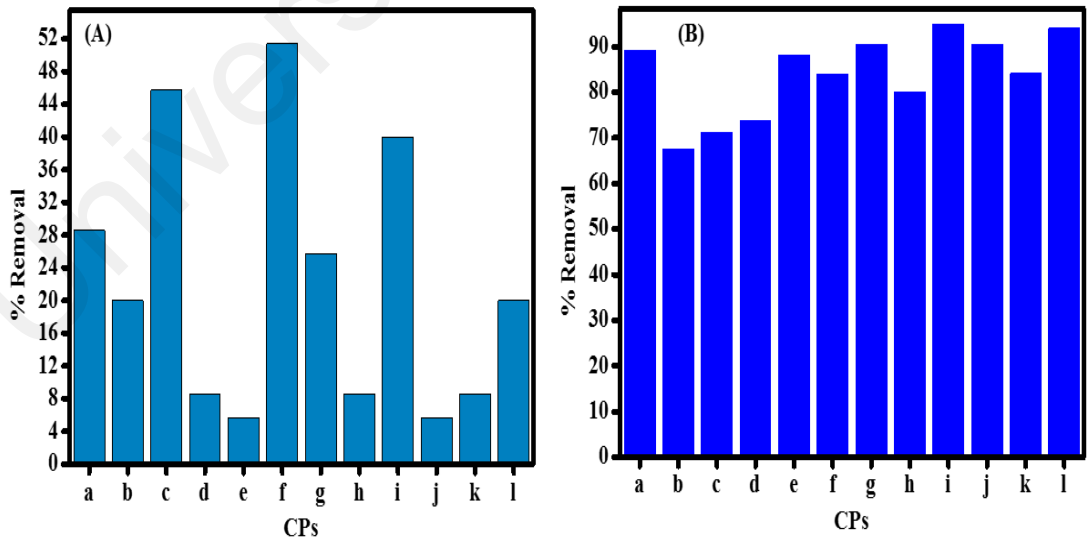

Figure 3.23:(A) % Removal of methylene blue by coordination polymers and (B) % removal of Chicago sky blue by coordination polymers.

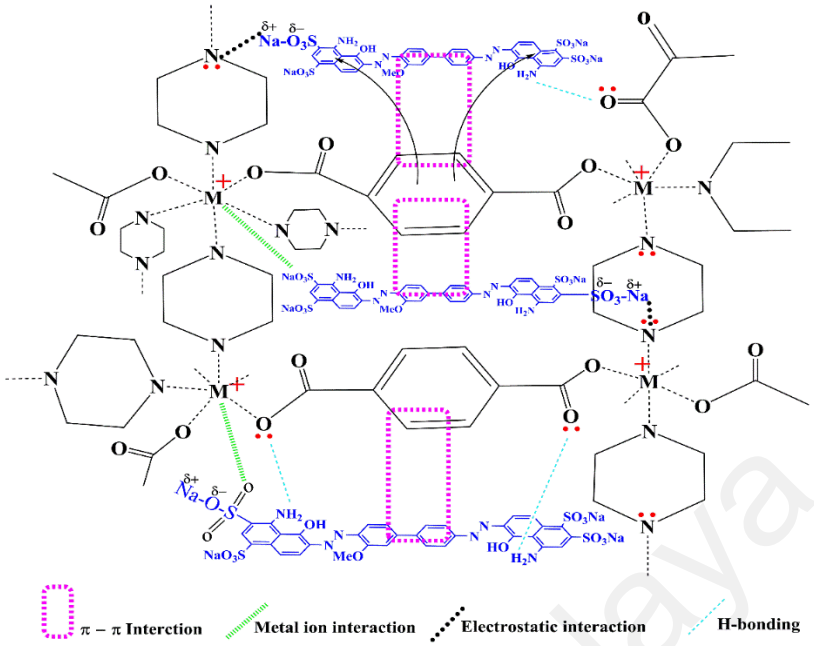

Figure 3.24: Proposed adsorption mechanism of CSB by coordination polymer.

On the other hand, in the case of methylene blue, there were also some interactions between MB and the coordination polymers because of the presence of the benzene rings, but due the repulsive interactions between cationic groups (metal ion, nitrogen atoms in CPs and nitrogen atoms in MB) decreases the adsorption of the dye.

Screening results of MB shows that all the zinc containing coordination polymers show comparatively good adsorption than Cu and Ni containing compounds because Zn has d^{10} system (which has high stability due to filled d orbital) and the repulsive force toward MB is comparatively less than Cu and Ni. That‘s why we select ABim-Zn-CP (**f**) which shows good percentage removal towards both dyes (CSB and MB) for the further adsorption studies.

3.3.3 Optimization factors affecting adsorption process

For the quantitative removal of CSB and MB dye, different parameters were optimized (i.e., adsorbent dosage, pH solution, adsorption time as well as CSB and MB concentration).

3.3.3.1 Effect of the ABim-Zn-CP (f) amount on CSB and MB

The mass of ABim-Zn-CP were studied within the range of 5 to 30 mg. The result in Figure.3.25a show that the removal of CSB and MB increased with increase in content of **f**. Quantitative removal of the CSB and MB was obtained using 10 mg and 5 mg of **f** respectively. At above 10 mg and 5 mg of adsorbent, the CSB and MB removal remained nearly constant. Therefore, 10 mg and 5mg of adsorbent were used for further experiments

3.3.3.2 Effect of solution pH on the removal of CSB and MB

pH plays an important role in adsorption process because it affects the degree of ionization of the material present in the solution and the dissociation of functional groups on the active sites of the adsorbent (Kamboh *et al*., 2013). The effect of pH (4.5–10.5) on the removal of CSB and MB dye using **f** was examined. As shown in Figure.3.25b, 88 % removal of CSB dye and 64 % removal of MB dye were achieved at pH 7.5. It was found that above pH 7.5 percent removal was decrease in MB and remains constant in CSB. The adsorption mechanism of CSB and MB onto **f** depend not only on the surface charge but also depend on the types of various interactions**.** As obvious from the zeta potential value of **f** (Figure 3.26) that the surface charge on the adsorbent is less negative (more towards positive) at pH 7.5 while more negative in basic and acid pH.

The adsorption of CSB at lower pH decrease due to the presence of excess H+ ions because:

- **Competition of anionic dye and high negatively charge adsorbent:**

Competition of anionic dye and high negatively charge adsorbent toward excess of H+ ions decrease the adsorption process.

- **Repulsion between anionic dye and negatively charge surface of adsorbent**

Electrostatic force of repulsion between anionic dye and negatively charge surface of adsorbent also decrease the adsorption of dye.

Similarly, in basic pH the adsorption decrease because:

- **Repulsion between dye anion and the excess of OH^- in the solution**

The excess of OH^- increase the surface charge and negatively charged surface site on the adsorbent does not favour the adsorption of dye anions due to electrostatic repulsion thus decreases the percent removal. At pH 7.5 there was low negative charge (more toward positive) on the surface, no competition with H^+ and OH^- ion and the lone pair of oxygen of SCB dye show coordination toward adsorbent cation (metal ion), which suggests a strong metal dye interaction, Therefore, by virtue of strong metal dye interaction, the dye is extracted.

Moreover, the adsorption of MB at low pH also effected due the excess of H^+ ion because:

- **Competition between excess of H^+ ion and cationic dye:**

Competition between excess of H^+ ion and cationic dye toward adsorbent site decrease the adsorption while in high pH:

- **Competition between OH^- and surface charge of adsorbent:**

The excess of OH^- in the solution compete with the surface charge of adsorbent for the dye cation to decrease the adsorption. The maximum adsorption of MB at pH 7.5 is due the interaction of surface charge of adsorbent and dye cation and there is no competition with H^+ and OH^- ions Thus, pH 7.5 is selected as optimum pH for both dyes for further experiment.

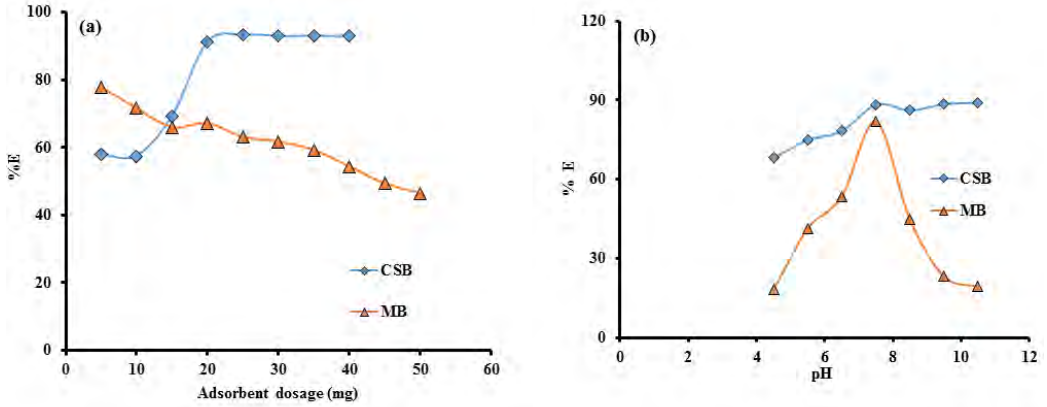

Figure 3.25: (a) Effect of content and (b) solution pH on the adsorption of CSB and MB dye.

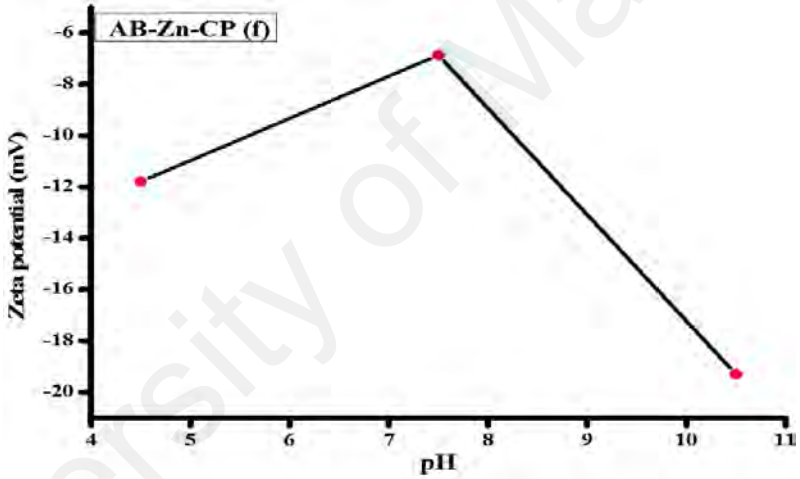

Figure 3.26: Effect of pH on the zeta potential of ABim-Zn-CP (f).

3.3.3.3 Effect of contact time and kinetic study

The effect of contact time for the removal of CSB and MB dyes were studied using **f** at different adsorption times (5 to 60 min), as shown in Figure. 3.27a. The adsorption capacity for the removal of CSB and MB increases during the first 30 min, and then remained constant afterward. Thus, 30 min was sufficient to reach to equilibrium, 30 min is selected as optimal shaking time for further experiments.

The validity of the adsorption rate of CSB onto f was investigated through kinetics models, i.e. pseudo-first-order and pseudo-second order kinetic models. The pseudo-first-order kinetic parameters were calculated using Eq. 3.4

$$ln(q_e - q_t) = ln\, q_e - k_1 t \qquad \text{Eq. (3.4)}$$

where k_1 (min^{-1}) is the adsorption rate constant, and q_e (mg g^{-1}) and q_t (mg g^{-1}) are the adsorption capacity at equilibrium time and at time *t*, respectively. The pseudo-second-order constants were calculated using Eq.3.5.

$$\frac{d_q}{d_t} = k_2(q_e - q_t)^2 \qquad \text{Eq. (3.5)}$$

where k_2 (g mg^{-1} min^{-1}) is the pseudo-second-order rate constant.

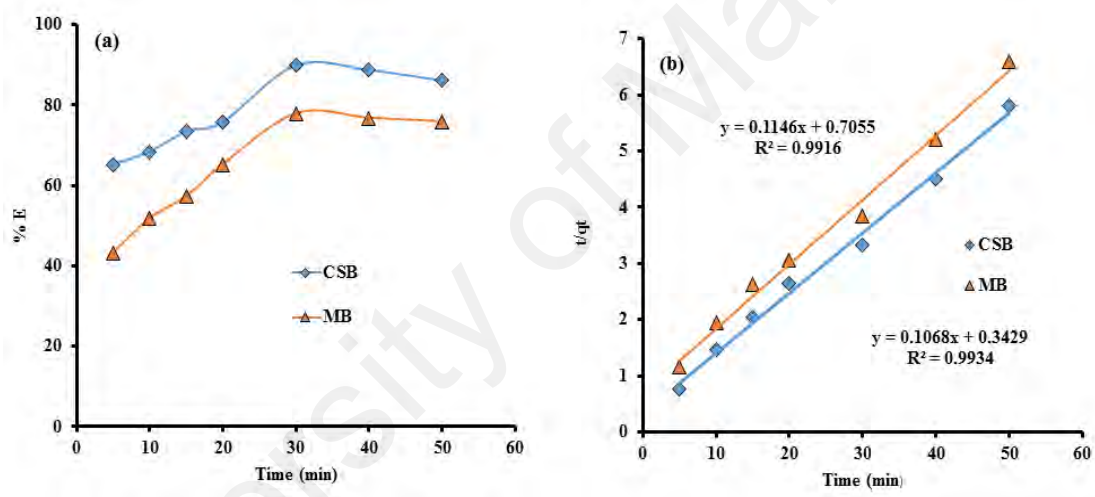

Figure 3.27: (a) Effect of contact time on adsorption capacity and (b) pseudo-second-order linear form.

The calculative parameters of both tested models are presented in Table 3.13 and Figure. 3.27 (a, b). The experimental data is well fitted in pseudo-second-order model with determination of coefficient (R^2) of 0.993 and 0.991 for both dyes. In addition, the obtained theoretical value of q_e (9.36 and 8.74 mg/g) for the pseudo-second-order model matches satisfactorily with experimental values at equilibrium time (9.00 and 7.79 mg/g). Thus, experimental data fit the pseudo-second-order model.

Table 3.13: Kinetic study, modelling constants, and coefficient of determination for CSB and MB adsorption onto **f**.

Model	Kinetic constants	**CSB**	**MB**
Pseudo-first-order	q_e(mg g^{-1})	119.6	98.4
	k_1 (min^{-1})	0.00001	0.00002
	R^2	0.813	0.790
Pseudo-second-order	q_e (mg g^{-1})	9.36	8.74
	k_2 (g mg^{-1} min^{-1})	0.3429	0.7055
	R^2	0.993	0.991

3.3.3.4 Initial concentration and adsorption isotherm

The effect of initial CSB and MB concentration on the adsorption capacity of **f** was investigated under equilibrium condition at room temperature (Figure. 3.28 (a, b)). The plot between q_e and C_e shows that adsorption capacity increase with the increase in CSB and MB concentration until the adsorbent site becomes saturated. The adsorption capacity of **f** toward CSB and MB dye were calculated using Eq. 2.9.

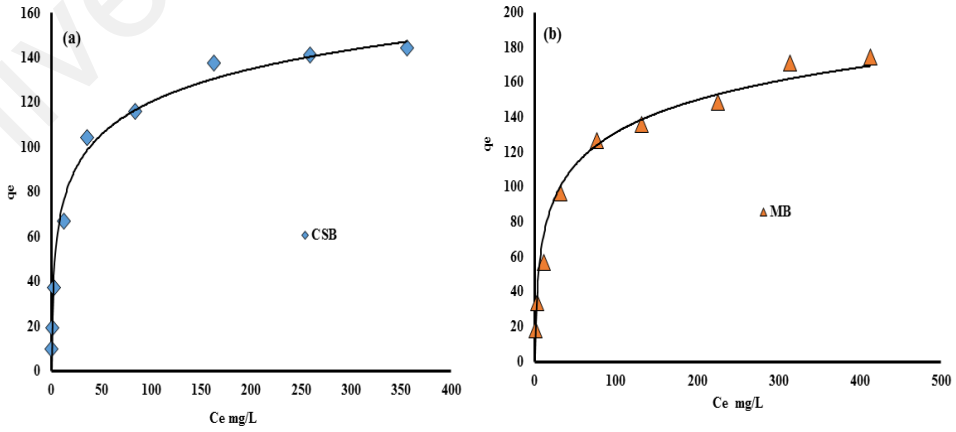

Figure 3.28: **(a)** Adsorption capacity for CSB and (b) adsorption capacity for MB.

The validity of the adsorption experiments were investigated by Langmuir and Freundlich isotherm models (Quiñones & Guiochon, 1996). The relationship between adsorption of CSB and MB dye onto **f** and the equilibrium concentrations were studied using linearized form of Eqs.3.6 and 3.7. The Langmuir and Freundlich models correspond to the monolayer and multilayer adsorption, respectively (Sa Kutsal, 1996).

$$\frac{C_e}{q_e} = \frac{C_e}{q_m} + \frac{1}{q_m} \qquad \text{Eq. (3.6)}$$

where q_e (mg g^{-1}) is the amount of CSB and MB adsorbed at equilibrium, c_e (mg L^{-1}) is the equilibrium CSB and MB concentration, and q_m (L mg^{-1}) is the Langmuir constant related to the maximum adsorption capacity.

$$lnq_e = lnK_F + \left(\frac{1}{n}\right) lnC_e \qquad \text{Eq. (3.7)}$$

where n is the dimensionless exponent of the Freundlich equation, and K_F ([(mg/L)/$(mg/g)^{1/n}$]) is the Freundlich constant related to the adsorption capacity. Comparison of R^2 values shows that adsorption of CSB and MB onto the **f** follow the Langmuir model better than Freundlich isotherm respectively. Moreover, the obtained theoretical value of q_m (144.9 and 178.5 mg/g) for the Langmuir model matches satisfactorily with experimental values at equilibrium (144.2 and 174 mg/g). The k_F values for CSB and MB were 16.5 and 17.9 respectively. The calculative parameters of both tested models are tabulated in Table 3.14 and Figure. 3.29 a, b. The applicability of Langmuir adsorption model suggests the monolayer coverage of CSB and MB on the surface of **f**.

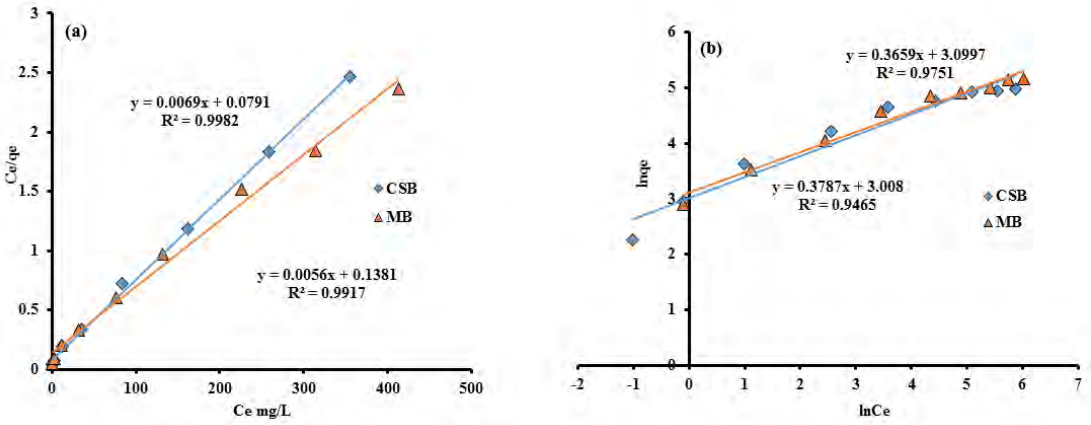

Figure 3.29: **(a)** Langmuir isotherm and (b) Freundlich plots for the adsorption of CSB and MB onto **f**.

Table 3.14: Isotherms parameters for CSB and MB adsorption onto ABim-Zn-CP **(f).**

Model	**Isotherm constant**	**CSB**	**MB**
Langmuir isotherm	q_m (mg g^{-1})	144.92	178.57
	b (L mg^{-1})	0.0872	0.4055
	R^2	0.998	0.991
Freundlich isotherm	K_F ((mg g^{-1})(L mg^{-1})$^{1/n}$)	16.50	17.98
	$1/n$ (g mg^{-1} min^{-1})	2.64	2.73
	R^2	0.975	0.946

3.3.3.5 Adsorption of mixture of dyes (CSB+MB) by ABim-Zn-CP (f)

Mixture of dyes (CSB+MB) were also study in order to further investigate the percentage removal efficiency of adsorbent (**f**) towards binary mixture of CSB and MB. For the mixture preparation we mixed both dyes with concentration of 10 ppm to make it 10 mL solution and analyzed by UV-vis spectrometer. It can be observed that mixture of dye gives its own peak at wavelength of 600 cm^{-1}, which shows that after mixing the CSB and MB dye, their properties are quite changed from the individual dye (CSB and

MB). When we added the prepared adsorbent (**f**) (10 mg) in the binary mixture (10 mL) of dyes, the removal efficiency of adsorbent (**f**) increase up to 94 %. The result indicates the synthesized adsorbent also has an excellent removal efficiency toward mixture of CSB and MB.

3.3.3.6 Real sample analysis

In order to authenticate the field application of the newly synthesized adsorbent (**f**), lake water (from University of Malaya) was analysed. 10 ppm mixture of dyes were spiked into the lake water and added 10 mg of adsorbent. It was found that the recovery in real sample is about 98 %, indicated that the synthesized adsorbent was applicable for the removal of mixture of dyes in environmental water samples.

3.3.3.7 Comparison of current adsorbent with reported materials

A comparison of the synthesized adsorbents (**f**) for the removal of carcinogenic azo dye CSB and MB with previously reported materials is given in Table 3.15. The absorption capacity of the prepared coordination polymer is comparatively higher than the other reported materials.

Table 3.15: Comparison of the adsorption capacity of carcinogenic azo dyes of the current study with several published materials

Adsorbent	**Type of Dye**	**Adsorption capacity *qe (mg/g)***	**Ref**
ABim-Zn-CP (f)	**CSB**	**144.92**	**Current study**
ABim-Zn-CP (f)	**MB**	**178.57**	**Current study**
Polymer 1 based on β cyclodextrin	CSB	7	(Yilmaz *et al*., 2010)
Polymer 2 base on β cyclodextrin	CSB	12	(Yilmaz *et al*., 2010)
p-tert-Butylcalix[4]arene	CSB	97	(Kamboh *et al*., 2013)
CNTs	MB	112.2	(Ma *et al*., 2012)
HKUST-1/GO	MB	183.49	(Li *et al*., 2013)
Activated carbon	MB	26	(Hameed *et al*., 2007)
MOF-235	MB	187	(Haque *et al*., 2011)

CHAPTER 4: MISCELLANEOUS STUDY

Synthesis, characterization, photoluminescence, and electrochemical studies of novel mononuclear Cu(II) and Zn(II) complexes with the 1-benzylimidazolium ligand

4.1 Introduction

Recently, coordination complexes have become attractive for use in the production of medicines and drugs, primarily because most metals and organic compounds have some biological activity, such as antifungal agents, antibiotics, and anticancer (Hackenberg & Tacke, 2014; Salehi *et al*., 2012). However, coordination complexes also have physical and chemical applications, such as in catalysis, luminescence, hydrometallurgy, and sensors (Parthiban *et al*., 2016; Yam *et al*., 2015; Prier *et al*., 2013). In addition, coordination complexes have been widely used in electrochemical studies because of the different oxidation state of transition metal (Begum *et al*., 2016; Wang *et al*., 2015).

Coordination complexes contain ligands, which can be ions or neutral molecules, that have lone pairs that can be donated to the central metal atom (Wang *et al*., 2016; Malone & Crowston, 1990). The ligand can be varied by the donor atom, for example, N, S, O, or P in phosphines (Sutra & Igau, 2016), alkoxides, imides (Tsai *et al*., 2015), phosphoramidites (Duursma *et al*., 2003), and more (Brändén & Reinhammar, 1975). Benzylimidazole is a popular N-donor ligand often used in coordination chemistry. The imidazole ring of benzylimidazole is an important component of numerous natural products, including purine, histidine, histamine, and nucleic acids. The exposed imidazole nitrogen atom of benzylimidazole can bind as a monodentate ligand to a central metal atom (González-Ortega & Guzmán, 2015; Nardecchia *et al.*, 2013). Benzylimidazole is also known to be good Lewis base and

metal coordinator because of its pK_a value (approximately 7), and the rotational freedom around the C-N bond in benzylimidazole allows changes in molecular conformation that lead to distinct coordination compound structures (Kovalevsky *et al.,* 2010; Wu *et al*., 1996). A large number of d-block transition metal and imidazole complexes and their derivatives are known to have biological and physiochemical properties (Majumder *et al*., 2006), and the coordination capability of a number of monodentate benzylimidazole derivatives (Maru & Shah, 2012; Goodgame *et al*., 1972).

In this study, we explore two novel crystal structures of benzylimidazole-based complexes: $[Cu(bim)_4Cl_2]\cdot 2H_2O$ (**1**) and $[Zn(bim)_2Cl_2]$ (**2**). The $[Zn(bim)_2Cl_2]$ (**2**) complex has been previously reported by Pettinari and coworkers, although no crystal structure (Pettinari *et al.,* 1998). Therefore, here, we report the synthesis, spectroscopic characterization, single crystal structure, X-ray diffraction (XRD) measurements, and thermogravimetric (TGA) analysis of complexes **1** and **2** and their electrochemical behavior. The electrochemical studies of both complexes were carried out using cyclic voltammetry (CV).

4.2 Experimental

4.2.1 Materials and measurements

1-Benzylimidazole (Sigma–Aldrich, 99%, Germany) $CuCl_2.2H_2O$, $ZnCl_2$ (98%; R&M chemicals, UK). Ultrapure water (Milli-Q water purification system, Millipore, Billerica, MA, USA) was used as the working solution. All reagents are commercially available and were used without further purification.

IR, UV-vis, Powder X-ray diffraction (PXRD) and TGA instruments and their methods are similar as it is explained in Section 2.1.2. Fluorescence spectra were measured using a JASCO FP-6500 spectrofluorometer.

X-ray single crystal data for complexes **1** and **2** were collected at 304(4) and 293(2) K on a Bruker AXS SMART APEX II diffractometer with a CCD area detector (Mo Kα = 0.71073 Å, monochromator = graphite). High-quality crystals were chosen under a polarizing microscope and mounted on a glass fiber. Data processing and absorption correction were accomplished using the APEXII software package (Bruker, 2005). The structures were solved by the same method as explained in section 2.1.2.

Cyclic voltammograms were recorded on a CHI602E electrochemical analyzer using a three-electrode cell.

4.2.2 Synthesis of $[Cu(bim)_4Cl_2].2H_2O$ (1)

An aqueous solution (20 mL) of $CuCl_2.6H_2O$ (0.0025 M, 0.426 g) was added to a methanol solution (20 mL) of 1-benzylimidazole (0.01 M, 1.582 g) at a molar ratio of 1:4. The mixture was stirred for 4 to 5 h at room temperature, and then the resultant clear solution was filtered off and allowed to stand for crystallization. Dark blue crystals formed after a week and were analyzed by single crystal X-ray diffraction technique. Anal. Calc.for $C_{40}H_{44}Cl_2CuN_8O_2$: C, 59.81; H, 5.52; N, 13.95; Found: C, 58.62; H, 4.33; N, 11.26. mp = 135–148 °C. Yield = 83%.

4.2.3 Synthesis of $[Zn(bim)_2Cl_2]$ (2)

A DMF solution (20 mL) of $ZnCl_2$ (0.0025 M, 0.341 g) was added to a methanol solution (20 mL) of 1-benzylimidazole (0.01 M, 1.582 g) at a molar ratio of 1:4 and the mixture was stirred for 4 to 5 h at room temperature. Colorless crystals were obtained from the filtrate after a week and analyzed by single crystal X-ray diffraction technique. Anal. Calc. for $C_{81}H_{80}Cl_8N_{15}Zn_4$: C, 53.03; H, 4.45; N, 12.38; Found: C, 52.55; H, 4.48; N, 11.58. The mp of 162–174 °C is in the range of previously reported proposed complex (Pettinari *et al.,* 1998). Yield = 94%.

4.3 Results and discussion

General and spectroscopic characterization

4.3.1 IR analysis

Table 4.1 lists the FT-IR spectral analysis of the ligand benzylimidazole and its complexes, **1** and **2**. The infrared spectrum of the benzylimidazole ligand contains a prominent band at 3137 cm^{-1}, which can be attributed to N-H stretching vibrations. The IR band appearing at 1178 cm^{-1} can be assigned to N-C stretching of the benzylimidazole ring (Katsyuba *et al.,* 2004). As evident from Table 5.1, the IR spectra of the ligand and the complexes contain peaks in a similar region. However, some significant variations are seen in the spectra of the metal complexes and their free ligands. By comparing the infrared spectra of the free ligand with those of its complexes, the coordination modes and parts of the ligand bound to the metal ion were explored. On coordination, the stretching vibrations for the υ(N-H) and υ(C-N) bonds show a significant shift, with υ(N-H) shifting from 3137 to 3122 and 3115 cm^{-1}, whereas υ(C-N) shifted from 1178 to 1158 and 1150 cm^{-1} in metal complexes **1** and **2**, respectively. New characteristic peaks, which were absent in the spectrum of the ligand, were observed in metal complexes at 510 and 530 cm^{-1}, indicating M-N linkages (Jayaseelan *et al.,* 2013) for complexes **1** and **2**, respectively.

Table 4.1: IR spectral data of ligand benzylimodazole and its complexes **1** and **2**.

Compound	**υ(N-H)**	**υ(C-N)**	**υ(M-N)**
Ligand (benzylimidazole)	3137	1178	-
Complex **1**	3126	1158	510
Complex **2**	3115	1104	530

4.3.2 UV-visible absorption spectroscopy

Figure 4.1 shows the solid state UV-Visible spectra of the ligand and its complexes **1** and **2**. As evident from the spectrum of the free ligand, a prominent absorption band appears between 200 and 300 nm with maxima at 212, 234, and 270 nm; these may be assigned to the π-π* transitions of benzylimidazole (Saral *et al*., 2017; Xing *et al*., 2008). The absorption spectra of complexes **1** and **2** displayed different absorption patterns compared to that of the free ligand. The absorption bands observed with maxima at 335 nm in the spectrum of **1** and 211, 231, and 264 nm in the spectrum of **2** were assigned to the π-π* transitions of the imidazole group. Complex **1** exhibited broad and sharp absorption bands between 500 and 800 nm, which may be attributed to d-d transitions, a unique characteristic of transition metal ions (Cu^{2+}), whereas the spectrum of complex **2**, which has a d^{10} metal ion (Zn^{2+}) configuration, does not contain any peaks arising from d-d (Begum *et al*., 2016) The shifting of the absorption bands in the spectra of the complexes towards higher wavelengths for complex **1** and lower intensity for complex **2** is indicative of the metal ion coordination with the benzylimidazole ring.

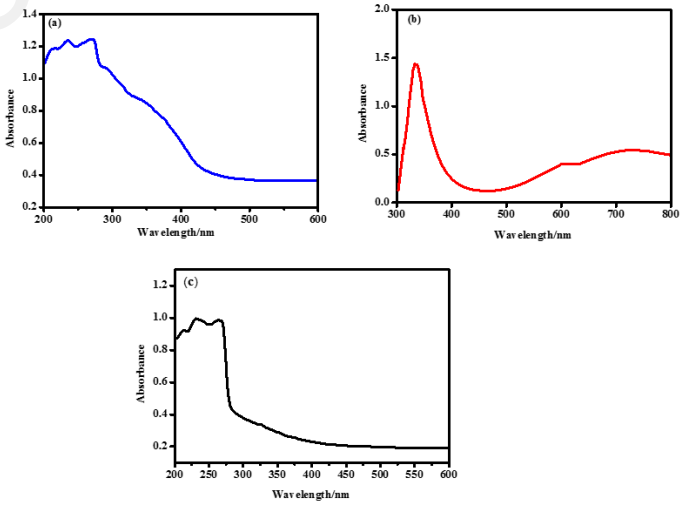

Figure 4.1: Solid state UV-Visible spectra of (a) free ligand (benzylimidazole), (b) complex **1** (c) complex **2**.

4.3.3 Fluorescence spectroscopy

Figure 4.2 shows the solid-state fluorescence emission spectra of the free ligand and its complexes, **1** and **2**, at ambient temperature. As obvious from the figure, the emission spectrum of the free ligand contains three significant emission peaks at λ_{max} = 308, 367, and 420 nm upon excitation at 270 nm, and these may be assigned to the π-π* transitions of the delocalized π electrons in the imidazole ring and the n-π* transitions of the n-electrons of the nitrogen atoms of imidazole (Cheng *et al*., 2014). The emission spectrum of complex **1** contains two emission peaks at 375 and 497 nm upon excitation at 335 nm, whereas complex **2** displayed two emission peaks at 297 and 419 nm upon excitation at 264 nm. Comparing the emission spectral data of the free benzylimidazole ligand with those of its complexes, the emergence of new peaks in the emission spectra of the complexes can be attributed to the π-π* transition of the benzylimidazole ligands with metal ion charge transitions. In addition, there is fluorescence quenching in complexes **1** and **2**. The fluorescence quenching of a ligand by transition metal ions during complexation is a common phenomenon and can be explained by processes such as magnetic perturbation, redox activity, and electronic energy transfer (Erkarslan *et al*., 2016; Hopa & Cokay, 2016; Yasemin, 2016). On the formation of metal complexes, the energy of the ligand excited states, which are responsible for the emission spectrum, transfers to the metal ions, leading to a decrease in the fluorescence intensity (Önal *et al*., 2011).

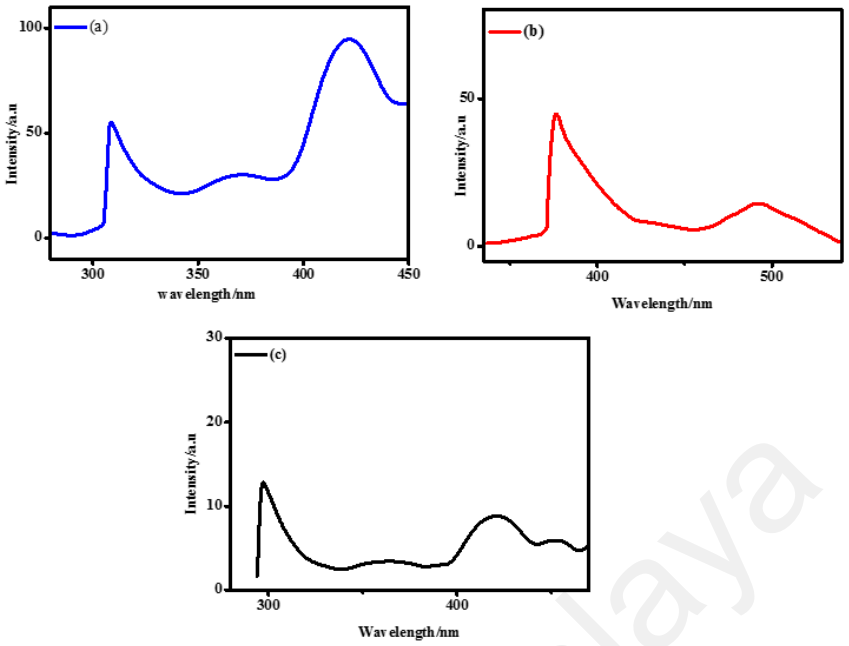

Figure 4.2: Fluorescence spectra for (a) free ligand (benzylimidazole) (b) complex **1** (c) Complex **2**.

4.3.4 Crystal structure description

Complex **1** crystallized in the monoclinic space group $P2_1/c$. The crystal data and structural refinement parameters are shown in Table 4.2.

Complex **1** (tetrabenzylimidazole dichlorocopper(II) dihydrate) possesses one half-molecule with the center of symmetry at the Cu1 atom in the asymmetric unit, and the molecular structure is shown in Figure 4.3. However, the octahedral geometry is due to the long-range interactions of Cu1 with the two Cl atoms occupying the axial positions. The Cu-Cl1 distances are 3.0897(7) Å. Similar observations has been observed in *catena*-poly[bis(1-methyl-1-tetrazole-κN4)copper(II)]-di-μ-bromo], in which the Cu-Br bond length is 3.101(4) Å (Ivashkevich *et al.,* 2005). The N2, N2A, N3, and N3A nitrogen atom of the imidazole rings occupy equatorial positions, with N2–Cu1–N3 and N2–Cu1–N3 bond angles of 86.94(7) and 93.06(7)°, respectively, making the geometry slightly distorted. The Cu1–N2 and Cu1-N3 bond lengths of

1.9887(17) and 2.0253(16) Å, respectively, are longer than that in [Cu(bhs)(Hdmpz)] (1.924(2) Å) (Paul *et al*., 2008). Other bond length and angles are normal and comparable to the Zn complex (Table 4.3). The cis imidazole rings, N1/N2/C8-C10 and N3/N4/ (C11-C13), are not coplanar but are twisted with an angle of 45.98°.

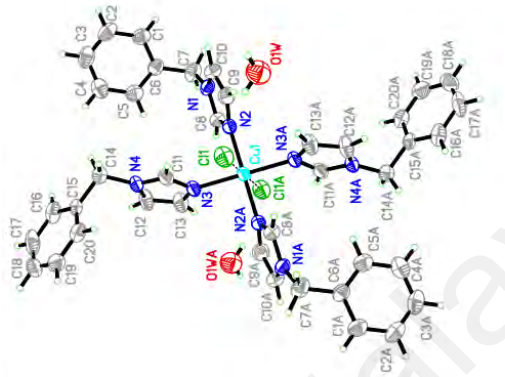

Figure 4.3: Molecular structure of complex **1**.

In the crystal packing structure of complex **1**, the interactions are dominated by C11-H11···Cl1 and intermolecular hydrogen bonds between the water molecules and chloride atoms, forming a two-dimensional network (Figure 4.4). All the symmetry codes are given in Table 4.4.

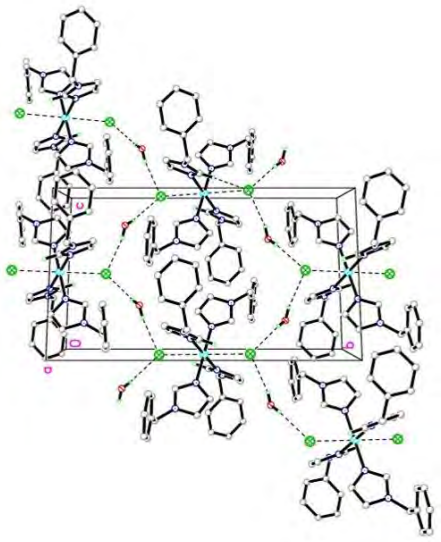

Figure 4.4: Crystal packing of complex 1 viewed down a axis. The dashed lines indicate hydrogen bond except chlorine to Cu atoms.

Complex **2** (dibenzylimidazoledichlorozinc(II)) crystallized in the triclinic space group *P*-1. The asymmetric unit contains four crystallographic independent complexes. In the molecular structure of complex **2**, the Zn atom is coordinated by two nitrogen atoms (from two benzylimidazole ligands) and two chlorides, resulting in a tetrahedral coordination geometry (Figure. 4.5**)**.

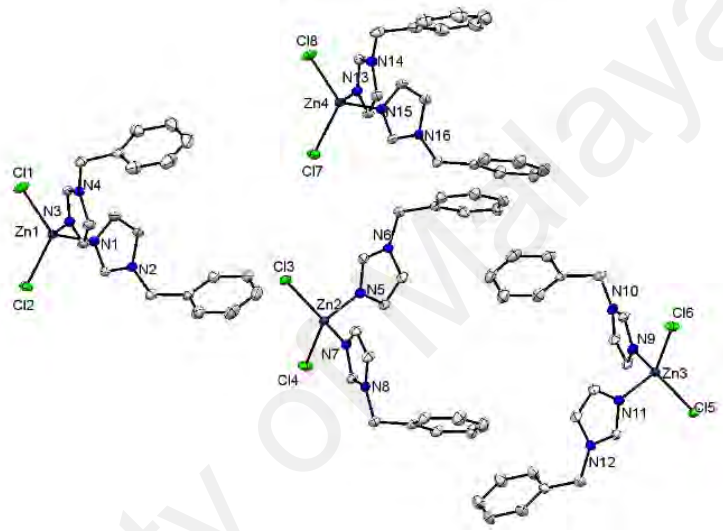

Figure 4.5: Asymmetric unit of complex **2.**

The two chloride atoms located at the basal position have Cl1-Zn1-Cl2, Cl3-Zn2-Cl4, Cl5-Zn3-Cl6, and Cl7-Zn4-Cl8 bond angles ranging from 117.45(2) to 119.87 (2)°, while the two nitrogen atoms of the imidazole rings are in equatorial positions with N1-Zn1-N3, N7-Zn2-N5, N9-Zn3-N11, and N13-Zn4-N15 bond angles of 108.02(7) to 108.52(7)°, resulting in a significantly distorted tetrahedral geometry. The cis benzylimidazole rings are not coplanar. The Zn-N bond lengths (Zn1-N1, Zn1-N3, Zn2-N7, Zn2-N5, Zn3-N9, Zn3-N11, Zn4-N13, and Zn4-N15) range from 2.0022(17) to 2.0106(17) Å, and these are slightly shorter than those in $[ZnCl_2(C_{14}H_{12}N_2)_2]$, which have bond lengths ranging from 2.0048(17) to 2.0225(17) Å to the imidazole group

(Deng *et al.,* 2016; Bouhfid *et al*., 2014). Other bond lengths and angles are within normal ranges (Table 4.3).

As shown in the crystal packing diagram, the intermolecular interactions are dominated by C-H···Cl and C-H···π interactions (blue dotted line), resulting in three-dimensional layers (Figure 4.6). There are no classical hydrogen bonds in the structure.

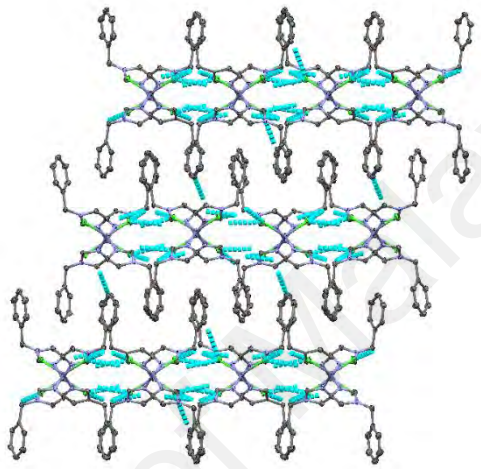

Figure 4.6: Crystal packing of complex 2 viewed down a axis.

Table 4.2: Crystal data and structure parameters for crystal complex **1** and complex **2**.

	1	**2**
CCDC No	1478266	1519004
Empirical formula	$C_{40}H_{44}Cl_2CuN_8O_2$	$C_{81}H_{80}Cl_8N_{15}Zn_4$
Formula weight	803.27	1808.68
Temperature/K	304(2) K	293(2)
Crystal system	monoclinic	triclinic
Space group	$P2_1/c$	P-1
a/Å	10.9435(7)	12.3756(4)
b/Å	17.8491(13)	14.5480(4)
c/Å	10.5662(6)	24.7577(7)
α /°	90	106.590(2)
β/°	109.201(2)	104.191(3)
γ /°	90	90.275(3)
Volume/ $Å^3$	1949.1(2)	4128.1(2)
Z	2	2
Density (calculated) /g/m^3	1.369	1.455
Absorption coefficient/ mm^{-1}	0.743	4.119
F(000)	838.0	1854.0
Crystal size/ mm^3	0.430 × 0.240 × 0.160	0.3 × 0.3 × 0.3
Theta range for data collection	3.0 to 28.3°.	7.4 to 149.4°
Reflections collected	63639	28752
Independent reflections	4845 [R(int) = 0.0587]	16214 [R(int) = 0.0262]
Completeness to theta = 28.3°	99 %	99 %
Max. and min. transmission	0.8903 and 0.7405	0.088 and 1.000
Refinement method	Full-matrix least-squares on F^2	Full-matrix least-squares on F^2
Goodness-of-fit on F2	1.062	1.005
Final R indices [I>2sigma(I)]	R1 = 0.0448, wR2 =0.0927	R1 = 0.0409, wR2 = 0.1141
R indices	R1 = 0.0775, wR2 = 0.1067	R1 = 0.0470, wR2 = 0.122
Largest diff. peak and hole/ e.Å-3	0.23 and -0.88	0.77 and -0.78

Table 4.3: Selected bond lengths (Å) and bond angles (°) for complex **1** and **2**.

Complex 1			
Atom	**Length/Å**	**Atom**	**Angle / °**
Cu1–N2	1.9887(17)	H(1WA)-O(1W)-H(1WB)	107(4)
Cu1-N3	2.0253 (16)	N(2A)-Cu(1)-N(2)	180.0
Cu1-Cl1	3.0897(7)	N2–Cu1–N3	86.94(7)
N(3)-C(1)	1.310	N2–Cu1–N3A	93.03(7)
Complex 2			
Atom	**Length/Å**	**Atom**	**Angle/ °**
Zn(1)-N(1)	2.0096(17)	N(1)-Zn(1)-N(3)	108.35(7)
Zn(1)-N(3)	2.0106(17)	N(7)-Zn(2)-N(5)	108.52(7)
Zn(1)-Cl(1)	2.2511(6)	N(9)-Zn(3)-N(11)	108.20(7)
Zn(1)-Cl(2)	2.2572(5)	N(13)-Zn(4)-N(15)	108.02(7)
Zn(2)-N(7)	2.0060(16)	Cl(1)-Zn(1)-Cl(2)	117.45(2)
Zn(2)-N(5)	2.0087(17)	Cl(4)-Zn(2)-Cl(3)	118.24(2)
Zn(2)-Cl(4)	2.2500(5)	Cl(5)-Zn(3)-Cl(6)	119.87(2)
Zn(2)-Cl(3)	2.2535(5)	Cl(8)-Zn(4)-Cl(7)	117.85(2)
Zn(3)-N(9)	2.0079(17)	N(15)-Zn(4)-Cl(7)	102.3(5)
Zn(3)-N(11)	2.0111(17)	N(1)-Zn(1)-Cl(1)	112.30(5)
Zn(3)-Cl(5)	2.2507(5)	N(7)-Zn(2)-Cl(4)	102.41(5)
Zn(3)-Cl(6)	2.2531(5)	N(9)-Zn(3)-Cl(5)	111.35(5)
Zn(4)-N(13)	2.0022(17)	N(13)-Zn(4)-Cl(8)	104.01(5)
Zn(4)-N(15)	2.0160(17)	N(3)-Zn(1)-Cl(2)	113.30(5)
Zn(4)-Cl(7)	2.2526(5)	N(5)-Zn(2)-Cl(4)	111.97(5)
Zn(4)-Cl(8)	2.2495(5)	N(11)-Zn(3)-Cl(6)	111.52(5)

Table 4.4: Hydrogen Bond (Å) for complex **1**.

Complex 1				
D-H……A	**d(D-H)**	**d(H…..A)**	**d(D…A)**	**d(D-H…..A)**
2O(1W)-H(1WA)…Cl1	0.82(2)	2.52(2)	3.293(3)	158(3)
2O(1W)-H(1WB)….Cl1	0.82(4)	2.65(4)	3.424(3)	158(4)
C(11)-H(11)…….Cl1	0.93	2.77	3.462(2)	132

x,1/2-y,1/2+z

4.3.5 X-ray powder diffraction pattern

Figure 4.7 shows the experimental powder X-ray diffraction patterns for the Cu(II) and Zn(II) coordination complexes, which agree well with the simulated patterns calculated from the single crystal structures of complexes **1** and **2**, indicating that the samples are single phase and free from impurities.

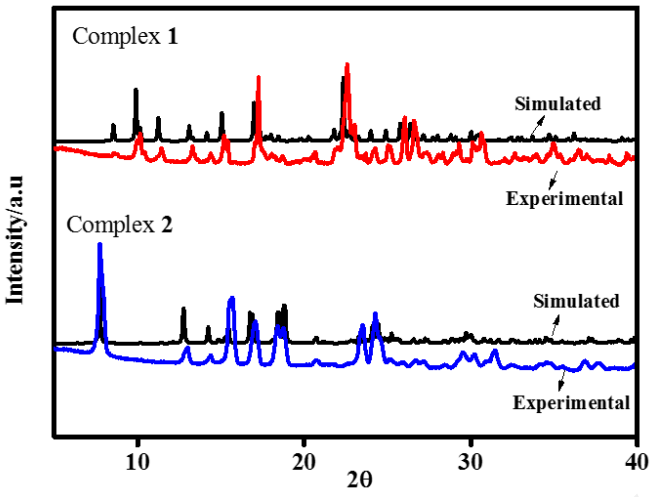

Figure 4.7: X-ray powder diffraction pattern of complex 1 and complex 2 (Black-simulated from CIFs, Red and Blue Experimental).

4.3.6 Electrochemical study

Electrochemical studies were performed for complexes **1** and **2**. Due to the different metal oxidation states, some redox properties are expected. Electrochemical measurements were carried out using a glassy carbon electrode in the presence of four different electrolytes: KCl, phosphate buffer, TRIS, and ammonium chloride (Table 4.5) at a scan rate of 50 mVs^{-1}. As shown in Figure 4.8, the peak potential separations ($E_{pc} - E_{pa}$) for complex **1** were 107, 93, 122, and 102 mV in KCl, phosphate buffer, TRIS, and NH_4Cl electrolyte solutions, respectively, and the ratios of cathodic current to anodic current I_{pc}/I_{pa} are 0.9, 0.86, 0.81, and 0.87, respectively, indicating that the redox reaction of the complex was quasi-reversible. Only one redox couple was detected for complex **1** using the previously mentioned conditions, which suggests that the cathodic peak is due to the reduction of Cu(II) to Cu(I). When the potential scan was reversed to positive potentials, anodic waves were observed at 0.01, 0.13, 0.12, and 0.15 V, respectively, indicating the oxidation of Cu(I) to Cu(II) (Mamun *et al*., 2010). In contrast, under the same condition, only one reduction peak was observed for complex **2**, which indicates that Zn(II) was reduced to Zn(0) at -0.68 V. The absence of an anodic

peak in the reverse scan suggests that the reduced form of complex **2** is more redox stable

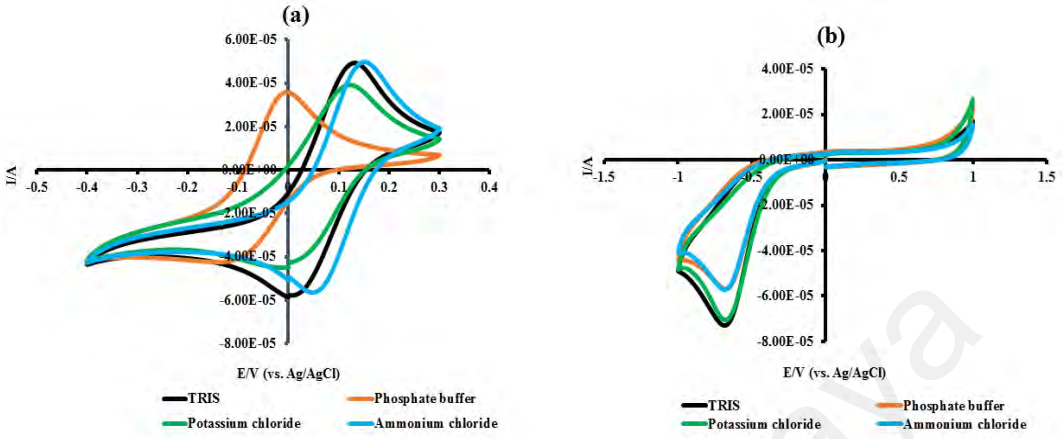

Figure 4.8: Cyclic voltammogram at a scan rate of 50 $mVs^{-1}$for (a) complex 1 (b) complex 2 using glassy carbon electrode (diameter = 2mm) in the presence 50mM KCl , phosphate buffer,TRIS,and ammonium chloride electrolyte solution.Scanning was performed against Ag/AgCl (sat.KCl) reference electrode.

Table 4.5: Electrochemical study Complex **1** and Complex **2** in different electrolytes solutions using glassy carbon electrode.

Complex **1**			
	Glassy carbon		
Electrolytes	$\mathbf{E_{P,A}}$	$\mathbf{E_{P,C}}$	$\mathbf{E_{1/2}}$
Phosphate buffer	0.00977	0.10254	0.05615
TRIS	0.13184	0.00977	0.07080
KCl	0.12451	0.01709	0.13794
NH_4Cl	0.15137	0.04883	0.10010
Complex **2**	**Glassy carbon**		
Electrolytes	$\mathbf{E_{P,A}}$	$\mathbf{E_{P,C}}$	$\mathbf{E_{1/2}}$
Phosphate buffer	No	0.67871	No
TRIS	No	0.68359	No
KCl	No	0.67627	No
NH_4Cl	No	0.68359	No

CHAPTER 5: CONCLUSION

A total of 12 compounds based on benzylimidazole and piperazine ligand (TBim-Ni-CP (**a**), TBim-Cu-CP (**b)**, TBim-Zn-CP (**c**), ABim-Ni-CP (**d**), ABim-Cu-CP (**e**), ABim-Zn-CP (**f**), TP-Ni-CP (**g**), TP-Cu-CP (**h**), TP-Zn-CP (**i**), AP-Ni-CP (**j**), AP-Cu-CP (**k**), AP-Zn-CP (**l**)) were successfully synthesized and characterised using various analytical techniques, including IR spectroscopy, elemental analysis, powder X-ray diffraction, single crystal X-ray diffraction, BET surface area analysis, thermogravimetric analysis and electrical impedance spectroscopy (conductivity analysis).

The synthesized coordination polymers were modified with carbon paste electrode (CPs/CPE) to study the electrochemical behaviour of ferricyanide and electrochemical sensing of H_2O_2. The electrochemical study of ferricyanide at CPs/CPE show that the newly synthesized coordination polymers have excellent potential as electrode modifier for the redox reaction of ferricyanide. The redox reaction of ferricyanide was reversible and diffusion controlled and the calculated diffusion coefficient value for ferricyanide at CPs/CPE were in the range of 1.89×10^{-5} -5.96×10^{-5} $cm^2\ s^{-1}$.

On the basis of good pore size (361.57 Å) and high conductivity (1.28×10^{-3} S/cm), AP-Ni-CP was applied for the electrochemical detection of H_2O_2. Under optimum condition, the voltammetric reduction of H_2O_2 at AP-Ni-CP/CPE in phosphate buffer solution has been studied. Under selected conditions, there was a linear relationship between the peak current and certain concentration range (0.004 to 60 mM) of H_2O_2 with low LOD (0.0009 mM). Moreover, it also showed good reproducibility, stability and good selectivity. In addition, high percentage recovery (94.7 % to 107 %) in real samples (lens cleaner solutions), suggested that the AP-Ni-CP modified to CPE

is a promising method to improve the CPE material in electrochemical analysis and extend its application in the scope of electrochemical sensing.

The synthesized compounds were further study for the adsorption of two oppositely charged dyes CSB and MB (Chicago sky blue and methylene blue) by batch method. The percentage removal for Chicago sky blue and methylene blue are in the range of 65-95 % and 4-48% respectively, which indicates that coordination polymers have more adsorption behaviour toward Chicago sky blue than methylene blue. On the basis of good results of percentage removal toward both dyes, ABim-Zn-CP was applied for kinetic and isotherm study of CSB and MB. The results show that pseudo-second-order kinetic model and Langmuir model matched well with the adsorption of CSB and MB onto ABim-Zn-CP (**f**). Under optimum condition the adsorption capacity (qe) of ABim-Zn-CP (**f**) toward CSB and MB were 144.26 mg/g and 174.60 mg/g respectively. Furthermore, the binary mixture of both dyes were also study in order to investigate the adsorption behaviour of ABim-Zn-CP in real sample (lake water). The high percentage of removal of binary mixture of dyes by using ABim-Zn-CP (**f**) in lake water (98 %), suggested that the ABim-Zn-CP (**f**) is a promising adsorbent for the removal of the dyes from an environmental water samples.

The miscellaneous study is about the synthesis of crystal structures of those complexes which were related to the synthesized coordination polymers but without linker. In this study we successfully synthesized and structurally characterized two new coordination complexes $[Cu(bim)_4Cl_2]\cdot 2H_2O$ (**1**) and $[Zn(bim)_2Cl_2]$ (**2**). Spectroscopic techniques confirmed the metal-ligand coordination, and single X-ray diffraction results show that Cu(II) complex is octahedral geometry, while the Zn(II) complex is tetrahedral. Both complexes exhibit photoluminescence properties. In the electrochemical measurements, the voltammogram of complex **1** shows quasi-reversible

redox reaction, while complex **2** shows only one reduction peak and no oxidation peak, arising from its stability in reduced form.

Future Research Plan

The applications of coordination polymers in analytical chemistry have attracted more interest in recent years due to their specific surface area, high porosity and good thermal stability. In future we will further expand the applications of coordination polymers in photocatalysis, bioactivity, ion exchange, and removal of heavy metals to meet the environment friendly demands. Further improvement to synthesized more porous coordination polymers with good conductivity for analytical applications. Meanwhile, we are able to get two crystal structures of coordination polymers in this study, so in future effort is being carried out towards establishing more good methods to get the crystal structures of the remaining compounds.

REFERENCES

Adeyemo, A. A., Adeoye, I. O., & Bello, O. S. (2012). Metal organic frameworks as adsorbents for dye adsorption: overview, prospects and future challenges. *Toxicological and Environmental Chemistry, 94*(10), 1846-1863.

Al-Degs, Y. S., El-Barghouthi, M. I., Issa, A. A., Khraisheh, M. A., & Walker, G. M. (2006). Sorption of Zn (II), Pb (II), and Co (II) using natural sorbents: equilibrium and kinetic studies. *Water Research, 40*(14), 2645-2658.

Azad, F. N., Ghaedi, M., Dashtian, K., Hajati, S., & Pezeshkpour, V. (2016). Ultrasonically assisted hydrothermal synthesis of activated carbon–HKUST-1-MOF hybrid for efficient simultaneous ultrasound-assisted removal of ternary organic dyes and antibacterial investigation: Taguchi optimization. *Ultrasonics Sonochemistry, 31*, 383-393.

Baca, B. T., del Castillo, L. F., Vera-Cruz, P., Toscano, R. A., Rodríguez-Hernández, J., & Balmaseda, J. (2016). Synthesis, characterization, and crystal structure of two zinc linear dicarboxylates. *Powder Diffraction, 31*(03), 229-232.

Bahadori, L., Manan, N. S. A., Chakrabarti, M. H., Hashim, M. A., Mjalli, F. S., AlNashef, I. M., Low, C. T. J. (2013). The electrochemical behaviour of ferrocene in deep eutectic solvents based on quaternary ammonium and phosphonium salts. *Physical Chemistry Chemical Physics, 15*(5), 1707-1714.

Balzani, V., Juris, A., Venturi, M., Campagna, S., & Serroni, S. (1996). Luminescent and redox-active polynuclear transition metal complexes. *Chemical Reviews, 96*(2), 759-834.

Banerjee, R., Phan, A., Wang, B., Knobler, C., Furukawa, H., O'keeffe, M., & Yaghi, O. M. (2008). High-throughput synthesis of zeolitic imidazolate frameworks and application to CO_2 capture. *Science, 319*(5865), 939-943.

Barrera, G., Bruno, J., Barron, T., & Allan, N. (2005). Negative thermal expansion. *Journal of Physics: Condensed Matter, 17*(4), R217.

Batten, S. R., Champness, N. R., Chen, X.M., Garcia-Martinez, J., Kitagawa, S., Öhrström, L., Reedijk, J. (2012). Coordination polymers, metal–organic frameworks and the need for terminology guidelines. *Crystal Engineering Communication, 14*(9), 3001-3004.

Batten, S. R., Neville, S. M., & Turner, D. R. (2009). *Coordination polymers: design, analysis and application*: Royal Society of Chemistry.

Bedekar, P. A., Kshirsagar, S. D., Gholave, A. R., & Govindwar, S. P. (2015). Degradation and detoxification of methylene blue dye adsorbed on water hyacinth in semi continuous anaerobic–aerobic bioreactors by novel microbial consortium-SB. *RSC Advances, 5*(120), 99228-99239.

Begum, M., Zangrando, E., Howlader, M., Sheikh, M., Miyatake, R., Hossain, M., Hasnat, M. (2016). Synthesis, characterization, photoluminescence and electrochemical studies of Ni (II), Cu (II), Zn (II), Cd (II) and Pd (II) complexes of the bidentate S-hexyl-β-N-(2-thienyl) methylenedithiocarbazate ligand. *Polyhedron, 105*, 56-61.

Bibi, S., Mohamad, S., Manan, N. S. A., Ahmad, J., Kamboh, M. A., Khor, S. M., Halim, S. N. A. (2017). Synthesis, characterization, photoluminescence, and electrochemical studies of novel mononuclear Cu (II) and Zn (II) complexes with the 1-benzylimidazolium ligand. *Journal of Molecular Structure, 1141*, 31-38.

Biradha, K., Ramanan, A., Vittal, J. J. (2009). Coordination polymers versus metal− organic frameworks. *Crystal Growth and Design, 9*(7), 2969-2970.

Bouhfid, R., Essassi, E., Saadi, M., & El Ammari, L. (2014). Bis (1-benzyl-1H-benzimidazole-κN_3) dichloridozinc. *Acta Crystallographica Section E: Structure Reports Online, 70*(3), m94-m95.

Brändén, R., & Reinhammar, B. (1975). EPR studies on the anaerobic reduction of fungal laccase: Evidence for participation of type 2 copper in the reduction mechanism. *Biochimica et Biophysica Acta (BBA)-Protein Structure, 405*(2), 236.

Bruker, A. (2005). Saint and SADABS. *Bruker AXS Inc., Madison, Wisconsin, USA*.

Cai, X., Ogorevc, B., Tavčar, G., Wang, J. (1995). Indium–tin oxide film electrode as catalytic amperometric sensor for hydrogen peroxide. *Analyst, 120*(10), 2579-2583.

Chandra, D., Kasture, M. W., & Bhaumik, A. (2008). A new microporous MOF material based on Zn (II)-polycarboxylate coordination polymer synthesized with the aid of 1, 6-diaminohexane as template. *Microporous and Mesoporous Materials, 116*(1), 204-209.

Chen, C.T., & Suslick, K. S. (1993). One-dimensional coordination polymers: Applications to material science. *Coordination Chemistry Reviews, 128*(1-2), 293-322.

Chen, D., Shen, W., Wu, S., Chen, C., Luo, X., & Guo, L. (2016). Ion exchange induced removal of Pb (II) by MOF-derived magnetic inorganic sorbents. *Nanoscale, 8*(13), 7172-7179.

Chen, S., Brown, L., Levendorf, M., Cai, W., Ju, S.-Y., Edgeworth, J., Piner, R. D. (2011). Oxidation resistance of graphene-coated Cu and Cu/Ni alloy. *ACS Nano, 5*(2), 1321-1327.

Chen, S., Yuan, R., Chai, Y., & Hu, F. (2013). Electrochemical sensing of hydrogen peroxide using metal nanoparticles: a review. *Microchimica Acta, 180*(1-2), 15-32.

Chen, S., Zhang, J., Zhang, C., Yue, Q., Li, Y., & Li, C. (2010). Equilibrium and kinetic studies of methyl orange and methyl violet adsorption on activated carbon derived from Phragmites australis. *Desalination, 252*(1), 149-156.

Chen, X., Wu, G., Cai, Z., Oyama, M., & Chen, X. (2014). Advances in enzyme-free electrochemical sensors for hydrogen peroxide, glucose, and uric acid. *Microchimica Acta, 181*(7-8), 689-705.

Cheng, Z., Yang, B., Yang, M., & Zhang, B. (2014). Structural study and fluorescent property of a novel organic microporous crystalline material. *Journal of the Brazilian Chemical Society, 25*(1), 112-118.

Cho, H.Y., Kim, J., Kim, S.N., & Ahn, W.S. (2013). High yield 1-L scale synthesis of ZIF-8 via a sonochemical route. *Microporous and Mesoporous Materials, 169*, 180-184.

Choi, H. J., & Suh, M. P. (1999). Synthesis, crystal structure, and properties of a 3-D network assembled by nickel (II) macrocyclic complex and terephthalato bridge. *Inorganic Chemistry, 38*(26), 6309-6312.

Choi, J.S., Son, W.J., Kim, J., & Ahn, W.S. (2008). Metal–organic framework MOF-5 prepared by microwave heating: factors to be considered. *Microporous and Mesoporous Materials, 116*(1), 727-731.

Chui, S. S.Y., Lo, S. M.F., Charmant, J. P., Orpen, A. G., & Williams, I. D. (1999). A chemically functionalizable nanoporous material [Cu_3 $(TMA)_2$ $(H_2O)_3$] n. *Science, 283*(5405), 1148-1150.

Coasne, B., Alba-Simionesco, C., Audonnet, F., Dosseh, G., & Gubbins, K. E. (2009). Adsorption and structure of benzene on silica surfaces and in nanopores. *Langmuir, 25*(18), 10648-10659.

Comminges, C., Barhdadi, R., Laurent, M., & Troupel, M. (2006). Determination of viscosity, ionic conductivity, and diffusion coefficients in some binary systems: ionic liquids+ molecular solvents. *Journal of Chemical and Engineering Data, 51*(2), 680-685.

Cravillon, J., M n zer, S., Lohmeier, S.J., Feldhoff, A., Huber, K., & Wiebcke, M. (2009). Rapid room-temperature synthesis and characterization of nanocrystals of a prototypical zeolitic imidazolate framework. *Chemistry of Materials, 21*(8), 1410-1412.

Crini, G. (2006). Non-conventional low-cost adsorbents for dye removal: a review. *Bioresource Technology, 97*(9), 1061-1085.

Cui, G.H., He, C.H., Jiao, C.H., Geng, J.C., & Blatov, V. A. (2012). Two metal–organic frameworks with unique high-connected binodal network topologies: synthesis, structures, and catalytic properties. *Crystal Engineering Communication, 14*(12), 4210-4216.

Dai, J.C., Wu, X.T., Fu, Z.Y., Cui, C.P., Hu, S.M., Du, W.X., Sun, R.Q. (2002). Synthesis, structure, and fluorescence of the novel cadmium (II)− trimesate coordination polymers with different coordination architectures. *Inorganic Chemistry, 41*(6), 1391-1396.

Day, P., & Underhill, A. E. (1999). *Metal-organic and organic molecular magnets*: Royal Society of Chemistry.

De Combarieu, G., Morcrette, M., Millange, F., Guillou, N., Cabana, J., Grey, C.P., Margiolaki, I., Férey, G. and Tarascon, J.M. (2009). Influence of the Benzoquinone sorption on the structure and electrochemical performance of the MIL-53 (Fe) hybrid porous material in a lithium-ion battery. *Chemistry of Materials*, *21*(8), 1602-1611.

Deng, Y., Zhao, Y., Zhang, X.D., Kang, Y.S., & Sun, W.Y. (2016). Coordination polymers with mixed 1, 3-bis (1-imidazolyl)-5-(imidazol-1-ylmethyl) benzene and multicarboxylate ligands: Synthesis, structure and property. *Microporous and Mesoporous Materials, 231*, 163-170.

Dey, C., Kundu, T., Biswal, B. P., Mallick, A., & Banerjee, R. (2014). Crystalline metal-organic frameworks (MOFs): synthesis, structure and function. *Acta Crystallographica Section B: Structural Science, Crystal Engineering and Materials, 70*(1), 3-10.

Ding, B., Yi, L., Liu, Y., Cheng, P., Dong, Y.B., & Ma, J.P. (2005). Hydrothermal synthesis of a novel three-dimensional complex with strong blue luminescent properties. *Inorganic Chemistry Communications, 8*(1), 38-40.

Ding, S.F., Xu, M.Q., Zhao, G.C., & Wei, X.W. (2007). Direct electrochemical response of Myoglobin using a room temperature ionic liquid, 1-(2-hydroxyethyl)-3-methyl imidazolium tetrafluoroborate, as supporting electrolyte. *Electrochemistry Communications, 9*(2), 216-220.

Dolomanov, O. V., Bourhis, L. J., Gildea, R. J., Howard, J. A., & Puschmann, H. (2009). OLEX2: a complete structure solution, refinement and analysis program. *Journal of Applied Crystallography, 42*(2), 339-341.

Dubbeldam, D., Walton, K. S., Ellis, D. E., & Snurr, R. Q. (2007). Exceptional negative thermal expansion in isoreticular metal–organic frameworks. *Angewandte Chemie*, *119*(24), 4580-4583.

Duursma, A., Hoen, R., Schuppan, J., Hulst, R., Minnaard, A. J., & Feringa, B. L. (2003). First examples of improved catalytic asymmetric CC bond formation using the monodentate ligand combination approach. *Organic Letters, 5*(17), 3111-3113.

Effendy, ‡, Marchetti, F., Pettinari, C., Pettinari, R., Ricciutelli, M., Skelton, B. W., White, A. H. (2004). (Bis (1, 2, 4-triazol-1-yl) methane) silver (I) phosphino complexes: Structures and spectroscopic properties of mixed-ligand coordination polymers. *Inorganic Chemistry, 43*(6), 2157-2165.

El-Gohary, F., & Tawfik, A. (2009). Decolorization and COD reduction of disperse and reactive dyes wastewater using chemical-coagulation followed by sequential batch reactor (SBR) process. *Desalination, 249*(3), 1159-1164.

El-Naas, M. H., Al-Muhtaseb, S. A., & Makhlouf, S. (2009). Biodegradation of phenol by Pseudomonas putida immobilized in polyvinyl alcohol (PVA) gel. *Journal of Hazardous Materials, 164*(2), 720-725.

Erkarslan, U., Oylumluoglu, G., Coban, M. B., Öztürk, E., & Kara, H. (2016). Cyanide-bridged trinuclear Mn^{III}–Fe^{III} assembly: Crystal structure, magnetic and photoluminescence behavior. *Inorganica Chimica Acta, 445*, 57-61.

Evans, O. R., Lin, W. (2002). Crystal engineering of NLO materials based on metal−organic coordination networks. *Accounts of Chemical Research, 35*(7), 511-522.

Fateeva, A., Horcajada, P., Devic, T., Serre, C., Marrot, J., Grenèche, J.M., Morcrette, M., Tarascon, J.M., Maurin, G. and Férey, G. (2010). Synthesis, Structure, Characterization, and Redox Properties of the Porous MIL-68 (Fe) Solid. *European Journal of Inorganic Chemistry*, *2010*(24), 3789-3794.

Feldmann, C., Jüstel, T., Ronda, C. R., & Schmidt, P. J. (2003). Inorganic luminescent materials: 100 years of research and application. *Advanced Functional Materials, 13*(7), 511-516.

Férey, G., Mellot-Draznieks, C., Serre, C., Millange, F., Dutour, J., Surblé, S., & Margiolaki, I. (2005). A chromium terephthalate-based solid with unusually large pore volumes and surface area. *Science, 309*(5743), 2040-2042.

Férey, G., Millange, F., Morcrette, M., Serre, C., Doublet, M. L., Grenèche, J. M., & Tarascon, J. M. (2007). Mixed-Valence Li/Fe-Based Metal–Organic Frameworks with Both Reversible Redox and Sorption Properties. *Angewandte Chemie International Edition, 46*(18), 3259-3263.

Fu, R., Xiang, S., Hu, S., Wang, L., Li, Y., Huang, X., & Wu, X. (2005). Assembled bright green fluorescent zinc coordination polymer. *Chemical Communications* (42), 5292-5294.

Gagnon, K. J., Perry, H. P., & Clearfield, A. (2011). Conventional and unconventional metal–organic frameworks based on phosphonate ligands: MOFs and UMOFs. *Chemical Reviews, 112*(2), 1034-1054.

Gale, R., Gilbert, B., & Osteryoung, R. (1979). Electrochemical and spectral investigations of nickel (II) ion equilibriums in room-temperature chloroaluminate solvents. *Inorganic Chemistry, 18*(10), 2723-2725.

Gándara, F., Furukawa, H., Lee, S., & Yaghi, O. M. (2014). High Methane Storage Capacity in Aluminum Metal–Organic Frameworks. *Journal of the American Chemical Society, 136*(14), 5271-5274.

Gao, J., Wei, W., Shi, M., Han, H., Lu, J., & Xie, J. (2016). A controlled solvethermal approach to synthesize nanocrystalline iron oxide for congo red adsorptive removal from aqueous solutions. *Journal of Materials Science, 51*(9), 4481-4494.

Gao, R., Cao, B., Hu, Y., Feng, Z., Wang, D., Hu, W., Xu, K. (2013). Human infection with a novel avian-origin influenza A (H7N9) virus. *New England Journal of Medicine, 368*(20), 1888-1897.

Gedanken, A. (2004). Using sonochemistry for the fabrication of nanomaterials. *Ultrasonics Sonochemistry, 11*(2), 47-55.

Givaja, G., Amo-Ochoa, P., Gómez-García, C. J., & Zamora, F. (2012). Electrical conductive coordination polymers. *Chemical Society Reviews, 41*(1), 115-147.

Golka, K., Kopps, S., & Myslak, Z. W. (2004). Carcinogenicity of azo colorants: influence of solubility and bioavailability. *Toxicology Letters, 151*(1), 203-210.

González-Ortega, O., & Guzmán, R. (2015). Purification of Human Serum Immunoglobulins Using Immobilized Metal Affinity Chromatography with Ethylenediamine Triacetic Acid as Chelating Agent. *Journal of Liquid Chromatography & Related Technologies, 38*(1), 74-81.

Goodgame, D., Goodgame, M., & Canham, G. R. (1972). Spectroscopic studies of substituted imidazole complexes. III. 2-methylbenzimidazole complexes of divalent cobalt, nickel, copper, and zinc. *Inorganica Chimica Acta, 6*, 245-247.

Groeneman, R. H., MacGillivray, L. R., & Atwood, J. L. (1999). One-dimensional coordination polymers based upon bridging terephthalate ions. *Inorganic Chemistry, 38*(2), 208-209.

Gu, A., Wang, G., Gu, J., Zhang, X., & Fang, B. (2010). An unusual H_2O_2 electrochemical sensor based on Ni $(OH)_2$ nanoplates grown on Cu substrate. *Electrochimica Acta, 55*(24), 7182-7187.

Gu, T., & Hasebe, Y. (2006). DNA–Cu (II) poly (amine) complex membrane as novel catalytic layer for highly sensitive amperometric determination of hydrogen peroxide. *Biosensors and Bioelectronics, 21*(11), 2121-2128.

Gupta, V. K., Mergu, N., Kumawat, L. K., & Singh, A. K. (2015). A reversible fluorescence ~~–~~off–on–off" sensor for sequential detection of aluminum and acetate/fluoride ions. *Talanta*, *144*, 80-89.

Hackenberg, F., & Tacke, M. (2014). Benzyl-substituted metallocarbene antibiotics and anticancer drugs. *Dalton Transactions, 43*(22), 8144-8153.

Hameed, B., Din, A. M., & Ahmad, A. (2007). Adsorption of methylene blue onto bamboo-based activated carbon: kinetics and equilibrium studies. *Journal of Hazardous Materials, 141*(3), 819-825.

Hao, H.J., Liu, F.J., Su, H.F., Wang, Z.H., Wang, D.F., Huang, R.B., & Zheng, L.S. (2012). Syntheses, structures and fluorescence of two coordination complexes of Zn (II) and 1, 3-bis (2-methylimidazolyl) propane: solvent effect. *Crystal Engineering Community, 14*(20), 6726-6731.

Haque, E., Jun, J. W., & Jhung, S. H. (2011). Adsorptive removal of methyl orange and methylene blue from aqueous solution with a metal-organic framework material, iron terephthalate (MOF-235). *Journal of Hazardous Materials, 185*(1), 507-511.

Haque, E., Lee, J. E., Jang, I. T., Hwang, Y. K., Chang, J.S., Jegal, J., & Jhung, S. H. (2010). Adsorptive removal of methyl orange from aqueous solution with metal-organic frameworks, porous chromium-benzenedicarboxylates. *Journal of Hazardous Materials, 181*(1), 535-542.

Hasan, Z., & Jhung, S. H. (2015). Removal of hazardous organics from water using metal-organic frameworks (MOFs): plausible mechanisms for selective adsorptions. *Journal of Hazardous Materials, 283*, 329-339.

Hasegawa, S., Horike, S., Matsuda, R., Furukawa, S., Mochizuki, K., Kinoshita, Y., & Kitagawa, S. (2007). Three-dimensional porous coordination polymer functionalized with amide groups based on tridentate ligand: selective sorption and catalysis. *Journal of the American Chemical Society, 129*(9), 2607-2614.

He, W., Liu, Y., Yuan, J., Yin, J.J., Wu, X., Hu, X., Ji, Y. (2011). Au@ Pt nanostructures as oxidase and peroxidase mimetics for use in immunoassays. *Biomaterials, 32*(4), 1139-1147.

Heli, H., & Pishahang, J. (2014). Cobalt oxide nanoparticles anchored to multiwalled carbon nanotubes: Synthesis and application for enhanced electrocatalytic reaction and highly sensitive nonenzymatic detection of hydrogen peroxide. *Electrochimica Acta, 123*, 518-526.

Hopa, C., & Cokay, I. (2016). Designing a heterotrinuclear Cu^{II}—Ni^{II}—Cu^{II} complex from a mononuclear Cu^{II} Schiff base precursor with dicyanamide as a coligand: synthesis, crystal structure, thermal and photoluminescence properties. *Acta Crystallographica Section C: Structural Chemistry, 72*(8) 601-606.

Horcajada, P., Serre, C., Maurin, G., Ramsahye, N. A., Balas, F., Vallet-Regi, M., Férey, G. (2008). Flexible porous metal-organic frameworks for a controlled drug delivery. *Journal of the American Chemical Society, 130*(21), 6774-6780.

Horikoshi, R., Mochida, T., & Moriyama, H. (2002). Synthesis and characterization of redox-active coordination polymers generated from ferrocene-containing bridging ligands. *Inorganic Chemistry, 41*(11), 3017-3024.

Hoskins, B., & Robson, R. (1990). Design and construction of a new class of scaffolding-like materials comprising infinite polymeric frameworks of 3D-linked molecular rods. A reappraisal of the zinc cyanide and cadmium cyanide structures and the synthesis and structure of the diamond-related frameworks $[N(CH_3)_4][Cu^{I}Zn^{II}(CN)_4]$ and Cu^{I} [4, 4', 4", 4"'-tetracyanotetraphenylmethane] $BF_4.xC_6H_5NO_2$. *Journal of the American Chemical Society, 112*(4), 1546-1554.

Hosseini, H., Ahmar, H., Dehghani, A., Bagheri, A., Fakhari, A. R., & Amini, M. M. (2013). Au-SH-SiO_2 nanoparticles supported on metal-organic framework (Au-

SH-SiO_2@ Cu-MOF) as a sensor for electrocatalytic oxidation and determination of hydrazine. *Electrochimica Acta, 88*, 301-309.

Hosseini, H., Ahmar, H., Dehghani, A., Bagheri, A., Tadjarodi, A., & Fakhari, A. R. (2013). A novel electrochemical sensor based on metal-organic framework for electro-catalytic oxidation of L-cysteine. *Biosensors and Bioelectronics, 42*, 426-429.

Hosseini, H., Rezaei, S. J. T., Rahmani, P., Sharifi, R., Nabid, M. R., & Bagheri, A. (2014). Nonenzymatic glucose and hydrogen peroxide sensors based on catalytic properties of palladium nanoparticles/poly (3, 4-ethylenedioxythiophene) nanofibers. *Sensors and Actuators B: Chemical, 195*, 85-91.

Hu, M. (2011). *Design, Synthesis and Applications of Metal Organic Framework.* Doctoral dissertation, Worcester Polytechnic Institute.

Hu, X.L., Liu, F.H., Qin, C., Shao, K.Z., & Su, Z.M. (2015). A 2D bilayered metal–organic framework as a fluorescent sensor for highly selective sensing of nitro explosives. *Dalton Transactions, 44*(17), 7822-7827.

Huang, Y., Liu, S., Lin, Z., Li, W., Li, X., & Cao, R. (2012). Facile synthesis of palladium nanoparticles encapsulated in amine-functionalized mesoporous metal–organic frameworks and catalytic for dehalogenation of aryl chlorides. *Journal of Catalysis, 292*, 111-117.

Ivashkevich, L. S., Lyakhov, A. S., Degtyarik, M. M., & Gaponik, P. N. (2005). An X-ray powder diffraction study of catena-poly [[bis (1-methyl-1H-tetrazole-κN4) copper (II)]-di-μ-bromo]. *Acta Crystallographica Section E: Structure Reports Online, 61*(2), m394-m396.

Jain, R., Gupta, V. K., Jadon, N., & Radhapyari, K. (2010). Voltammetric determination of cefixime in pharmaceuticals and biological fluids. *Analytical Biochemistry*, *407*(1), 79-88.

Janiak, C. (2003). Engineering coordination polymers towards applications. *Dalton Transactions,* (14), 2781-2804.

Jayaseelan, P., Akila, E., Rani, M. U., & Rajavel, R. (2013). Synthesis, spectral characterization, electrochemical, anti-microbial, DNA binding and cleavage studies of new binuclear Schiff base metal (II) complexes derived from o-hydroxyacetophenone. *Journal of Saudi Chemical Society 20*(6), 625-634.

Jhung, S. H., Khan, N. A., & Hasan, Z. (2012). Analogous porous metal–organic frameworks: synthesis, stability and application in adsorption. *Crystal Engineering Communication, 14*(21), 7099-7109.

Jhung, S. H., Lee, J. H., Yoon, J. W., Serre, C., Férey, G., & Chang, J. S. (2007). Microwave Synthesis of Chromium Terephthalate MIL-101 and Its Benzene Sorption Ability. *Advanced Materials, 19*(1), 121-124.

Jiao, Y., Pei, J., Yan, C., Chen, D., Hu, Y., & Chen, G. (2016). Layered nickel metal–organic framework for high performance alkaline battery-supercapacitor hybrid devices. *Journal of Materials Chemistry A, 4*(34), 13344-13351.

Kachoosangi, R. T., Wildgoose, G. G., & Compton, R. G. (2007). Room temperature ionic liquid carbon nanotube paste electrodes: overcoming large capacitive currents using rotating disk electrodes. *Electroanalysis, 19*(14), 1483-1489.

Kamboh, M. A., Akoz, E., Memon, S., & Yilmaz, M. (2013). Synthesis of amino-substituted p-tert-butylcalix [4] arene for the removal of chicago sky blue and tropaeolin 000 azo dyes from aqueous environment. *Water, Air, and Soil Pollution, 224*(2), 1424.

Kamboh, M. A., Solangi, I. B., Sherazi, S., & Memon, S. (2009). Synthesis and application of calix [4] arene based resin for the removal of azo dyes. *Journal of Hazardous Materials, 172*(1), 234-239.

Kan, W.Q., Ma, J. F., Liu, Y.Y., & Yang, J. (2012). A series of coordination polymers based on 5-(2-carboxybenzyloxy) isophthalic acid and bis (imidazole) ligands: syntheses, topological structures and photoluminescent properties. *Crystal Engineering Community, 14*(6), 2316-2326.

Kaskel, S. (2002). Porous Metal-Organic Frameworks. *Handbook of Porous Solids*, 1190-1249.

Katsyuba, S. A., Dyson, P. J., Vandyukova, E. E., Chernova, A. V., Vidiš, A. (2004). Molecular Structure, Vibrational Spectra, and Hydrogen Bonding of the Ionic Liquid 1-Ethyl-3-methyl-1H-imidazolium Tetrafluoroborate. *Helvetica Chimica Acta, 87*(10), 2556-2565.

Khani, H., Rofouei, M. K., Arab, P., Gupta, V. K., & Vafaei, Z. (2010). Multi-walled carbon nanotubes-ionic liquid-carbon paste electrode as a super selectivity sensor: application to potentiometric monitoring of mercury ion (II). *Journal of Hazardous Materials*, *183*(1), 402-409.

Khlobystov, A. N., Blake, A. J., Champness, N. R., Lemenovskii, D. A., Majouga, A. G., Zyk, N. V., & Schröder, M. (2001). Supramolecular design of one-dimensional coordination polymers based on silver (I) complexes of aromatic nitrogen-donor ligands. *Coordination Chemistry Reviews, 222*(1), 155-192.

Kitagawa, S. (2014). Metal–organic frameworks (MOFs). *Chemical Society Reviews, 43*(16), 5415-5418.

Kitagawa, S., Kitaura, R., & Noro, S. I. (2004). Functional porous coordination polymers. *Angewandte Chemie International Edition, 43*(18), 2334-2375.

Kitagawa, S., & Munakata, M. (1993). Molecular architecture of copper (I) coordination polymers towards crystal lattice design. *În: Trends Inorginic Chemistry, 3*, 437-462.

Kitagawa, S., & Noro, S. (2004). Coordination polymers: infinite systems. *ChemInform, 35*(47).

Kligler, B., Buonora, M., Gabison, J., McKee, D., Filshie, J., Minchom, A., Gunapala, R. (2016). Abstracts from the Society for Acupuncture Research 2015 International Conference Reaching Across Disciplines to Broaden the Acupuncture Research Network November 12–14, 2015 Boston, MA. *The Journal of Alternative and Complementary Medicine, 22*(1), A1-A46.

Klimakow, M., Klobes, P., Th ne mann, A. F., Rademann, K., Emmerling, F. (2010). Mechanochemical synthesis of metal− organic frameworks: a fast and facile approach toward quantitative yields and high specific surface areas. *Chemistry of Materials, 22*(18), 5216-5221.

Klinowski, J., Paz, F. A. A., Silva, P., & Rocha, J. (2011). Microwave-assisted synthesis of metal–organic frameworks. *Dalton Transactions, 40*(2), 321-330.

Kobayashi, Y., Jacobs, B., Allendorf, M. D., & Long, J. R. (2010). Conductivity, doping, and redox chemistry of a microporous dithiolene-based metal− organic framework. *Chemistry of Materials, 22*(14), 4120-4122.

Kovalevsky, A., Chatake, T., Shibayama, N., Park, S.Y., Ishikawa, T., Mustyakimov, M., Morimoto, Y. (2010). Protonation states of histidine and other key residues in deoxy normal human adult hemoglobin by neutron protein crystallography. *Acta Crystallographica Section D: Biological Crystallography, 66*(11), 1144-1152.

Kovalevsky, A. Y., Chatake, T., Shibayama, N., Park, S.Y., Ishikawa, T., Mustyakimov, M., Morimoto, Y. (2010). Direct determination of protonation states of histidine

residues in a 2 Å neutron structure of deoxy-human normal adult hemoglobin and implications for the Bohr effect. *Journal of Molecular Biology, 398*(2), 276-291.

Krishnamurthy, G., & Agarwal, S. (2014). Room Temperature Synthesis and Characterization of a Zn (II) based Metal-organic Framework with Mixed Ligands, 1, 4-Benzenedicarboxylic Acid and 1-methyle Imidazole. *Procedia Materials Science, 5*, 1258-1265.

Kumar, P., Deep, A., Kim, K.-H., & Brown, R. J. (2015). Coordination polymers: Opportunities and challenges for monitoring volatile organic compounds. *Progress in Polymer Science, 45*, 102-118.

Kurmoo, M. (2009). Magnetic metal–organic frameworks. *Chemical Society Reviews, 38*(5), 1353-1379.

Kuppler, R. J., Timmons, D. J., Fang, Q. R., Li, J. R., Makal, T. A., Young, M. D., & Zhou, H. C. (2009). Potential applications of metal-organic frameworks. *Coordination Chemistry Reviews*, *253*(23), 3042-3066.

Lee, J., Farha, O. K., Roberts, J., Scheidt, K. A., Nguyen, S. T., & Hupp, J. T. (2009). Metal–organic framework materials as catalysts. *Chemical Society Reviews, 38*(5), 1450-1459.

Lee, Y.R., Cho, S.M., Ahn, W.S., Lee, C.H., Lee, K.H., & Cho, W.S. (2015). Facile synthesis of an IRMOF-3 membrane on porous Al_2O_3 substrate via a sonochemical route. *Microporous and Mesoporous Materials, 213*, 161-168.

Lee, Y.R., Kim, J., & Ahn, W.S. (2013). Synthesis of metal-organic frameworks: A mini review. *Korean Journal of Chemical Engineering, 30*(9), 1667-1680.

Leng, F., Wang, W., Zhao, X. J., Hu, X. L., & Li, Y. F. (2014). Adsorption interaction between a metal–organic framework of chromium–benzenedicarboxylates and uranine in aqueous solution. *Colloids and Surfaces A: Physicochemical and Engineering Aspects, 441*, 164-169.

Li, B.L., Wang, H.N., Zhao, L., Li, G.Z., & Su, Z.M. (2016). A pillar-layer MOF used as a luminescent probe for detecting small molecules acetone. *Inorganic Chemistry Communications, 66*, 87-89.

Li, C.P., Chen, J., & Du, M. (2010a). Mixed-ligand metallosupramolecular complexes with Brn-terephthalic acid (n= 1 or 4) and a versatile bent dipyridyl tecton: Structural modulation by substituent effect of the ligand and metal ion. *Polyhedron, 29*(1), 463-469.

Li, C.P., Chen, J., & Du, M. (2010b). Structural diversification and metal-directed assembly of coordination architectures based on tetrabromoterephthalic acid and a bent dipyridyl tecton 2, 5-bis (4-pyridyl)-1, 3, 4-oxadiazole. *Crystal Engineering Community, 12*(12), 4392-4402.

Li, F., Guo, S., Hartog, N., Yuan, Y., & Yang, X. (2016). Isolation and characterization of heavy polycyclic aromatic hydrocarbon-degrading bacteria adapted to electrokinetic conditions. *Biodegradation, 27*(1), 1-13.

Li, H.H., Zeng, X.H., Wu, H.Y., Jie, X., Zheng, S.T., & Chen, Z.R. (2014). Incorporating Guest Molecules into Honeycomb Structures Constructed from Uranium (VI)-Polycarboxylates: Structural Diversities and Photocatalytic Activities for the Degradation of Organic Dye. *Crystal Growth & Design, 15*(1), 10-13.

Li, H., Eddaoudi, M., O'Keeffe, M., & Yaghi, O. M. (1999). Design and synthesis of an exceptionally stable and highly porous metal-organic framework. *Nature, 402*(6759), 276-279.

Li, H. H., Ma, Y. J., Zhao, Y. Q., & Cui, G. H. (2015). Synthesis and characterization of three cobalt (II) coordination polymers with tetrabromoterephthalic acid and flexible bis (benzimidazole) ligands. *Transition Metal Chemistry, 40*(1), 21-29.

Li, L., Liu, X. L., Geng, H. Y., Hu, B., Song, G. W., & Xu, Z. S. (2013). A MOF/graphite oxide hybrid (MOF: HKUST-1) material for the adsorption of methylene blue from aqueous solution. *Journal of Materials Chemistry A, 1*(35), 10292-10299.

Li, S. L., & Xu, Q. (2013). Metal–organic frameworks as platforms for clean energy. *Energy & Environmental Science*, *6*(6), 1656-1683.

Li, Y., Huangfu, C., Du, H., Liu, W., Li, Y., & Ye, J. (2013). Electrochemical behavior of metal–organic framework MIL-101 modified carbon paste electrode: An excellent candidate for electroanalysis. *Journal of Electroanalytical Chemistry, 709*, 65-69.

Li, Z.Q., Qiu, L.G., Xu, T., Wu, Y., Wang, W., Wu, Z.Y., & Jiang, X. (2009). Ultrasonic synthesis of the microporous metal–organic framework $Cu_3(BTC)_2$ at ambient temperature and pressure: an efficient and environmentally friendly method. *Materials Letters, 63*(1), 78-80.

Lightfoot, P., Woodcock, D. A., Maple, M. J., Villaescusa, L. A., & Wright, P. A. (2001). The widespread occurrence of negative thermal expansion in zeolites basis of a presentation given at Materials Discussion No. 3, 26–29 September,

2000, University of Cambridge, UK. *Journal of Materials Chemistry, 11*(1), 212-216.

Lin, K.Y. A., & Lee, W.D. (2016). Self-assembled magnetic graphene supported ZIF-67 as a recoverable and efficient adsorbent for benzotriazole. *Chemical Engineering Journal, 284*, 1017-1027.

Lin, Z.J., Lü, J., Hong, M., & Cao, R. (2014). Metal–organic frameworks based on flexible ligands (FL-MOFs): structures and applications. *Chemical Society Reviews, 43*(16), 5867-5895.

Liu, J., Bo, X., Yang, J., Yin, D., & Guo, L. (2017). One-step synthesis of porphyrinic iron-based metal-organic framework/ordered mesoporous carbon for electrochemical detection of hydrogen peroxide in living cells. *Sensors and Actuators B: Chemical*, *248*, 207-213.

Liu, X.B., Huang, C.M., Dong, G.Y., & Cui, G.H. (2015). Three nickel (II) coordination polymers with flexible bis (benzimidazole) and tetrabromoterephthalate ligands. *Transition Metal Chemistry, 40*(8), 847-856.

Liu, Y., Ma, Y., Zhao, Y., Sun, X., Gándara, F., Furukawa, H., Suenaga, K. (2016). Weaving of organic threads into a crystalline covalent organic framework. *Science, 351*(6271), 365-369.

Lock, N., Wu, Y., Christensen, M., Cameron, L. J., Peterson, V. K., Bridgeman, A. J., Iversen, B. B. (2010). Elucidating negative thermal expansion in MOF-5. *The Journal of Physical Chemistry C, 114*(39), 16181-16186.

Low, K.H., Roy, V., Chui, S. S.Y., Chan, S. L.F., & Che, C.M. (2010). Highly conducting two-dimensional copper (i) 4-hydroxythiophenolate network. *Chemical Communications, 46*(39), 7328-7330.

Lu, X., Zhai, T., Zhang, X., Shen, Y., Yuan, L., Hu, B., Zhou, J. (2012). WO3–x@ Au@ MnO2 Core–Shell Nanowires on Carbon Fabric for High-Performance Flexible Supercapacitors. *Advanced Materials, 24*(7), 938-944.

Ma, D.Y., Guo, H.F., Qin, L., Li, Y., Ruan, Q.T., Huang, Y.W., & Xu, J. (2014). Construction of a new 2D cadmium (II) coordination polymer based on N-and O-donor ligands: synthesis, luminescence and biological activities. *Journal of Chemical Crystallography, 44*(2), 63-69.

Ma, J., Yu, F., Zhou, L., Jin, L., Yang, M., Luan, J., Chen, J. (2012). Enhanced adsorptive removal of methyl orange and methylene blue from aqueous solution

by alkali-activated multiwalled carbon nanotubes. *ACS Applied Materials & Interfaces, 4*(11), 5749-5760.

Ma, W., Jiang, Q., Yu, P., Yang, L., & Mao, L. (2013). Zeolitic imidazolate framework-based electrochemical biosensor for in vivo electrochemical measurements. *Analytical Chemistry, 85*(15), 7550-7557.

Macrae, C.F., Bruno, I.J., Chisholm, J.A., Edgington, P.R., McCabe, P., Pidcock, E., Rodriguez-Monge, L., Taylor, R., Streek, J.V. and Wood, P.A. (2008). Mercury CSD 2.0–new features for the visualization and investigation of crystal structures. *Journal of Applied Crystallography, 41*(2), 466-470.

Majumder, A., Rosair, G. M., Mallick, A., Chattopadhyay, N., & Mitra, S. (2006). Synthesis, structures and fluorescence of nickel, zinc and cadmium complexes with the N, N, O-tridentate Schiff base N-2-pyridylmethylidene-2-hydroxy-phenylamine. *Polyhedron, 25*(8), 1753-1762.

Mamun, M., Ahmed, O., Bakshi, P., & Ehsan, M. (2010). Synthesis and spectroscopic, magnetic and cyclic voltammetric characterization of some metal complexes of methionine:$[(C_5H_{10}NO_2S)_2\ M^{II}]$; M^{II}= Mn (II), Co (II), Ni (II), Cu (II), Zn (II), Cd (II) and Hg (II). *Journal of Saudi Chemical Society, 14*(1), 23-31.

Marimuthu, T., Mahmoudian, M., Mohamad, S., & Alias, Y. (2014). Synthesis and characterization of non-enzymatic hydrogen peroxide sensor of polypyrrole coated cobalt nanocomposites. *Sensors and Actuators B: Chemical, 202*, 1037-1043.

Martinez Joaristi, A., Juan-Alca iz , J., Serra-Crespo, P., Kapteijn, F., & Gascon, J. (2012). Electrochemical synthesis of some archetypical Zn^{2+}, Cu^{2+}, and Al^{3+} metal organic frameworks. *Crystal Growth & Design, 12*(7), 3489-3498.

Maru, M., & Shah, M. (2012). Journal of Chemical and Pharmaceutical Research, 2012, 4 (3): 1638-1643. *Journal Chemical and Pharmaceutical Research., 4*(3), 1638-1643.

Mittal, A., Malviya, A., Kaur, D., Mittal, J., & Kurup, L. (2007). Studies on the adsorption kinetics and isotherms for the removal and recovery of Methyl Orange from wastewaters using waste materials. *Journal of Hazardous Materials, 148*(1), 229-240.

Moon, H. R., Kim, J. H., & Suh, M. P. (2005). Redox-Active Porous Metal–Organic Framework Producing Silver Nanoparticles from Ag^{I} Ions at Room Temperature. *Angewandte Chemie, 117*(8), 1287-1291.

Morozan, A., & Jaouen, F. (2012). Metal organic frameworks for electrochemical applications. *Energy & Environmental Science, 5*(11), 9269-9290.

Morsali, A., & Hashemi, L. (2017). *Main Group Metal Coordination Polymers: Structures and Nanostructures*: John Wiley & Sons.

Mowat, J. P., Groves, J. A., Wharmby, M. T., Miller, S. R., Li, Y., Lightfoot, P., & Wright, P. A. (2009). Lanthanide N, N′-piperazine-bis (methylenephosphonates)(Ln= La, Ce, Nd) that display flexible frameworks, reversible hydration and cation exchange. *Journal of Solid State Chemistry, 182*(10), 2769-2778.

Mueller, U., Puetter, H., Hesse, M., Schubert, M., Wessel, H., Huff, J., & Guzmann, M. (2009). Method for the controlled storage and release of gases using an electrochemically produced crystalline, porous, organometallic skeleton material: Google Patents.

Mueller, U., Schubert, M., Teich, F., Puetter, H., Schierle-Arndt, K., & Pastre, J. (2006). Metal–organic frameworks—prospective industrial applications. *Journal of Materials Chemistry, 16*(7), 626-636.

Mukhopadhyay, A., Padmaja, G., Pal, S., & Pal, S. (2003). Square-planar nickel (II) complexes with a tridentate Schiff base and monodentate heterocycles: self-assembly to dimeric and one-dimensional array via hydrogen bonding. *Inorganic Chemistry Communications, 6*(4), 381-386.

Munakata, M., Wu, L. P., & Kuroda-Sowa, T. (1998). Toward the construction of functional solid-state supramolecular metal complexes containing copper (I) and silver (I). *Advances in Inorganic Chemistry, 46*, 173-303.

Nardecchia, S., Carriazo, D., Ferrer, M. L., Gutiérrez, M. C., & del Monte, F. (2013). Three dimensional macroporous architectures and aerogels built of carbon nanotubes and/or graphene: synthesis and applications. *Chemical Society Reviews, 42(2), 794-830.*

Nezamzadeh-Ejhieh, A., & Esmaeilian, A. (2012). Application of surfactant modified zeolite carbon paste electrode (SMZ-CPE) towards potentiometric determination of sulfate. *Microporous and Mesoporous Materials, 147*(1), 302-309.

Nezamzadeh-Ejhieh, A., & Hashemi, H.S. (2012). Voltammetric determination of cysteine using carbon paste electrode modified with Co (II)-Y zeolite. *Talanta, 88*, 201-208.

Nia, P. M., Lorestani, F., Meng, W. P., & Alias, Y. (2015). A novel non-enzymatic H_2O_2 sensor based on polypyrrole nanofibers–silver nanoparticles decorated reduced graphene oxide nano composites. *Applied Surface Science, 332*, 648-656.

Niranjana, E., Swamy, B. K., Naik, R. R., Sherigara, B., & Jayadevappa, H. (2009). Electrochemical investigations of potassium ferricyanide and dopamine by sodium dodecyl sulphate modified carbon paste electrode: A cyclic voltammetric study. *Journal of Electroanalytical Chemistry, 631*(1), 1-9.

Nodeh, H. R., Ibrahim, W. A. W., Ali, I., & Sanagi, M. M. (2016). Development of magnetic graphene oxide adsorbent for the removal and preconcentration of As (III) and As (V) species from environmental water samples. *Environmental Science and Pollution Research international, 23*(10), 9759.

Önal, Z., Zengin, H., & Sönmez, M. (2011). Synthesis, characterization, and photoluminescence properties of Cu (II), Co (II), Ni (II), and Zn (II) complexes of N-aminopyrimidine-2-thione. *Turkish Journal of Chemistry, 35*(6), 905-914.

Oxford Diffraction, C. P., Oxford Diffr. Ltd., Abingdon, Oxfordshire, England. (2013). .

Park, J.H., Park, S.H., & Jhung, S.H. (2009). Microwave-Syntheses of Zeolitic Imidazolate Framework Material, ZIF-8. *Journal of the Korean Chemical Society, 53*(5), 553-559.

Parnham, E. R., & Morris, R. E. (2007). Ionothermal synthesis of zeolites, metal–organic frameworks, and inorganic–organic hybrids. *Accounts of Chemical Research, 40*(10), 1005-1013.

Parthiban, C., Ciattini, S., Chelazzi, L., & Elango, K. P. (2016). Colorimetric sensing of anions by Cu (II), Co (II), Ni (II) and Zn (II) complexes of naphthoquinone-imidazole hybrid—Influence of complex formation on selectivity and sensing medium. *Sensors and Actuators B: Chemical, 231,* 768-778.

Paul, S., Bag, S. K., Das, S., Harvill, E. T., & Dutta, C. (2008). Molecular signature of hypersaline adaptation: insights from genome and proteome composition of halophilic prokaryotes. *Genome Biology, 9*(4), R70.

Pettinari, C., Marchetti, F., Cingolani, A., Troyanov, S., & Drozdov, A. (1998). Ligation properties of N-substituted imidazoles: synthesis, spectroscopic and structural investigation, and behaviour in solution of zinc (II) and cadmium (II) complexes. *Polyhedron, 17*(10), 1677-1691.

Pichon, A., & James, S. L. (2008). An array-based study of reactivity under solvent-free mechanochemical conditions—insights and trends. *Crystal Engineering Communication, 10*(12), 1839-1847.

Pietraszkiewicz, O., Koźbiał, M., Pietraszkiewicz, M. (1998). Charge transfer complexes involving calix [4] resorcinarenes: potential candidates for non-linear optics. *Advanced Materials for Optics and Electronics, 8*(5), 277-284.

Polak, J., Jarosz-Wilkolazka, A., Szuster-Ciesielska, A., Wlizlo, K., Kopycinska, M., Sojka-Ledakowicz, J., & Lichawska-Olczyk, J. (2016). Toxicity and dyeing properties of dyes obtained through laccase-mediated synthesis. *Journal of Cleaner Production, 112*, 4265-4272.

Poulsen, R., Overgaard, J., Chevallier, M.A., Clausen, H., & Iversen, B. (2005). A gadolinium-based metal–organic framework, poly [[tris (μ4-benzene-1, 4-dicarboxylato) bis (μ2-N, N-diethylformamide) digadolinium (III)] monohydrate]. *Acta Crystallographica Section E: Structure Reports Online, 61*(7), m1337-m1339.

Prier, C. K., Rankic, D. A., & MacMillan, D. W. (2013). Visible light photoredox catalysis with transition metal complexes: applications in organic synthesis. *Chemical Reviews, 113*(7), 5322-5363.

Quiñones, I., & Guiochon, G. (1996). Derivation and application of a Jovanovic–Freundlich isotherm model for single-component adsorption on heterogeneous surfaces. *Journal of Colloid and Interface Science, 183*(1), 57-67.

Rachuri, Y., Parmar, B., Bisht, K. K., & Suresh, E. (2016). Mixed ligand two dimensional Cd (II)/Ni (II) metal organic frameworks containing dicarboxylate and tripodal N-donor ligands: Cd (II) MOF is an efficient luminescent sensor for detection of picric acid in aqueous media. *Dalton Transactions, 45*(18), 7881-7892.

Refat, M. S., El-Korashy, S. A., Kumar, D. N., & Ahmed, A. S. (2008). FTIR, magnetic, 1 H NMR spectral and thermal studies of some chelates of caproic acid: Inhibitory effect on different kinds of bacteria. *Spectrochimica Acta Part A: Molecular and Biomolecular Spectroscopy, 70*(1), 217-233.

Ramaswamy, P., Wong, N. E., & Shimizu, G. K. (2014). MOFs as proton conductors–challenges and opportunities. *Chemical Society Reviews*, *43*(16), 5913-5932.

Robin, A. Y., & Fromm, K. M. (2006). Coordination polymer networks with O-and N-donors: what they are, why and how they are made. *Coordination Chemistry Reviews, 250*(15), 2127-2157.

Rosi, N. L., Eckert, J., Eddaoudi, M., Vodak, D. T., Kim, J., O'keeffe, M., & Yaghi, O. M. (2003). Hydrogen storage in microporous metal-organic frameworks. *Science, 300*(5622), 1127-1129.

Rosi, N. L., Eddaoudi, M., Kim, J., O'Keeffe, M., & Yaghi, O. M. (2002). Advances in the chemistry of metal-organic frameworks. *Crystal Engineering Communication, 4*(68), 401-404.

Rowsell, J. L., Spencer, E. C., Eckert, J., Howard, J. A., & Yaghi, O. M. (2005). Gas adsorption sites in a large-pore metal-organic framework. *Science, 309*(5739), 1350-1354.

Rubianes, M. a. D., & Rivas, G. A. (2003). Carbon nanotubes paste electrode. *Electrochemistry Communications, 5*(8), 689-694.

Sabo, M., Henschel, A., Fröde, H., Klemm, E., & Kaskel, S. (2007). Solution infiltration of palladium into MOF-5: synthesis, physisorption and catalytic properties. *Journal of Materials Chemistry, 17*(36), 3827-3832.

Sachdev, D., Maheshwari, P. H., & Dubey, A. (2016). Piperazine functionalized mesoporous silica for selective and sensitive detection of ascorbic acid. *Journal of Porous Materials, 23*(1), 123-129.

Sa , Y. i., Kutsal, T. (1996). Fully Competitive Biosorption of Chromium (VI) and Iron (III) Ions from Binary Metal Mixtures by R-Arrhizus-Use of the Competitive Langmuir Model. *Process Biochemistry, 31*(6), 573-585.

Sahiner, N., Sel, K., Ozturk, O. F., Demirci, S., & Terzi, G. (2014). Facile synthesis and characterization of trimesic acid-Cu based metal organic frameworks. *Applied Surface Science, 314*, 663-669.

Salehi, M., Dutkiewicz, G., Rezaei, A., Amoozadeh, A., Rahmani, S., Grivani, G. H., & Kubicki, M. (2012). Synthesis, antibacterial studies and crystal structures of tridentate schiff base ligand and it‘s cobalt (III) complex. *Journal of Chemical Crystallography, 42*(8), 871-878.

Saral, H., Özdamar, Ö., Uçar, İ. (2017). Synthesis, structural and spectroscopic studies of two new benzimidazole derivatives: A comparative study. *Journal of Molecular Structure, 1130*, 46-54.

Schoedel, A., & Yaghi, O. M. (2016). *Porosity in Metal–Organic Compounds. Macrocyclic and Supramolecular Chemistry: How Izatt-Christensen Award Winners Shaped the Field, 200.*

Sel, K., Demirci, S., Meydan, E., Yildiz, S., Ozturk, O. F., Al-Lohedan, H., & Sahiner, N. (2015a). Benign Preparation of Metal-Organic Frameworks of Trimesic Acid and Cu, Co or Ni for Potential Sensor Applications. *Journal of Electronic Materials, 44*(1), 136.

Sel, K., Demirci, S., Meydan, E., Yildiz, S., Ozturk, O. F., Al-Lohedan, H., & Sahiner, N. (2015b). Benign Preparation of Metal–Organic Frameworks of Trimesic Acid and Cu, Co or Ni for Potential Sensor Applications. *Journal of Electronic Materials, 44*(1), 136-143.

Sel, K., Demirci, S., Ozturk, O. F., Aktas, N., & Sahiner, N. (2015). NH_3 gas sensing applications of metal organic frameworks. *Microelectronic Engineering, 136*, 71-76.

Seo, Y.K., Hundal, G., Jang, I. T., Hwang, Y. K., Jun, C.H., & Chang, J.S. (2009). Microwave synthesis of hybrid inorganic–organic materials including porous Cu_3 $(BTC)_2$ from Cu (II)-trimesate mixture. *Microporous and Mesoporous Materials, 119*(1), 331-337.

Seward, C., Jia, W. L., Wang, R. Y., Enright, G. D., & Wang, S. (2004). Luminescent 2D Macrocyclic Networks Based on Starburst Molecules:$[\{Ag(CF_3SO_3)\}_{1.5}$ (tdapb)] and $[\{Ag\ (NO_3)\ \}_3$ (tdapb)]. *Angewandte Chemie International Edition, 43*(22), 2933-2936.

Shahabuddin, S., Muhamad Sarih, N., Mohamad, S., & Joon Ching, J. (2016). SrTiO3 Nanocube-Doped Polyaniline Nanocomposites with Enhanced Photocatalytic Degradation of Methylene Blue under Visible Light. *Polymers, 8*(2), 27.

Shakeel, F., Haq, N., Alanazi, F. K., & Alsarra, I. A. (2016). Removal of methyl orange from aqueous solution by EA/Triton-X100/EG/water green nanoemulsions. *Desalination and Water Treatment, 57*(2), 747-753.

Shang, L., & Dong, S. (2009). Design of fluorescent assays for cyanide and hydrogen peroxide based on the inner filter effect of metal nanoparticles. *Analytical Chemistry, 81*(4), 1465-1470.

Sheldrick, G. M. (2015). Crystal structure refinement with SHELXL. *Acta Crystallographica Section C: Structural Chemistry, 71*(1), 3-8.

Sheng, S.N., Han, Y., Wang, B., Zhao, C., Yang, F., Zhao, M.J., Li, J.R. (2016). A novel porous anionic metal–organic framework with pillared double-layer structure for selective adsorption of dyes. *Journal of Solid State Chemistry, 233*, 143-149.

Son, W.J., Kim, J., Kim, J., & Ahn, W.S. (2008). Sonochemical synthesis of MOF-5. *Chemical Communications* (47), 6336-6338.

Song, L., Zhang, J., Sun, L., Xu, F., Li, F., Zhang, H., Liu, S. (2012). Mesoporous metal–organic frameworks: design and applications. *Energy & Environmental Science, 5*(6), 7508-7520.

Špalek, O., Balej, J., Paseka, I. (1982). Kinetics of the decomposition of hydrogen peroxide in alkaline solutions. *Journal of the Chemical Society, Faraday Transactions 1: Physical Chemistry in Condensed Phases, 78*(8), 2349-2359.

Spek, A. L. (2009). Structure validation in chemical crystallography. *Acta Crystallographica Section D: Biological Crystallography, 65*(2), 148-155.

Sponza, D. T. (2006). Toxicity studies in a chemical dye production industry in Turkey. *Journal of Hazardous Materials, 138*(3), 438-447.

Stock, N., & Biswas, S. (2011). Synthesis of metal-organic frameworks (MOFs): routes to various MOF topologies, morphologies, and composites. *Chemical Reviews, 112*(2), 933-969.

Suh, M. P., Moon, H. R., Lee, E. Y., & Jang, S. Y. (2006). A redox-active two-dimensional coordination polymer: preparation of silver and gold nanoparticles and crystal dynamics on guest removal. *Journal of the American Chemical Society, 128*(14), 4710-4718.

Sun, L., Hendon, C. H., Minier, M. A., Walsh, A., Dincă, M. (2015). Million-fold electrical conductivity enhancement in Fe_2 (DEBDC) versus Mn_2 (DEBDC)(E= S, O). *Journal of American Chemical Society, 137*(19), 6164-6167.

Sun, L., Miyakai, T., Seki, S., Dincă, M. (2013). Mn_2(2, 5-disulfhydrylbenzene-1, 4-dicarboxylate): A Microporous Metal–Organic Framework with Infinite (− Mn–S−)∞ Chains and High Intrinsic Charge Mobility. *Journal of the American Chemical Society, 135*(22), 8185-8188.

Suslick, K. S., Hammerton, D. A., & Cline, R. E. (1986). Sonochemical hot spot. *Journal of the American Chemical Society, 108*(18), 5641-5642.

Sutra, P., Igau, A. (2016). Anionic phosph (in) ito (–phosphoryl") ligands: Non-classical –actor" phosphane-type ligands in coordination chemistry. *Coordination Chemistry Reviews, 308,* 97-116.

Takaishi, S., Hosoda, M., Kajiwara, T., Miyasaka, H., Yamashita, M., Nakanishi, Y., .Kitagawa, H. (2008). Electroconductive porous coordination polymer Cu[Cu

$(pdt)_2$] composed of donor and acceptor building units. *Inorganic Chemistry, 48*(19), 9048-9050.

Tranchemontagne, D. J., Hunt, J. R., & Yaghi, O. M. (2008). Room temperature synthesis of metal-organic frameworks: MOF-5, MOF-74, MOF-177, MOF-199, and IRMOF-0. *Tetrahedron, 64*(36), 8553-8557.

Tsai, C. N., Mazumder, S., Zhang, X. Z., Schlegel, H. B., Chen, Y. J., & Endicott, J. F. (2015). Metal-to-Ligand Charge-Transfer Emissions of Ruthenium (II) Pentaammine Complexes with Monodentate Aromatic Acceptor Ligands and Distortion Patterns of their Lowest Energy Triplet Excited States. *Inorganic Chemistry, 54*(17), 8495-8508.

Unuabonah, E. I., Adebowale, K. O., & Dawodu, F. A. (2008). Equilibrium, kinetic and sorber design studies on the adsorption of Aniline blue dye by sodium tetraborate-modified Kaolinite clay adsorbent. *Journal of Hazardous Materials, 157*(2), 397-409.

Valente, C., Choi, E., Belowich, M. E., Doonan, C. J., Li, Q., Gasa, T. B., Stoddart, J. F. (2010). Metal–organic frameworks with designed chiral recognition sites. *Chemical Communications, 46*(27), 4911-4913.

Valvekens, P., Vermoortele, F., & De Vos, D. (2013). Metal–organic frameworks as catalysts: the role of metal active sites. *Catalysis Science & Technology, 3*(6), 1435-1445.

Wang, C., Zhang, T., & Lin, W. (2011). Rational synthesis of noncentrosymmetric metal–organic frameworks for second-order nonlinear optics. *Chemical Reviews, 112*(2), 1084-1104.

Wang, J., Groeneveld, A., Oikonomou, M., Prusova, A., Van As, H., van Lent, J. W., & Velders, A. H. (2016). Revealing and tuning the core, structure, properties and function of polymer micelles with lanthanide-coordination complexes. *Soft Matter, 12*(1), 99-105.

Wang, L., Li, Y.A., Yang, F., Liu, Q.K., Ma, J.P., & Dong, Y.B. (2014). Cd (II)-MOF: Adsorption, separation, and guest-dependent luminescence for monohalobenzenes. *Inorganic Chemistry, 53*(17), 9087-9094.

Wang, L., Yan, Z.H., Xiao, Z., Guo, D., Wang, W., & Yang, Y. (2013). Reactant ratio-modulated entangled Cd (II) coordination polymers based on rigid tripodal imidazole ligand and tetrabromoterephthalic acid: interpenetration, interdigitation and self-penetration. *Crystal Engineering Communication, 15*(27), 5552-5560.

Wang, M.Q., Zhang, Y., Bao, S.J., Yu, Y.N., & Ye, C. (2016). Ni (II)-Based Metal-Organic Framework Anchored on Carbon Nanotubes for Highly Sensitive Non-Enzymatic Hydrogen Peroxide Sensing. *Electrochimica Acta, 190,* 365-370.

Wang, Q., Xia, Y., & Jiang, C. (2014). Mesoporous nanobelts and nano-necklaces of Co_3O_4 converted from β-Co $(OH)_2$ nanobelts via a thermal decomposition route for the electrocatalytic oxidation of H_2O_2. *Crystal Engineering Communication, 16*(41), 9721-9726.

Wang, Y., Ma, X., Wen, Y., Xing, Y., Zhang, Z., & Yang, H. (2010). Direct electrochemistry and bioelectrocatalysis of horseradish peroxidase based on gold nano-seeds dotted TiO_2 nanocomposite. *Biosensors and Bioelectronics, 25*(11), 2442-2446.

Wang, Y., Zhang, C., Li, H., Zhu, G., Bao, S.S., Wei, S., Xu, Z. (2015). Synthesis, characterization and in vitro anticancer activity of the biomolecule-based coordination complex nanotubes. *Journal of Materials Chemistry B*, *3*(2), 296-305.

Wu, C. F., Chen, W. Y., & Lee, J. F. (1996). Microcalorimetric studies of the interactions of imidazole with immobilized Cu(II): Effects of pH value and salt concentration. *Journal of colloid and Interface Science, 183*(1), 236-242.

Wu, J., Xu, J.W., Liu, W.C., Yang, S.Z., Luo, M.M., Han, Y. Y., Batten, S. R. (2016). Designed metal–organic framework based on metal–organic polyhedron: Drug delivery. *Inorganic Chemistry Communications, 71*, 32-34.

Wu, Y., Kobayashi, A., Halder, G. J., Peterson, V. K., Chapman, K. W., Lock, N., Kepert, C. J. (2008). Negative Thermal Expansion in the Metal–Organic Framework Material Cu_3 (1, 3, 5-benzenetricarboxylate)$_2$. *Angewandte Chemie International Edition, 47*(46), 8929-8932.

Xing, Y. H., Han, J., Zhou, G. H., Sun, Z., Zhang, X. J., Zhang, B. L., Ge, M. F. (2008). Syntheses and structures of mononuclear and binuclear transition metal complexes (Cu, Zn, Ni) with (salicylideneglycine and imidazole). *Journal of Coordination Chemistry, 61*(5), 715-730.

Xu, Q., Wang, Y., Jin, G., Jin, D., Li, K., Mao, A., & Hu, X. (2014). Photooxidation assisted sensitive detection of trace Mn^{2+} in tea by NH_2-MIL-125 (Ti) modified carbon paste electrode. *Sensors and Actuators B: Chemical, 201*, 274-280.

Xu, Y., Jin, J., Li, X., Han, Y., Meng, H., Song, C., & Zhang, X. (2015). Magnetization of a Cu (II)1, 3, 5-benzenetricarboxylate metal-organic framework for efficient solid-phase extraction of Congo Red. *Microchimica Acta, 182*(13-14), 2313-2320.

Yaghi, O., Davis, C. E., Li, G., & Li, H. (1997). Selective guest binding by tailored channels in a 3-D porous zinc (II)-benzenetricarboxylate network. *Journal of the American Chemical Society, 119*(12), 2861-2868.

Yaghi, O. M. (2000). Departments-leading the Way-A molecular world full of holes. *Chemical Innovation, 30*(10), 3-4.

Yaghi, O. M., O'Keeffe, M., Ockwig, N. W., Chae, H. K., Eddaoudi, M., & Kim, J. (2003). Reticular synthesis and the design of new materials. *Nature, 423*(6941), 705-714.

Yam, V. W.W., Au, V. K.M., & Leung, S. Y.L. (2015). Light-Emitting Self-Assembled Materials Based on d^8 and d^{10} Transition Metal Complexes. *Chemical Reviews, 115*(15), 7589-7728.

Yang, D.A., Cho, H.Y., Kim, J., Yang, S.T., & Ahn, W.S. (2012). CO_2 capture and conversion using Mg-MOF-74 prepared by a sonochemical method. *Energy & Environmental Science, 5*(4), 6465-6473.

Yang, L., Peng, Y., Bian, F., Yan, S.p., Liao, D.z., Cheng, P., & Jiang, Z.h. (2005). Structure and magnetic properties of a dinuclear complex $[Cu_2(TPA)_2$ (o-phth)$](ClO_4)_2$. *Journal of Chemical Crystallography, 35*(7), 555-559.

Yang, L., Xu, C., Ye, W., & Liu, W. (2015). An electrochemical sensor for H_2O_2 based on a new Co-metal-organic framework modified electrode. *Sensors and Actuators B: Chemical, 215*, 489-496.

Yap, K. K., & Neuhaus, S. J. (2016). Making cancer visible–Dyes in surgical oncology. Surgical Oncology, 25(1), 30-36.

Yasemin, A. (2016). Photoluminescence properties of Gd (III) and Ce (III) lanthanide based metal organic frameworks. Acta Crystallography. Section. C. Structural. Chemistry, 72, 426-431..

Yilmaz, E., Memon, S., & Yilmaz, M. (2010). Removal of direct azo dyes and aromatic amines from aqueous solutions using two β-cyclodextrin-based polymers. *Journal of Hazardous Materials, 174*(1), 592-597.

Youngs, W. J., Tessier, C. A., & Bradshaw, J. D. (1999). Ortho-arene cyclynes, related heterocyclynes, and their metal chemistry. *Chemical Reviews, 99*(11), 3153-3180.

Yu, S., Jiang, Z., Ding, H., Pan, F., Wang, B., Yang, J., & Cao, X. (2015). Elevated pervaporation performance of polysiloxane membrane using channels and active

sites of metal organic framework CuBTC. *Journal of Membrane Science, 481*, 73-81.

Yuan, B., Zhang, J., Zhang, R., Shi, H., Guo, X., Guo, Y., Zhang, D. (2015). Electrochemical and electrocatalytic properties of a stable Cu-based metal–organic framework. *International Journal of Electrochemical Science, 10*, 4899-4910.

Zare, M. A., Husain, S. W., Tehrani, M. S., & Azar, P. A. (2017). Pentaazatetraethylene supported polyacrylamide (PAA-N5) as a novel adsorbent for the efficient removal of industrial dyes from aqueous solutions: adsorption isotherms and kinetics. *Monatshefte für Chemie-Chemical Monthly*, *2*(148), 191-197.

Zhang, C., Wang, M., Liu, L., Yang, X., & Xu, X. (2013). Electrochemical investigation of a new Cu-MOF and its electrocatalytic activity towards H_2O_2 oxidation in alkaline solution. *Electrochemistry Communications, 33*, 131-134.

Zhang, D., Zhang, J., Shi, H., Guo, X., Guo, Y., Zhang, R., & Yuan, B. (2015). Redox-active microsized metal-organic framework for efficient nonenzymatic H_2O_2 sensing. *Sensors and Actuators B: Chemical, 221*, 224-229.

Zhang, M., Chen, C., Wang, Q., Fu, W., Huang, K., & Zhou, W. (2017). A metal–organic framework functionalized with piperazine exhibiting enhanced CH_4 storage. *Journal of Materials Chemistry A, 5*(1), 349-354.

Zhang, Y., Bo, X., Luhana, C., Wang, H., Li, M., & Guo, L. (2013). Facile synthesis of a Cu-based MOF confined in macroporous carbon hybrid material with enhanced electrocatalytic ability. *Chemical Communications, 49*(61), 6885-6887.

Zhang, Z., Yoshikawa, H., & Awaga, K. (2014). Monitoring the solid-state electrochemistry of Cu(2, 7-AQDC)(AQDC= anthraquinone dicarboxylate) in a lithium battery: coexistence of metal and ligand redox activities in a metal–organic framework. *Journal of the American Chemical Society, 136*(46), 16112-16115.

Zhao, B., Liu, Z., Liu, Z., Liu, G., Li, Z., Wang, J., & Dong, X. (2009). Silver microspheres for application as hydrogen peroxide sensor. *Electrochemistry Communications, 11*(8), 1707-1710.

Zhu, H.F., Zhao, W., Okamura, T.a., Fei, B.L., Sun, W.Y., & Ueyama, N. (2002). Self-assembly of a snake-like blue photoluminescent coordination polymer from 4, 4′-bis (imidazol-1-ylmethyl) biphenyl and zinc acetate. *New Journal of Chemistry, 26*(10), 1277-1279.

LIST OF PUBLICATIONS AND PRESENTATIONS

1. **Sherino, B**., Mohamad, S., Manan, N. S. A., Ahmad, J., Kamboh, M. A., Khor, S. M., Halim, S. N. A. (2017). Synthesis, characterization, photoluminescence, and electrochemical studies of novel mononuclear Cu (II) and Zn (II) complexes with the 1-benzylimidazolium ligand. *Journal of Molecular Structure, 1141*, 31-38 (published).

2. **Sherino, B**., Mohamad, S., Halim, S. N. A., & Manan, N. S. A. (2018). Electrochemical detection of hydrogen peroxide on a new microporous Ni–metal organic framework material-carbon paste electrode. *Sensors and Actuators B: Chemical, 254*, 1148-1156 (published).

3. **Sherino, B**., Mohamad, S., Manan, N. S. A., Tareen, H., Yamin, B. M., & Halim, S. N. A. (2018). Structural, electrochemical, and adsorption studies of Ni and Zn benzylimidazole coordination polymers with terephthalate linkers. *Transition Metal Chemistry*, *43*(1), 53-64 (published)

4. **Bibi Sherino,** Siti Nadiah Abdul Halim, Ninie Suhana Abdul Manan. " Synthesis of Zn-decorated metal–organic framework materials as adsorbent for removal of carcinogenic textile dye", 7th IWA-ASPIRE CONFERENCE 2017 & Water Malaysia Exhibition 2017 KUALA LUMPUR, MALAYSIA is attending on 11th to 14th September 2017.

Journal of Molecular Structure 1141 (2017) 31–38

Contents lists available at ScienceDirect

Journal of Molecular Structure

journal homepage: http://www.elsevier.com/locate/molstruc

Synthesis, characterization, photoluminescence, and electrochemical studies of novel mononuclear Cu(II) and Zn(II) complexes with the 1-benzylimidazolium ligand

Sherino Bibi [a, b], Sharifah Mohammad [a], Ninie Suhana Abdul Manan [a, c], Jimmy Ahmad [a], Muhammad Afzal Kamboh [e], Sook Mei Khor [a], Bohari M. Yamin [d], Siti Nadiah Abdul Halim [a, *]

[a] Department of Chemistry, Faculty of Science, University of Malaya, 50603, Kuala Lumpur, Malaysia
[b] Department of Chemistry, Sardar Bahadur Khan Women University, Quetta, Balochistan, Pakistan
[c] Center for Ionic Liquids (UMCiL), University Malaya, 50603, Kuala Lumpur, Malaysia
[d] School of Chemical Sciences and Food Technology, University Kebangsaan, Malaysia
[e] School of Chemistry, Shaheed Benazir Bhutto University Shaheed, Benazirabad, Sindh, Pakistan

ARTICLE INFO

Article history:
Received 4 January 2017
Received in revised form
17 March 2017
Accepted 19 March 2017
Available online 21 March 2017

Keywords:
Synthesis
Cu(II) complex
Zn(II) complex
Benzylimidazole
Crystal structure

ABSTRACT

Two new mononuclear coordination complexes $[Cu(bim)_4Cl_2]\cdot 2H_2O$ (**1**) and $[Zn(bim)_2Cl_2]$ (**2**) containing the 1-benzylimidazole (bim) ligand were successfully synthesized. Both complexes were characterized by IR, UV–vis, and fluorescence spectroscopies, single crystal and powder X-ray diffraction measurements, and thermogravimetric analysis. Self-assembly during the recrystallization process resulted in the formation of octahedral and tetrahedral Cu(II) and Zn(II) complexes, respectively. The single crystals obtained are representative of the bulk material, as shown by the powder X-ray diffraction patterns. Cyclic voltammetry measurements showed that complex **1** undergoes a quasi-reversible redox reaction, while complex **2** undergoes reduction alone, and no oxidation peak was observed; this is due to the stability of the reduced form of complex **2**.

1. Introduction

Recently, coordination complexes have become attractive for use in the production of medicines and drugs, primarily because most metals and organic compounds have some biological activity, such as antifungal agents, antibiotics, and anticancer [1,2]. However, coordination complexes also have physical and chemical applications, such as in catalysis, luminescence, hydrometallurgy, and sensors [3–5]. In addition, coordination complexes have been widely used in electrochemical studies because of the different oxidation state of transition metal [6,7].

Coordination complexes contain ligands, which can be ions or neutral molecules, that have lone pairs that can be donated to the central metal atom [8,9]. The ligand can be varied by the donor atom, for example, N, S, O, or P in phosphines [10], alkoxides, imides [11], phosphoramidites [12], and more [13]. Benzylimidazole is a popular N-donor ligand often used in coordination chemistry. The imidazole ring of benzylimidazole is an important component of numerous natural products, including purine, histidine, histamine, and nucleic acids. The exposed imidazole nitrogen atom of benzylimidazole (shown in Fig. 1) can bind as a monodentate ligand to a central metal atom [14,15]. Benzylimidazole is also known to be good Lewis base and metal coordinator because of its pK_a value (approximately 7), and the rotational freedom around the C–N bond in benzylimidazole (shown in Fig. 1, blue color) allows changes in molecular conformation that lead to distinct coordination compound structures [16–18]. A large number of d-block transition metal and imidazole complexes and their derivatives are known to have biological and physiochemical properties [19], and the coordination capability of a number of monodentate benzylimidazole derivatives [20,21].

In this paper, we explore two novel crystal structures of benzylimidazole-based complexes: $[Cu(bim)_4Cl_2]\cdot 2H_2O$ (**1**) and

* Corresponding author.
E-mail address: nadiahhalim@um.edu.my (S.N. Abdul Halim).

http://dx.doi.org/10.1016/j.molstruc.2017.03.032
0022-2860/

Sensors and Actuators B 254 (2018) 1148–1156

Contents lists available at ScienceDirect

Sensors and Actuators B: Chemical

journal homepage: www.elsevier.com/locate/snb

Electrochemical detection of hydrogen peroxide on a new microporous Ni–metal organic framework material-carbon paste electrode

Bibi Sherino [a,b], Sharifah Mohamad [a,c], Siti Nadiah Abdul Halim [a], Ninie Suhana Abdul Manan [a,c,*]

[a] Department of Chemistry, Faculty of Science, University of Malaya, 50603 Kuala Lumpur, Malaysia
[b] Department of Chemistry, Sardar Bahadur Khan Women University, Quetta, Balochistan, Pakistan
[c] University of Malaya Centre for Ionic Liquids (UMCiL), University of Malaya, 50603 Kuala Lumpur, Malaysia

ARTICLE INFO

Article history:
Received 23 March 2017
Received in revised form 4 July 2017
Accepted 1 August 2017
Available online 2 August 2017

Keywords:
Metal organic framework
Piperazine
Adipic acid
MOF material
Electrochemical senor
H_2O_2

ABSTRACT

In this paper a new Ni^{2+} metal organic framework (based on adipic acid as the linker & piperazine as the ligand) (AP-Ni-MOF) was synthesized and has been used as an electrode material (AP-Ni-MOF/CPE) for the detection of H_2O_2. The morphology and formation of AP-Ni-MOF was confirmed by field emission scanning electron microscopy, FT-IR spectroscopy, energy-dispersive spectroscopy, X-ray diffraction, and TGA. AP-Ni-MOF showed high electrochemical activity for the detection of H_2O_2 due to high conductivity *i.e* 1.28×10^{-3} S/cm. Electrochemical studies were carried out for AP-Ni-MOF/CPE by cyclic voltammetry and chrono-amperometry methods. Under optimized condition AP-Ni-MOF/CPE show a dynamic range (0.004 mM to 60 mM) with the limit of detection of 0.0009 mM. The effect of interfering species on the reduction peak current response show a minor change of signals (>5%). The modified electrode has good repeatability due to lifetime stability. AP-Ni-MOF/CPE electrode was also used in real samples (lens cleaner solution) for the detection of H_2O_2 with the recoveries of 94.7–107%.

1. Introduction

The increasing demand of hydrogen peroxide (H_2O_2) sensor were more focused in recent years due to the significance role of hydrogen peroxide in various field such as food industry, fuel cell, chemical synthesis, biotechnology, environmental, clinical and pharmaceutical application [1–4]. In the past decade's electrochemical biosensor based on enzymes have been greatly studied due to their high performance [5–7]. However, the enzyme based electrochemical biosensors are expensive, complicated and effected by temperature and pH due to activity of enzyme. Alternatively, non-enzymatic electrochemical sensors are attracted more attention for the determination of H_2O_2 due to long term stability, high sensitivity, pH free, quick response time and low cost [8–10]. Transition metal oxide, Nobel metals, alloy and nano particles are employed as non-enzyme electrochemical sensor but their application were limited due to poor operating stability and low electronic conductivity [11–14]. In order to overcome these problems, the development of new highly sensitive, selective, fast, low cost non-enzymatic electrode material with the high performance for H_2O_2 detection is still needed.

Nowdays various studies focused on chemically modified electrodes due to their significant advantages. Carbon paste (CP) has become one of the most popular electrode materials used for the preparation of different types of sensors, electrodes and detectors. The CPEs are favoured due to low background, current, wide potential window and low costs. Carbon paste (CP) are being prepared from a non-conductive binder and graphite powder with specific mixing ratio [15]. Applications and properties of CPEs modified with zeolites and metal organic framework have attracted much attention due to its easy fabrication and good stability [16].

Microporous metal organic framework (MOF) materials are new class of crystalline materials formed by metal ions and multidente organic ligand through coordinate covalent bond. In recent years the research involving MOFs were more focused due to significant applications in various fields, such as separation science, ion exchange, gas storage, sensors, energy storage, proton conductivity and catalysis [17–22]. Design and synthesis of different types of metal organic framework for electroanalysis application

* Corresponding author at: Department of Chemistry, Faculty of Science, University of Malaya, 50603 Kuala Lumpur, Malaysia.
E-mail address: ninieman@um.edu.my (N.S. Abdul Manan).

http://dx.doi.org/10.1016/j.snb.2017.08.002
0925-4005/

Transition Metal Chemistry
https://doi.org/10.1007/s11243-017-0193-1

Structural, electrochemical, and adsorption studies of Ni and Zn benzylimidazole coordination polymers with terephthalate linkers

Bibi Sherino[1,2] · Sharifah Mohamad[1,3] · Ninie Suhana Abdul Manan[1,3] · Huma Tareen[2] · Bohari M. Yamin[4] · Siti Nadiah Abdul Halim[1]

Received: 11 August 2017 / Accepted: 3 November 2017

Abstract
Two coordination polymers, $[Ni(bim)_2(L1)(H_2O)_2]_n$ (CP-1) and $[Zn(bim)(L1)(Cl)]_n$ (CP-2) (bim = 1-benzylimidazole, L1 = terephthalic acid), were synthesized and characterized by physicochemical and spectroscopic methods. The Ni(II) center in CP-1 is octahedral, while the Zn(II) center in CP-2 is tetrahedral. CP-1 and CP-2 were used to modify carbon paste electrodes to assess their effect on the electrochemical behavior of ferricyanide. The redox reactions of ferricyanide on both electrodes proved to be reversible and diffusion controlled, with ferricyanide diffusion coefficients for CP-1 and CP-2 of 1.88×10^5 and 3.44×10^5 $cm^2\ s^{-1}$, respectively. These coordination polymers were also investigated for their adsorption behavior toward two dyes: Chicago sky blue and methylene blue. CP-1 and CP-2 both rapidly adsorbed the anionic Chicago sky blue dye by different intermolecular interactions; in contrast, the cationic methylene blue dye was adsorbed to a lesser extent. The adsorption of these CPs depends on the charge but not the size of the dye. Addition of methanolic potassium nitrate solution caused the release of the adsorbed dyes.

Introduction

Coordination polymers (CPs) are defined as inorganic or organometallic polymers containing metal centers linked by organic ligands. Alternatively, a CP can be viewed as a coordination compound with repeating units linked in 1, 2, or 3 dimensions [1, 2]. The investigation of CPs has been driven by the attractive properties of flexible frameworks based on different multifunctional organic bridging ligands and metal centers [3]. The flexibility and steric hindrance of the organic ligands are very important factors in the formation of coordination polymers [4, 5]. The ligand can be varied by the donor atom, for example, N, S, O, or P in phosphines [6], alkoxides, imides [7], phosphoramidites [8], and others [9]. In recent years, there have been many reports of flexible bis(benzimidazole) derivatives which have been used as common N-containing ligands due to their excellent coordination capabilities and potential applications as functional materials. Arylaliphatic spacers can be used to selectively construct the flexible frameworks of CPs [10–12].

Benzylimidazole is a popular N donor ligand often used in coordination chemistry. Its exposed imidazole nitrogen atom is available for coordination to a metal atom. Benzylimidazole is also known to be good Lewis base and metal coordinator because of its pKa value (approximately 7), while the rotational freedom around the C–N bond in benzylimidazole allows for a variety of coordination structures [13]. Furthermore, the presence of $-(CH_2)_n-$ (n = 1–6) spacers provides additional flexibility, consequently allowing for the formation of strong and complex networks [14–17]. Furthermore, such ligands can act as hydrogen bond donors and also form π–π stacking interactions through their imidazole rings [18–20]. Meanwhile, aromatic dicarboxylates are well known to be good co- and bridging ligands, forming large

Electronic supplementary material The online version of this article (https://doi.org/10.1007/s11243-017-0193-1) contains supplementary material, which is available to authorized users.

✉ Siti Nadiah Abdul Halim
nadiahhalim@um.edu.my

[1] Department of Chemistry, Faculty of Science, University Malaya, 50603 Kuala Lumpur, Malaysia

[2] Department of Chemistry, Sardar Bahadur Khan Women University, Quetta, Balochistan, Pakistan

[3] University Malaya Centre for Ionic Liquids (UMCiL), University Malaya Kuala Lumpur, 50603 Kuala Lumpur, Malaysia

[4] Academy of Sciences Malaysia, Jalan Sultan Hj Ahmad Shah Off Jalan Tuanku Abdul Halim, 50480 Kuala Lumpur, Malaysia

Published online: 28 November 2017

APPENDIX

Appendix A: IR spectra of benzylimidazole based coordination polymers.

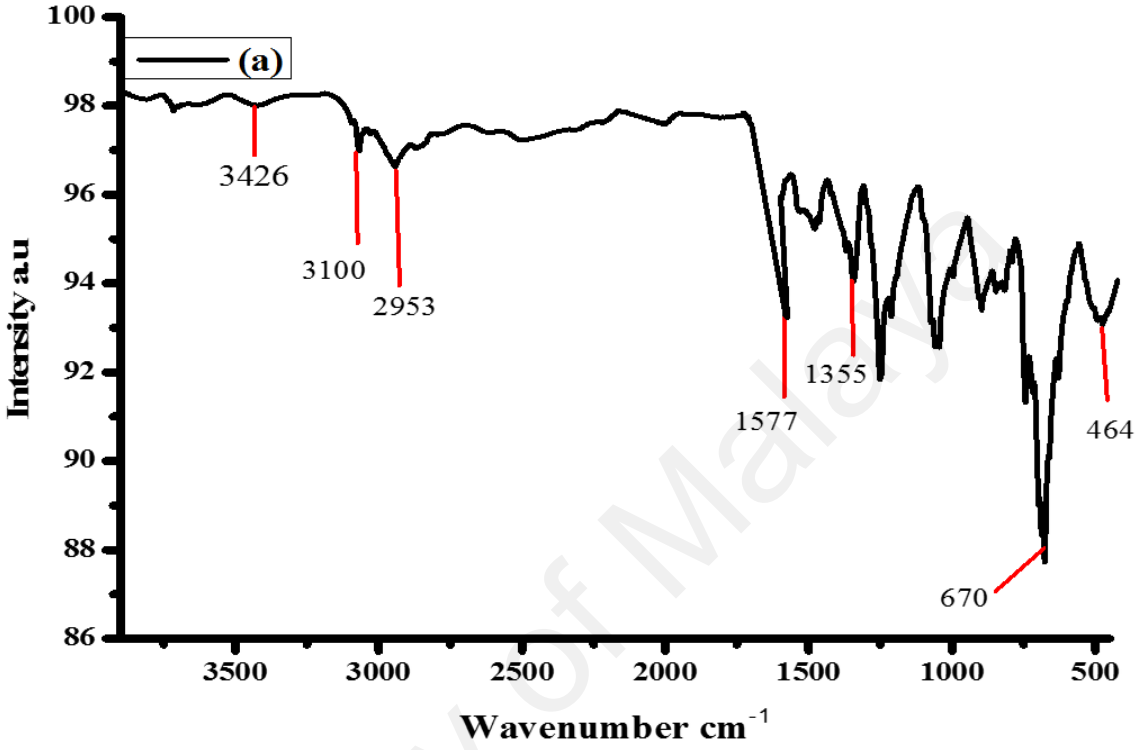

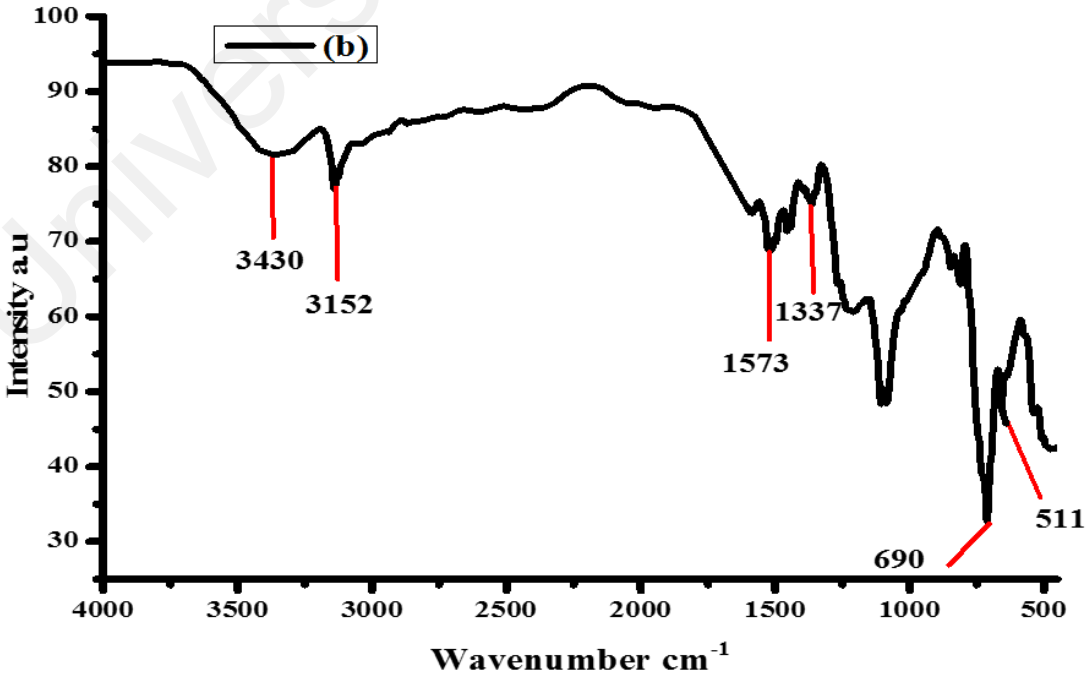

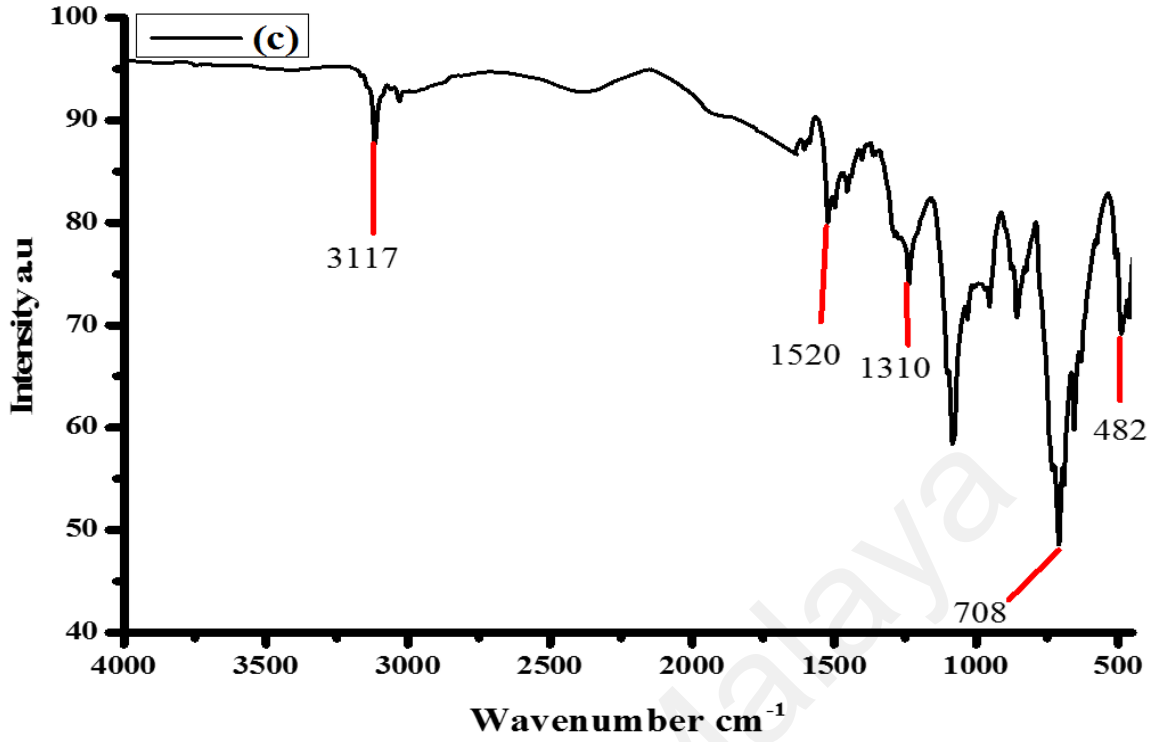

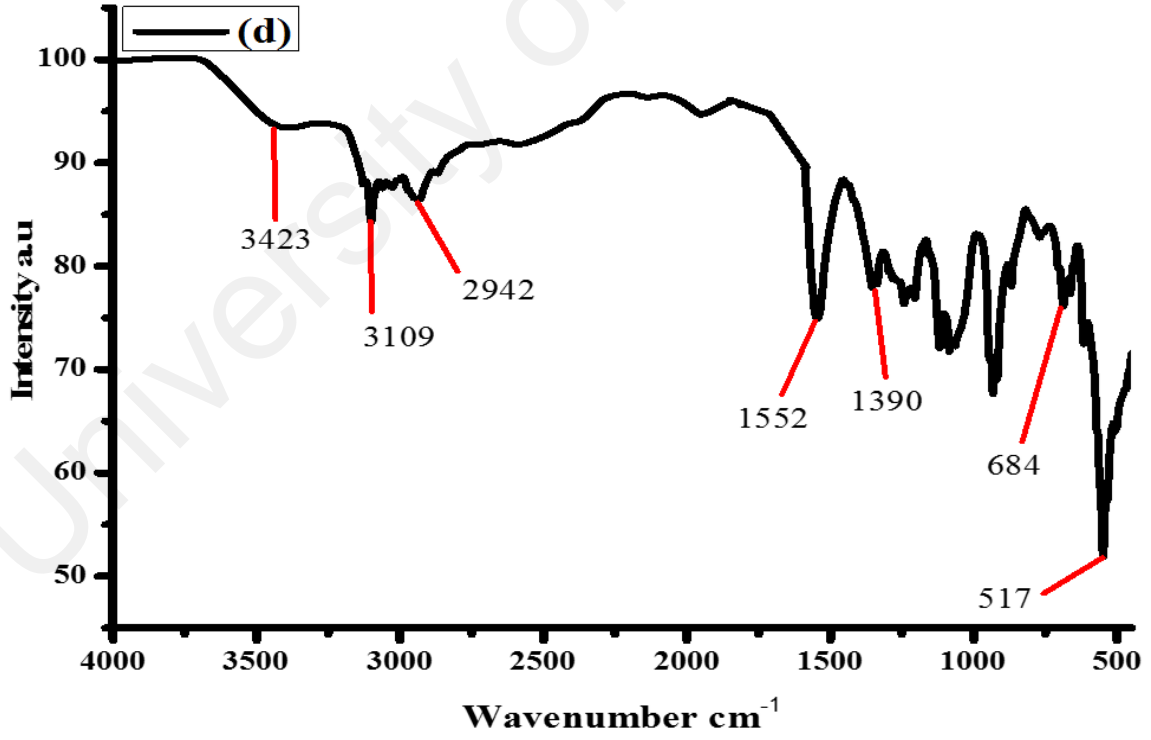

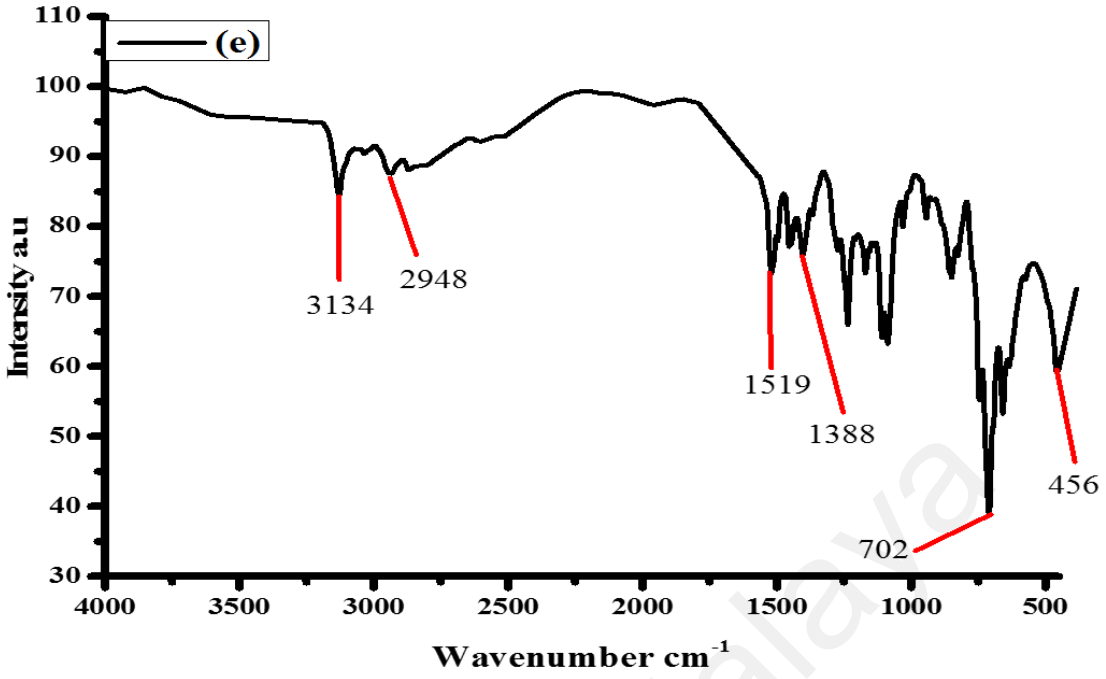

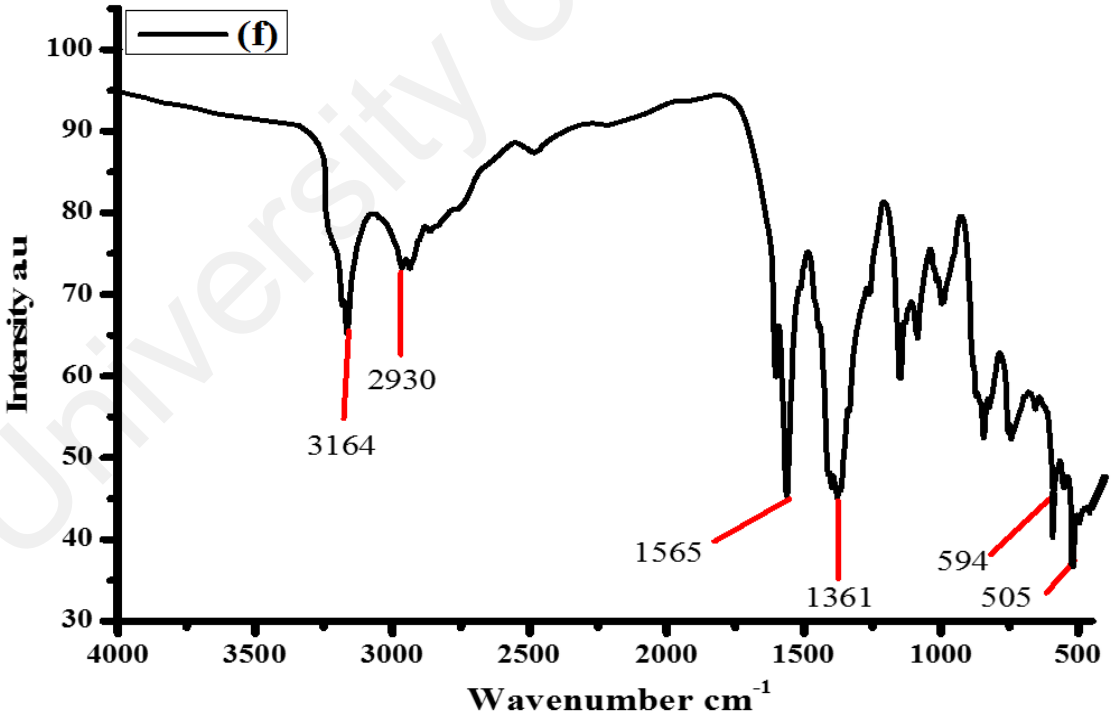

Appendix B: IR spectra of piperazine based coordination polymers.

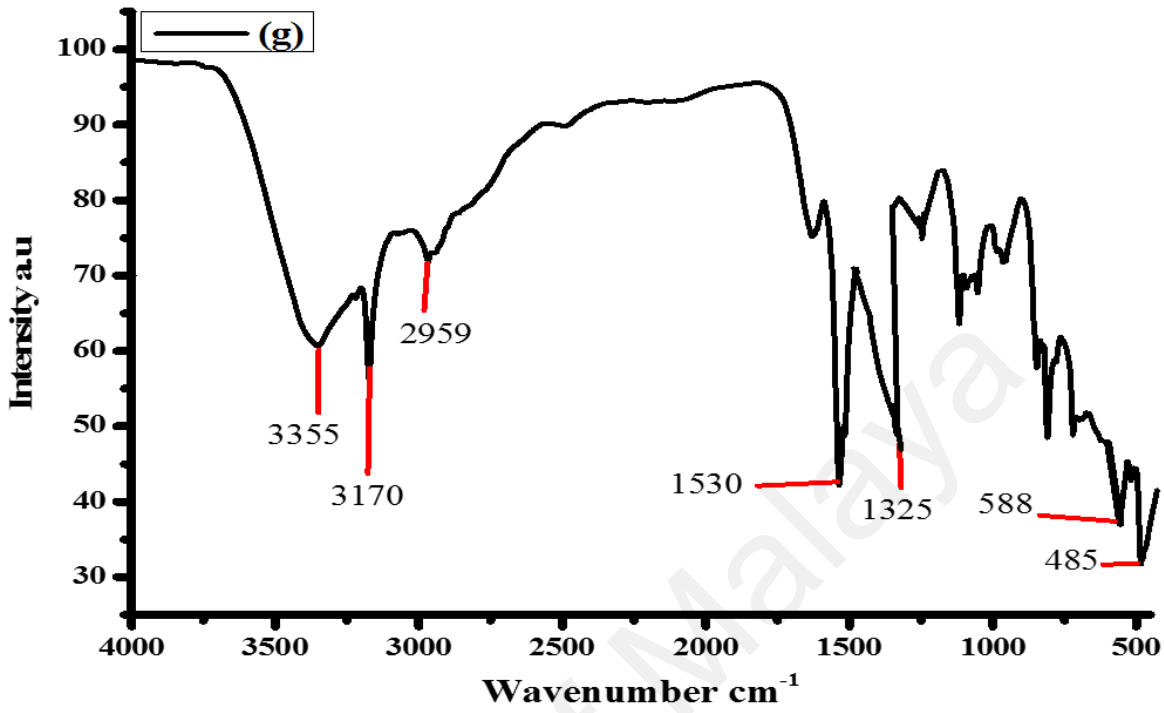

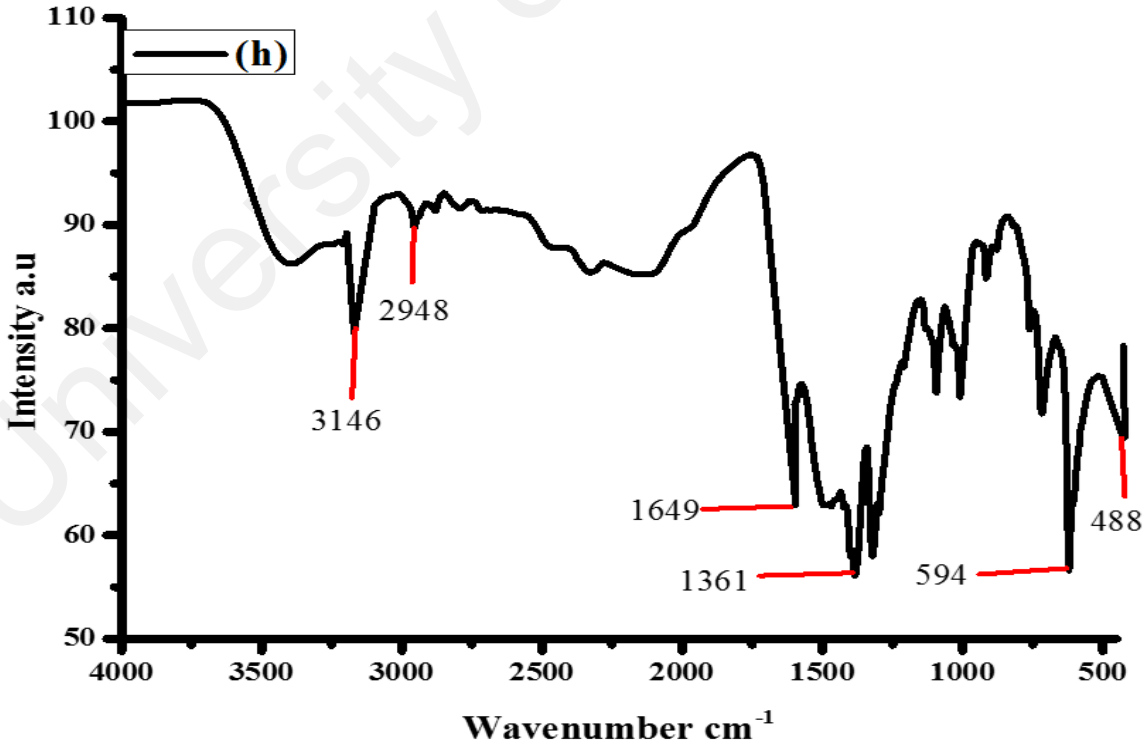

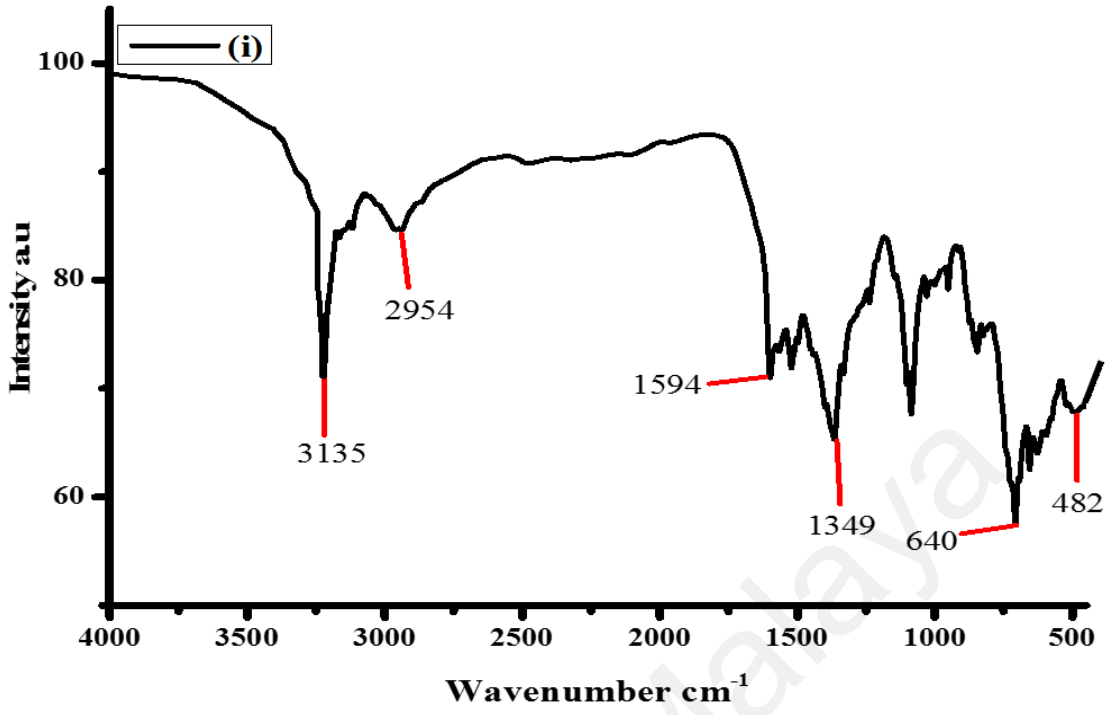

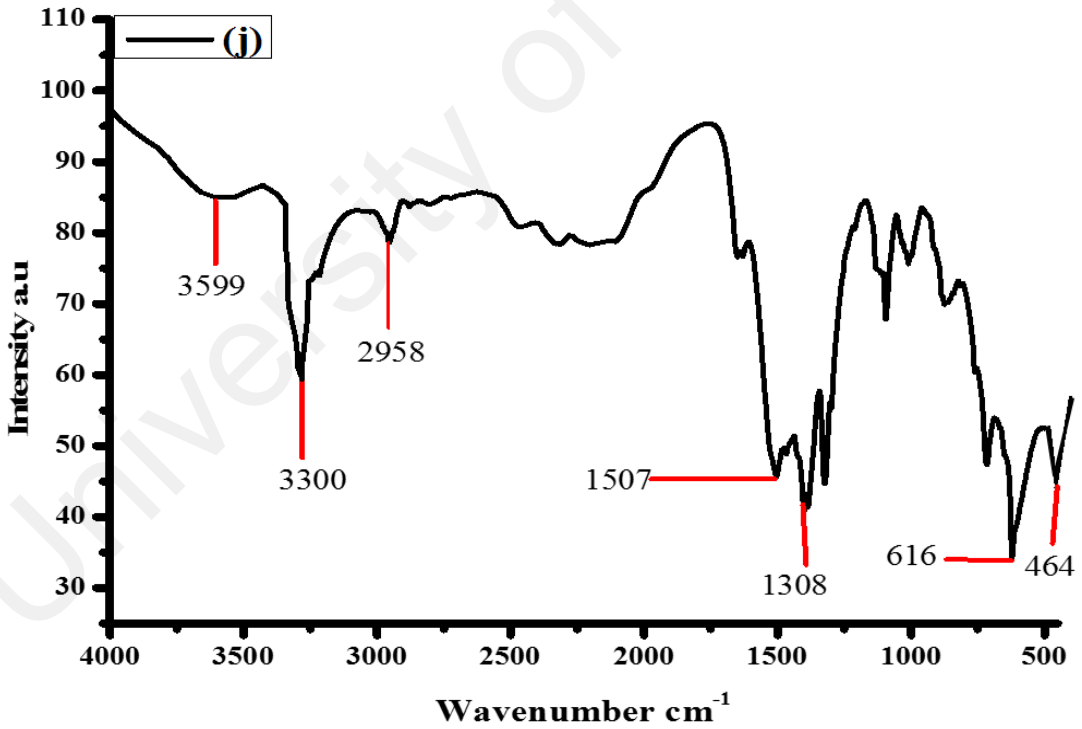

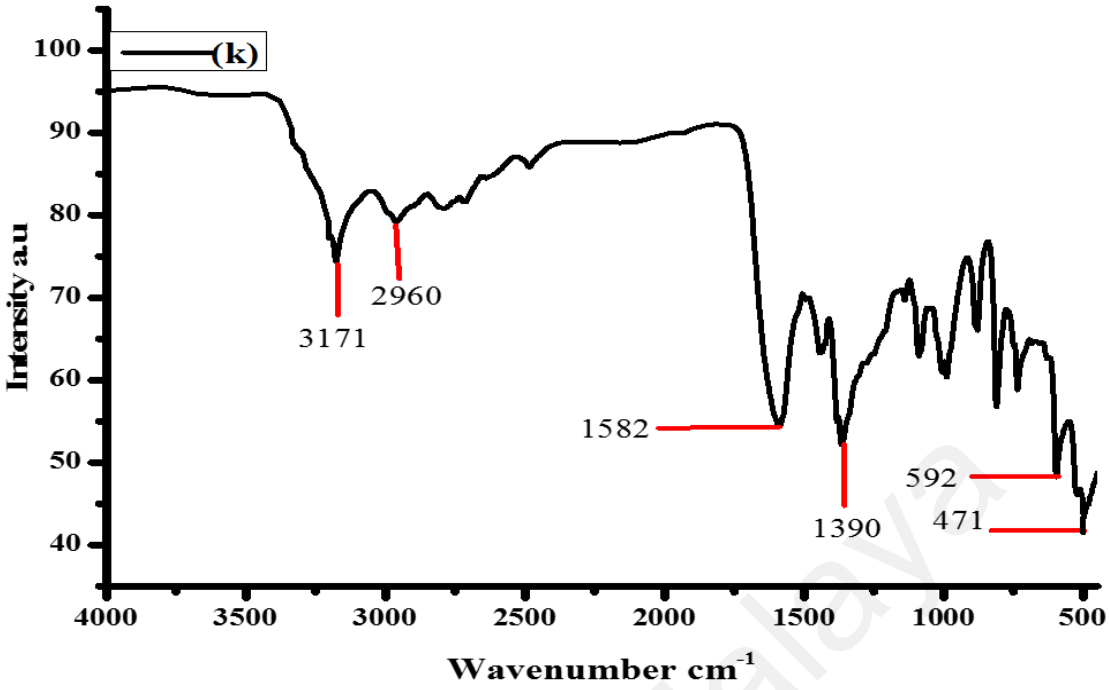

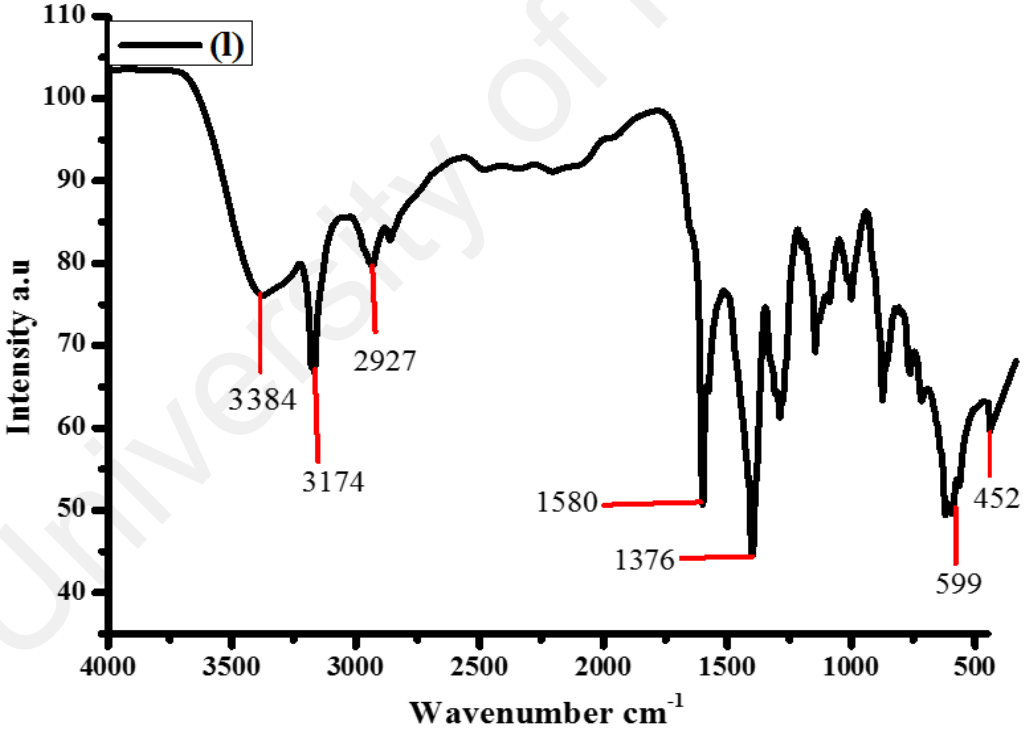

Appendix C: Cole-Cole plot of benzylimidazole series.

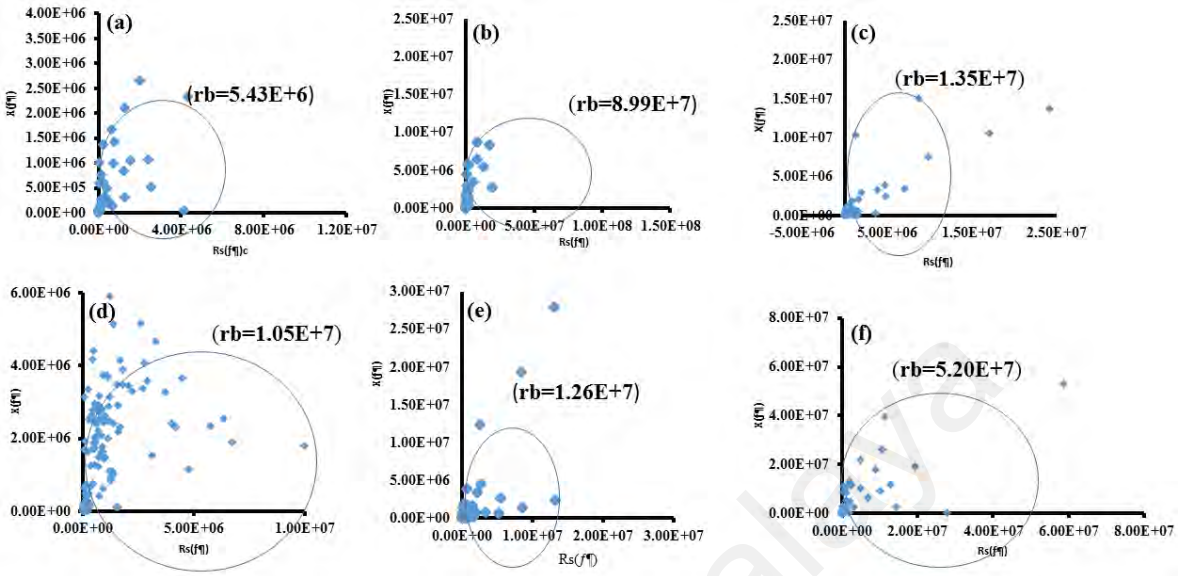

Appendix D: Cole-Cole plot of piperazine**.**